

Spectroscopy of the solid-state analogues of the hydrogen atom: donors and acceptors in semiconductors

A K Ramdas and S Rodriguez

Department of Physics, Purdue University, West Lafayette, Indiana 47907, USA

Abstract

Under suitable circumstances imperfections in semiconductors can bind electrons (holes) with a binding energy small compared to the intrinsic energy gap of the host; the wavefunctions characterising the energy levels of the imperfection are extended over many lattice spacings. This review discusses the electronic energy levels of chemical impurities in the classic group IV elemental and the III-V and II-VI compound semiconductors. The large dielectric constant of the host, the anisotropic effective mass tensor and/or the small effective mass of the charge carrier are the factors which play a significant role in the description of the electronic energy levels; they can be viewed as scaled-down versions of the hydrogen atom with bound states having binding energies orders of magnitude smaller than those of the hydrogen atom. In this review we present the experimental results on the spectroscopy of donors and acceptors in semiconductors together with the theory necessary for their interpretation. We discuss the experimental results and the theory of the bound states of impurities in the context of the symmetry and the effective-mass parameters of the band extrema with which they are associated. Effects of external perturbation—piezo- and magneto-spectroscopy—are presented both from experimental and theoretical points of view. The review concludes with the experimental observations on the linewidths of the excitation spectra of donors and acceptors in semiconductors and an analysis of the causes underlying them.

This review was received in June 1981.

Contents

	Page
1. Introduction	1299
2. Experimental techniques	1301
3. Theory of impurity states	1306
3.1. The effective-mass approximation	1306
3.2. Impurity states in the effective-mass approximation	1309
4. Experimental results in the absence of external fields	1319
4.1. Group V donors in silicon (Si) and germanium (Ge)	1319
4.2. Other donors in Si and Ge	1327
4.3. Group III acceptors in Si and Ge	1331
4.4. Other acceptors in Si and Ge	1337
4.5. Acceptors in diamond	1339
4.6. Donors and acceptors in compound semiconductors	1339
5. Impurity states under external perturbations	1345
5.1. Effects of uniaxial stress	1345
5.2. Effect of a magnetic field on donors and acceptors	1360
6. Linewidths of excitation lines	1370
6.1. Interaction of bound carriers and phonons	1370
6.2. Resonant electron-phonon interaction	1371
6.3. Electric-field broadening	1376
6.4. Concentration broadening	1379
7. Concluding remarks	1380
Acknowledgments	1381
References	1381

1. Introduction

The present semiconductor technology began during the Second World War when intense efforts were made to develop microwave detectors (Torrey and Whitmer 1948, Lark-Horovitz 1954). The group IV elemental semiconductors, silicon and germanium, were identified as the most promising materials. It was soon established that imperfections—their nature and concentration—played a decisive role in the magnitude and the type of conductivity; for example, at sufficiently low temperatures, the Hall coefficient of silicon with group V impurities like phosphorus in high enough concentrations is negative whereas it is positive when the impurities belong to group III of the periodic table of elements. In the former, electrons dominate the conductivity (*n* type) while holes constitute the majority current carriers in the latter (*p* type). The mastery of crystal growth and the introduction of known impurities in controlled amounts have proved to be the crucial factors in the remarkable range of semiconductor devices invented in the past quarter of a century. With the present state of the art of crystal growth it is possible to produce, for example, germanium crystals free of dislocations with impurity concentrations ranging from 10^8 – 10^{20} cm $^{-3}$. With such astonishing control, a wide range of phenomena of basic interest in solid-state physics becomes accessible to experimental investigation.

Much effort has gone into establishing the nature of imperfections in semiconductors. Foreign atoms in substitutional or interstitial positions, complexes of such atoms, vacancies or interstitials of the host atoms and non-stoichiometry in compound semiconductors are examples of imperfections which have received a great amount of attention (Flynn 1972). Consider, for example, the group V impurity phosphorus in silicon. A variety of evidence (Pearson and Bardeen 1949) can be adduced to prove that it enters the host in a site normally occupied by a silicon atom, i.e. substitutionally. Four of the five of its outermost electrons in the $3s^23p^3$ states form saturated (covalent) bonds with its four nearest neighbours; the fifth electron not incorporated in this bonding scheme is *donated* to the conduction band. However, it remains bound to the P^+ ion by the Coulomb attraction. It is clearly of interest to find out how tightly the ‘donor’ electron is bound and to establish its energy level scheme. The potential energy of the donor electron must take into account the adjustment of the charge density of the host in the field of the positively charged donor. The evaluation of this potential is a many-body problem. However, for distances, r , large compared to the lattice spacing, a , this adjustment can be viewed as a polarisation of the host described by its static dielectric constant, κ . In this limit the potential is

$$U_i(r) = -e^2/\kappa r. \quad (1.1)$$

Closer to the impurity $U_i(r)$ is more attractive, the dielectric screening being less effective, approaching $-e^2/r$ as r becomes comparable to the size of the P^+ ion. It should be recognised, however, that the donor wavefunction must be orthogonal to the core states of the P^+ ion. It can be shown that this constraint results in an approximate cancellation of the kinetic and potential energies close to the impurity centre which in turn justifies the potential in equation (1.1). In a crystal the electrons behave under an external field as particles with an effective mass m^* different from the free-electron mass, m , and often

much smaller. Under these assumptions, the donor electron will have hydrogen-like bound states given by

$$E_n = -m^*e^4/2\hbar^2\kappa^2n^2 \quad (1.2)$$

where $n = 1, 2, 3, \dots$. For example, in GaAs, $m^* = 0.06650 m$ and $\kappa = 12.58$ yield an ionisation energy, $E_I = -E_1 = 5.72$ meV and the corresponding Bohr radius $a^* = \hbar^2\kappa/m^*e^2 = 100$ Å (see Stillman *et al* 1971). Since $a^* \gg a$, the use of an effective kinetic energy ($p^2/2m^*$) is justified, thereby providing validity for equation (1.2). This simple model (Mott and Gurney 1940, Bethe 1942) needs to be modified for actual semiconductors in two important respects. (i) To the extent equation (1.1) fails to describe the true potential, the binding energies of different group V impurities in Si or Ge, for example, are not the same. (ii) The effective mass, m^* , for many semiconductors is a tensor rather than a scalar, reflecting the nature of the conduction band. In an analogous fashion one can develop a model for substitutional group III impurities in Si or Ge which bind the hole created in the valence band resulting from the formation of the covalent bonds with its nearest neighbours. These impurities which have *accepted* an electron from the valence band to complete the bonding scheme with its four nearest neighbours are called 'acceptors'. The details of the bound states of the acceptor reflect the characteristics of the valence band maximum of the host. (For a convenient summary of the symmetries and mass parameters of the band extrema of the semiconductors discussed in this review we refer the readers to appendix C of Long (1968).)

The concepts of donor and acceptor impurities are easily extended to compound semiconductors which are tetrahedrally bonded, e.g. GaAs or CdTe. In the III-V semiconductors, a group VI impurity like Te in a substitutional site on the lattice of the group V atoms and a group II impurity like Zn replacing a group III atom act as a donor and acceptor, respectively. A group IV impurity in a III-V semiconductor is a donor or an acceptor, depending on whether it substitutes a group III or a group V host atom (Whelan 1960).

We have thus seen that the donors and acceptors we have considered are solid-state analogues of the hydrogen atom. Indeed, the energy levels represented in equation (1.2) are simply a 'scaled-down' version of the energy levels of the hydrogen atom. It is easy to extend such considerations to substitutional group VI(II) impurities in Si or Ge which bind two electrons (holes) and hence constitute solid-state analogues of neutral helium.

The hydrogenic model of donors and acceptors in semiconductors, especially equation (1.2), immediately suggests optical observation of spectra similar to the well-known Lyman, Balmer, . . . , series of the hydrogen atom. Such spectra are expected in the near-to far-infrared in view of small m^* and large κ , which characterise typical semiconductors. Samples would have to be held at cryogenic temperatures in order to have neutral (un-ionised) donors or acceptors, which are characterised by small ionisation energies. In the early days of semiconductor physics it was felt (Torrey and Whitmer 1948) that the excited states of different impurity centres would overlap in view of their large radii, $a_n^* = n^2a^*$, their binding energies would correspondingly decrease, and they would merge with the conduction band. It was concluded that only the ground state would have a finite binding energy. Pioneering experiments by Burstein and co-workers (Burstein *et al* 1953, 1956, Picus *et al* 1956) on the Lyman spectra of donors and acceptors in silicon, however, showed that at sufficient dilution discrete ground and excited states do exist. Since these early observations, impurity states have been experimentally investigated using (i) absorption and photoconductivity spectroscopy in the near- and far-infrared,

(ii) Raman spectroscopy and (iii) luminescence. Such spectra have been reported for a large number of impurity species in several semiconductors and have been studied under the influence of elastic strain or magnetic field. In this entire development there has been an intimate interaction of theory and experiment. One of the satisfying by-products of such studies has been the development of some of the most sensitive infrared detectors based on the photoconductivity produced by the photoionisation of impurity centres (Putley 1964, Bratt 1977).

In the present review we focus our discussion on foreign atoms in otherwise perfect tetrahedrally bonded group IV elemental and III-V as well as II-VI compound semiconductors. Experimental results on the spectroscopy of donors and acceptors, with and without external perturbation, are reviewed along with theoretical developments. Recently Bassani *et al* (1974), Pantelides (1978) and Altarelli and Bassani (1980) have written comprehensive review articles on the theory of the impurity states. Reference should also be made to chapters 7 and 8 in the recent book by Bassani and Pastori Parravicini (1975). Experimental work prior to 1969 has been reviewed by Fisher and Ramdas (1969). In the present review we stress the experimental developments but provide sufficient theoretical background to make it self-contained.

2. Experimental techniques

Many impurities can be introduced into semiconductors during crystal growth in a deliberate and controlled manner, as dopants added to the melt in the Czochralski method or in the form of a suitable gaseous compound allowed to enter the vacuum chamber in which the crystal is grown by the floating zone technique (Hannay 1960, Gilman 1963, Laudise 1970). Impurities like lithium, magnesium or copper can be incorporated into an otherwise pure host crystal by diffusion followed by a quench (Reiss and Fuller 1960). An ingenious technique of introducing phosphorus in silicon is based on the nuclear transmutation of ^{30}Si into ^{31}P by the capture of a slow neutron followed by a β^- decay; the isotope ^{30}Si occurs in natural silicon with an abundance of 3.1%. A similar procedure can be utilised to convert ^{70}Ge into ^{71}Ga , ^{74}Ge into ^{75}As , and ^{76}Ge into ^{77}Se (Lark-Horovitz 1951, 1954, Tannenbaum and Mills 1961). Considerations important in the preparation of crystals doped with a specific impurity at a desired concentration are discussed by de Kock (1980). It should be emphasised here that, even in semiconductors like silicon, 'unknown' imperfections generated during crystal growth have been traced only after a considerable period of confusion and lack of appreciation of some aspect of the growth technique; oxygen and carbon in silicon can be cited as classic examples (Newman 1973).

In view of the small binding energies of group V donors and group III acceptors in Si and Ge and of the analogous centres in the III-V semiconductors, a significant fraction of the impurity centres are ionised at room temperature. Samples thus have to be cooled to sufficiently low temperatures in order to ensure that these centres are neutral and hence can be excited by electromagnetic radiation of the appropriate frequencies. For the semiconductors which have been extensively studied the suitable range of temperatures turns out to be between the boiling points of nitrogen and helium. An additional reason for performing optical measurements at cryogenic temperatures is the sharpening of the excitation lines. Optical cryostats of various designs and fabricated with either glass or stainless steel have been described in the literature and are commercially available

(Rose-Innes 1973). We give here a short description of a glass cryostat (figure 1) used for a number of years in our laboratory (Fisher *et al* 1963).

As can be seen from this diagram the cryostat consists of two parts. One unit consists of the liquid coolant reservoir and sample block and will be called the centre piece. The remainder we shall call the outer piece. The sample is clamped over one of two identical apertures in a copper block. Either the sample or the reference aperture can be interposed in the light beam by rotating the centre piece at the 29/42 joint. In figure 1, the top 35/20 ball can be used to connect the volume containing the coolant to a high-speed vacuum pump so that one can reduce the vapour pressure of the gas above the liquid and

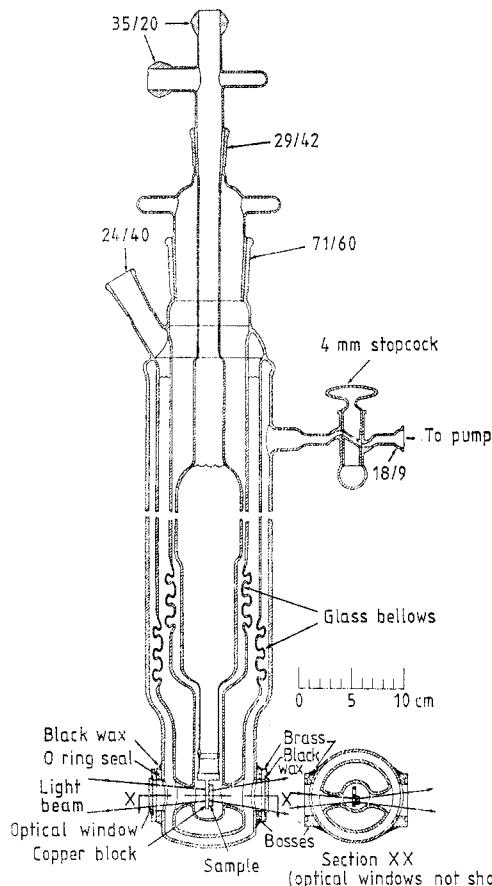


Figure 1. Glass optical cryostat with glass centre piece (from Fisher *et al* 1963).

thus lower the bath temperature and still allow rotation about 29/42. The outer piece consists of three coaxial tubes. The outermost tube forms the vacuum wall of the cryostat, the inner two constitute the liquid nitrogen radiation shield and are joined to the outer tube at the top in two ring seals and thence to the 71/60 cone. Thus the liquid nitrogen is open to the atmosphere only at the 24/40 cone which is used as the filling port. The inner and outer vacuum spaces are interconnected via the apertures through the two walls of the nitrogen jacket. The sizes of these apertures are chosen to just accommodate the light beam and so minimise the undesired room-temperature radiation reaching the sample. Since the two walls of the nitrogen shield are rigidly connected at the

top and the bottom, bellows are provided to permit independent expansion and contraction of these two tubes. The optical windows (alkali halide, sapphire, CaF_2 , crystalline quartz or Mylar) are mounted onto brass plates, which in turn are bolted to brass bosses waxed to the outside surface of the outer piece.

When uniaxial stress experiments are carried out, a stainless-steel centre piece, shown in figure 2, is inserted in place of the glass centre piece. The centre piece is mated to the optical cryostat by means of the stainless-steel cone joint G. The pressure head B is pressurised with nitrogen gas through the point A and the resultant force produced by

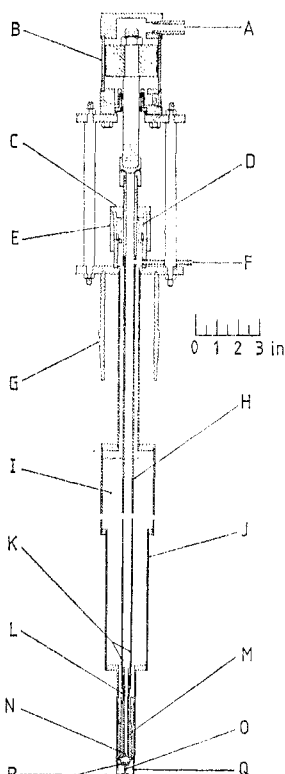


Figure 2. Stainless-steel-stress centre piece. This replaces the glass centre piece shown in figure 1 (from Tekippe *et al* 1972). A, gas pressure inlet; B, pressure head; C, height adjustment collar; D, M, bellows; E, safety collar; F, coolant outlet; G, stainless-steel cone joint; H, hollow push rod; I, coolant chamber; J, walls of the coolant reservoir; K, N, small holes allowing the coolant to flow into I from H; L, copper portion of the push rod; O, sample; P, copper cups; Q, copper tailpiece.

the piston is transmitted by a hollow push rod H which passes through the coolant I and makes contact with the sample O. The sample is compressed against the bottom of a hollow copper cylinder Q which is threaded to the coolant reservoir J. For measurements of the Zeeman effect a modification of the cryostat has been described by Fisher *et al* (1963). The above cryostats are designed for either transmission or photoconductivity measurements. For luminescence or light scattering experiments a third window whose axis is at right angles with respect to that of the other two is provided.

Because of the small binding energies of the impurity centres of interest, absorption and photoconductivity spectra are studied in the spectral range from a few to several

hundred microns. The various advances in near- and far-infrared spectroscopy in the past 30 years have been fully exploited in this field. The early work of Burstein and co-workers on group III and group V impurities in silicon utilised prism spectrometers which can extend up to $50\text{ }\mu\text{m}$ with CsI or KRS-5 optics. Grating spectrometers are essential beyond $50\text{ }\mu\text{m}$, the range where the excitation spectra of group III and group V impurities in germanium are found. Even for the impurities in silicon and those of germanium for which the spectra occur in the shorter wavelengths, grating spectrometers are to be preferred since they are capable of better resolution and have higher light gathering power. A variety of detectors—thermocouple, pneumatic cell (Golay cell), photoconductive semiconducting detectors based on the photoionisation of impurity centres, semiconducting bolometers—are currently available to the infrared

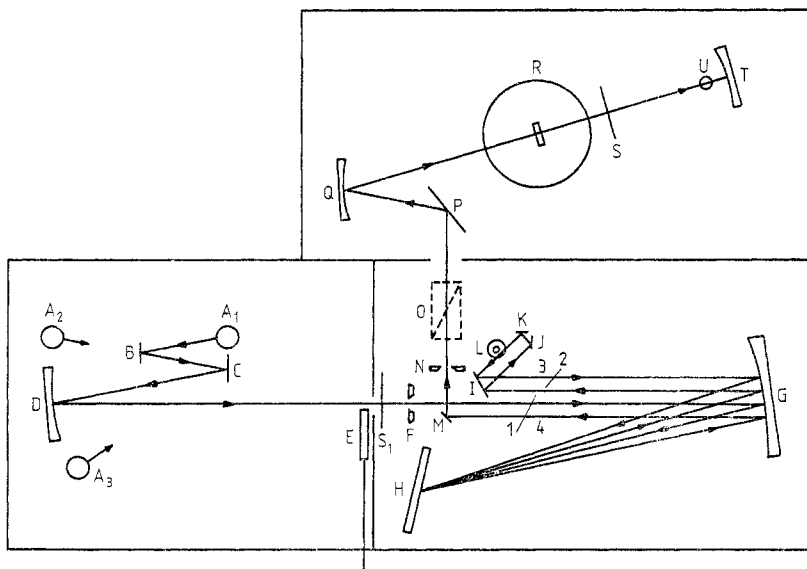


Figure 3. Schematic of a double-pass grating spectrometer incorporating a Perkin-Elmer Model 99G monochromator (from Jones 1968). A₁, A₂, A₃, source position; B, C, P, plane reflectors: aluminised mirrors or reststrahlen plates; D, Q, aluminised spherical mirrors; I, J, K, M, aluminised plane mirrors; E, shutter; F, entrance slit; G, off-axis paraboloid collimator; H, plane reflection grating; L, chopper; N, exit slit; O, polariser position; R, optical cryostat with sample; S, S₁, transmission filter position; T, thermocouple elliptical focusing mirror; U, thermocouple detector.

spectroscopist. The comprehensive treatises by Hadni (1967) and Möller and Rothschild (1971) give a wealth of information about all aspects of infrared spectroscopy.

Figure 3 shows a grating spectrometer incorporating a double-pass monochromator and the associated source and exit optics. Another comparatively recent type of spectrometer is the one based on the Michelson interferometer, the so-called Fourier transform spectrometer; here an interferogram is generated as a function of the displacement of the movable mirror and, when appropriately digitised and Fourier-transformed on a digital computer, yields the spectrum (Bell 1972); figure 4 shows such a spectrometer. A tunable diode laser spectrometer (Hinkeley *et al* 1976), which can currently cover a range $2\text{--}30\text{ }\mu\text{m}$, promises to be a convenient ultra-high-resolution spectrometer. Novel types of spectrometers incorporating a spin-flip Raman laser (Patel and Shaw 1970) or a difference frequency generator (Pine 1974) should see more use in this field in the com-

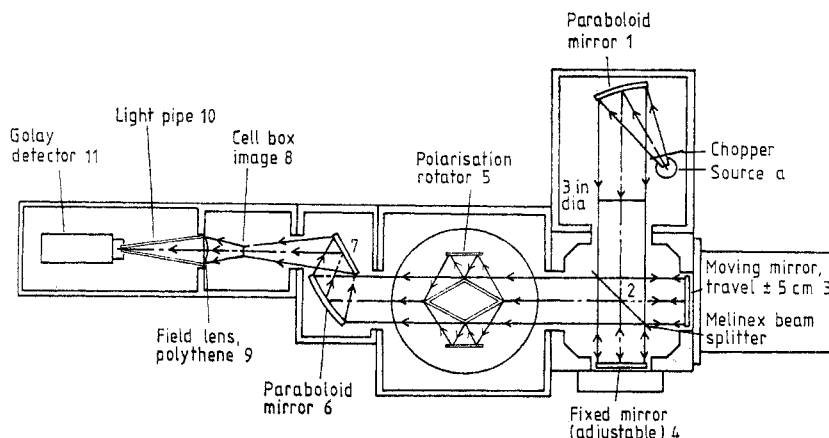


Figure 4. Schematic of the Beckman-RIIC FS-720 Fourier transform spectrometer modified to accommodate a polarisation rotator (from Jagannath 1980).

ing years. In some studies a backward wave tube (Gershenzon 1977) has been successfully used in the sub-millimetre range. Measurements of the Zeeman effect can be carried out by varying the applied magnetic field until the transition energy equals the energy of the photons from a monochromatic laser source (Stillman *et al* 1971).

Light scattering studies in the near-infrared have utilised a YAG(Nd) or a YAG(Ho) laser, a photoconductive detector or a photomultiplier, and the phase-sensitive technique or the photon counting technique (Mooradian 1972, Doehler *et al* 1974). A tunable dye laser in the visible has been used ingeniously for luminescence studies on the donor-acceptor pairs in gallium phosphide (Street and Senske 1976). In all of these investigations a grating double monochromator serves the purpose ideally. Figure 5 shows the experimental setup used by Mooradian and Wright (1966a, b), Wright and Mooradian

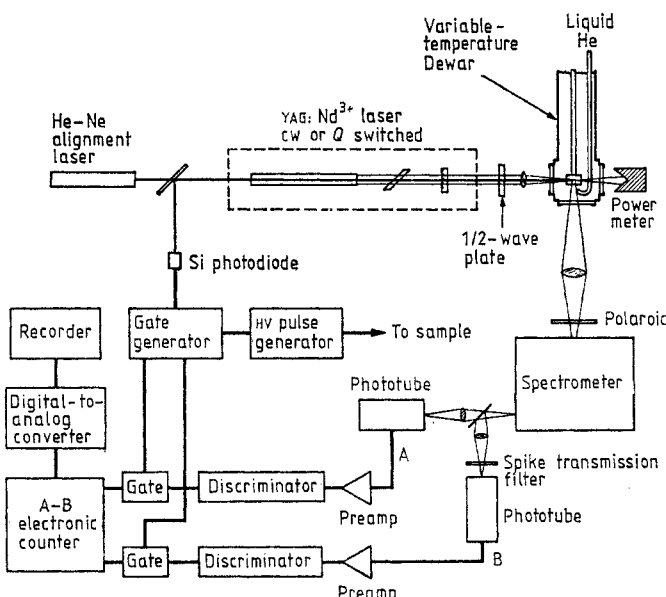


Figure 5. Experimental set-up for the study of electronic Raman scattering used by Mooradian (1972).

(1967) and Mooradian and McWhorter (1967) and described in a review article by Mooradian (1972). Wood *et al* (1977) and Aggarwal *et al* (1980) have carried out a novel experiment on n-type germanium in which they measure the third-order non-linear optical susceptibility, $\chi^{(3)}$, in a non-linear resonant four-wave mixing; impurity-induced resonances in $\chi^{(3)}$ characteristic of the donors are observed.

3. Theory of impurity states

In this section we present the theory of the stationary states of a charge carrier, say an electron, bound to an ionised impurity in a semiconductor. The potential energy of the electron is assumed to differ from that in the perfect crystal by $U_i(r)$. It is useful to first review the effective-mass theory for electrons in a perfect crystal.

3.1. The effective-mass approximation

In a crystal with periodic potential $U_0(r)$ the eigenfunctions of the Hamiltonian

$$H_0 = \frac{p^2}{2m} + U_0(r) \quad (3.1)$$

can be selected to have the Bloch form

$$\psi_{\nu k}(r) = N_c^{-1/2} \exp(i\mathbf{k} \cdot \mathbf{r}) u_{\nu k}(r) \quad (3.2)$$

normalised over the volume $V = N_c v_0$ of the crystal where N_c is the number of primitive cells, $u_{\nu k}(r)$ has the translational symmetry of $U_0(r)$ and is normalised over the volume v_0 of the primitive cell. The eigenvalue of H_0 in the state $\psi_{\nu k}$ is denoted by $E_{\nu}(\mathbf{k})$. In the periodic zone scheme, $E_{\nu}(\mathbf{k})$ is invariant under the translations of the reciprocal lattice. The periodic part $u_{\nu k}(r)$ of $\psi_{\nu k}(r)$ satisfies

$$H(\mathbf{k}) u_{\nu k}(r) = E_{\nu}(\mathbf{k}) u_{\nu k}(r) \quad (3.3)$$

where

$$H(\mathbf{k}) = H_0 + \frac{\hbar}{m} \mathbf{k} \cdot \mathbf{p} + \frac{\hbar^2 k^2}{2m}. \quad (3.4)$$

Let $E_{\nu}(\mathbf{k})$ have an extremum at $\mathbf{k} = \mathbf{k}_0$. Using quantum-mechanical perturbation theory, we construct the eigenstates of $H(\mathbf{k})$ assuming those of $H(\mathbf{k}_0)$ to be known. This development is expected to yield rapid convergence for values of \mathbf{k} near \mathbf{k}_0 . The perturbation is (Kane 1966)

$$H' = H(\mathbf{k}) - H(\mathbf{k}_0) = \frac{\hbar}{m} (\mathbf{k} - \mathbf{k}_0) \cdot \mathbf{p} + \frac{\hbar^2}{2m} (\mathbf{k}^2 - \mathbf{k}_0^2). \quad (3.5)$$

We remark that for fixed \mathbf{k} and all ν the set $\{u_{\nu k}\}$ forms a basis for functions with the periodicity of the lattice. The matrix elements of $H(\mathbf{k})$ in the representation $\{u_{\nu k_0}\}$ are

$$\langle \nu' k_0 | H(\mathbf{k}) | \nu k_0 \rangle = \left(E_{\nu}(\mathbf{k}_0) + \frac{\hbar^2}{2m} (\mathbf{k} - \mathbf{k}_0)^2 \right) \delta_{\nu' \nu} + \frac{\hbar}{m} (\mathbf{k} - \mathbf{k}_0) \cdot \mathbf{p}_{\nu' \nu} (1 - \delta_{\nu' \nu}). \quad (3.6)$$

Here

$$\mathbf{p}_{\nu' \nu} = \int_{(v_0)} u_{\nu' k_0}^* \mathbf{p} u_{\nu k_0} d\mathbf{r} \quad (3.7)$$

in deriving equation (3.6) we have used

$$\mathbf{p}_{\nu\nu} = \frac{m}{\hbar} \left(\frac{\partial E_{\nu}}{\partial \mathbf{k}} \right)_{\mathbf{k}=\mathbf{k}_0} - \hbar \mathbf{k}_0 = -\hbar \mathbf{k}_0 \quad (3.8)$$

since $E_{\nu}(\mathbf{k}_0)$ is an extremum of $E_{\nu}(\mathbf{k})$.

If the state $\psi_{\nu\mathbf{k}_0}$ is non-degenerate, to second order in $\mathbf{k}-\mathbf{k}_0$, perturbation theory yields

$$E_{\nu}(\mathbf{k}) = E_{\nu}(\mathbf{k}_0) + \frac{\hbar^2}{2m} (\mathbf{k}-\mathbf{k}_0) \cdot \boldsymbol{\alpha} \cdot (\mathbf{k}-\mathbf{k}_0) \quad (3.9)$$

where the tensor $\boldsymbol{\alpha}$ is

$$\boldsymbol{\alpha} = \mathbf{1} + \frac{2}{m} \sum'_{\nu'} \frac{\mathbf{p}_{\nu\nu'} \mathbf{p}_{\nu'\nu}}{E_{\nu}(\mathbf{k}_0) - E_{\nu'}(\mathbf{k}_0)}. \quad (3.10)$$

The sum over ν' extends over all bands except that labelled by ν . We consider now the case in which $E_{\nu}(\mathbf{k}_0)$ is degenerate. Since the matrix element

$$\frac{\hbar}{m} (\mathbf{k}-\mathbf{k}_0) \cdot \mathbf{p}_{\nu'\nu} (1 - \delta_{\nu\nu'})$$

is already off-diagonal we obtain the energy to second order in $\mathbf{k}-\mathbf{k}_0$ by diagonalising the sub-matrix whose $\nu'\nu$ element is

$$\left(E_{\nu}(\mathbf{k}_0) + \frac{\hbar^2}{2m} (\mathbf{k}-\mathbf{k}_0)^2 \right) \delta_{\nu\nu'} + \frac{\hbar^2}{m^2} \sum'_{\lambda} \frac{(\mathbf{k}-\mathbf{k}_0) \cdot \mathbf{p}_{\nu'\lambda} \mathbf{p}_{\lambda\nu} \cdot (\mathbf{k}-\mathbf{k}_0)}{E_{\nu}(\mathbf{k}_0) - E_{\lambda}(\mathbf{k}_0)}.$$

Here ν and ν' range over the states at \mathbf{k}_0 having the energy $E_{\nu}(\mathbf{k}_0)$ and the sum over λ is over all other states. This sum can be simplified using symmetry considerations. In the semiconductors we consider, the degeneracy of interest is that of the valence band maximum occurring at $\mathbf{k}=0$.

Neglecting spin, this state has the three-fold degeneracy associated with the Γ_5^+ irreducible representation of the group O_h . Here we follow Koster *et al* (1963) in labelling the irreducible representations. Then, this matrix element is

$$\left(E_0 + \frac{\hbar^2 k^2}{2m} \right) \delta_{\nu\nu'} + \frac{\hbar^2}{m^2} \mathbf{k} \cdot \sum'_{\lambda} \frac{\mathbf{p}_{\nu'\lambda} \mathbf{p}_{\lambda\nu} \cdot \mathbf{k}}{E_0 - E_{\lambda}}$$

where, for short, we write $E_{\lambda} = E_{\lambda}(0)$ and $E_{\nu}(0) = E_0$, the energy of the top of the valence band; the components of

$$\sum'_{\lambda} \frac{\mathbf{p}_{\nu'\lambda} \mathbf{p}_{\lambda\nu}}{E_0 - E_{\lambda}}$$

form a second-rank symmetric tensor in the indices ν and ν' . If $E_0=0$ is three-fold degenerate, the Hamiltonian matrix can be written as (Luttinger and Kohn 1955, Bir and Pikus 1974)

$$\mathcal{D}(\mathbf{k}) = Ak^2 - 3B \sum_i k_i^2 (I_i^2 - \frac{1}{3} I^2) - 2D \sqrt{3} \sum_{i < j} k_i k_j \{I_i I_j\} \quad (3.11)$$

where A , B and D are constants and I_x , I_y , I_z are the matrix elements of the angular momentum operators for $l=1$ in the x , y , z representation, i.e.

$$I_x = \begin{pmatrix} 0 & 0 & 0 \\ 0 & 0 & -i \\ 0 & i & 0 \end{pmatrix} \quad I_y = \begin{pmatrix} 0 & 0 & i \\ 0 & 0 & 0 \\ -i & 0 & 0 \end{pmatrix} \quad I_z = \begin{pmatrix} 0-i & 0 \\ i & 0 \\ 0 & 0 \end{pmatrix}. \quad (3.12)$$

The sums over i and j run over x , y , z and $\{I_i I_j\}$ is the symmetrised product of I_i and I_j , $\frac{1}{2}(I_i I_j + I_j I_i)$. Here x , y , z are the cubic axes of the crystal. Equation (3.11) is demonstrated using Unsöld's theorem for the construction of the invariant operators which are quadratic in the components of k .

It is customary to write $\mathcal{D}(k)$ in the form

$$\mathcal{D}(k) = \begin{pmatrix} Lk_x^2 + M(k_y^2 + k_z^2) & Nk_x k_y & Nk_x k_z \\ Nk_y k_x & Lk_y^2 + M(k_z^2 + k_x^2) & Nk_y k_z \\ Nk_z k_x & Nk_z k_y & Lk_z^2 + M(k_x^2 + k_y^2) \end{pmatrix} \quad (3.13)$$

where

$$L = A + 2B$$

$$M = A - B \quad (3.14)$$

$$N = D\sqrt{3}.$$

If we consider the spin of the electron, the three-fold degenerate state Γ_5^+ becomes a sextuplet $\Gamma_5^+ \times \Gamma_6^+ = \Gamma_7^+ + \Gamma_8^+$; the spin-orbit interaction splits this multiplet into a four-fold degenerate Γ_8^+ analogous to a $p_{3/2}$ atomic state and a two-fold Γ_7^+ state similar to an atomic $p_{1/2}$ state. The spin-orbit interaction can be expressed by

$$H_{s-0} = \frac{1}{3}\lambda \mathbf{I} \cdot \boldsymbol{\sigma} \quad (3.15)$$

where λ is the only non-vanishing matrix element of

$$\frac{3i\hbar}{4m^2c^2} \left(\frac{\partial U_0}{\partial x} p_y - \frac{\partial U_0}{\partial y} p_x \right).$$

The 6×6 Hamiltonian replacing equation (3.11) contains the contribution H_{s-0} , in addition to the direct product $\mathcal{D}(k) \times \sigma_0$ where σ_0 is the 2×2 unit matrix; σ is the Pauli spin matrix.

In the vicinity of $k=0$, for λ sufficiently large, the matrix $H_{s-0} + \mathcal{D}(k) \times \sigma_0$ can be separated into two sub-matrices with the aid of the Wigner-Eckart theorem as

$$\mathcal{D}_{3/2}(k) = Ak^2 - B \sum_i k_i^2 (J_i^2 - \frac{1}{3}J^2) - \frac{2D}{\sqrt{3}} \sum_{i < j} k_i k_j \{J_i J_j\} \quad (3.16)$$

and

$$\mathcal{D}_{1/2}(k) = -\lambda + Ak^2. \quad (3.17)$$

Here we neglect matrix elements connecting the $\frac{3}{2}$ and $\frac{1}{2}$ states; also we have shifted the origin of the energy by $-\frac{1}{3}\lambda$. In equation (3.16) J_x , J_y and J_z are the angular momentum matrices for $j=\frac{3}{2}$.

3.2. Impurity states in the effective-mass approximation

The theory of the quantum-mechanical states of point imperfections in semiconductors can be developed in a number of ways. We follow here the method of Luttinger and Kohn (1955) which is particularly suited for ‘shallow’ donors and acceptors, i.e. for imperfections with ionisation energies comparable to that given by equation (1.2). Their energy levels are given by the solutions of the Schrödinger equation:

$$H\psi = \left(\frac{p^2}{2m} + U_0(\mathbf{r}) + U_i(\mathbf{r}) \right) \psi = E\psi. \quad (3.18)$$

Instead of the Bloch functions for a perfect crystal, Luttinger and Kohn use

$$\chi_{\nu k}(\mathbf{r}) = N_c^{-1/2} \exp(i\mathbf{k} \cdot \mathbf{r}) u_{\nu k_0}(\mathbf{r}) \quad (3.19)$$

which also constitute a complete orthonormal set. We restrict \mathbf{k} to the reduced Brillouin zone. As already mentioned, we assume that $E_\nu(\mathbf{k})$ has an extremum at \mathbf{k}_0 .

In the representation (3.19), the matrix elements of H are

$$\langle \nu' \mathbf{k}' | H | \nu \mathbf{k} \rangle = \langle \nu' \mathbf{k}' | H_0 + H_1 + U_i | \nu \mathbf{k} \rangle \quad (3.20)$$

where

$$\langle \nu' \mathbf{k}' | H_0 | \nu \mathbf{k} \rangle = \left(E_\nu(\mathbf{k}_0) + \frac{\hbar^2}{2m} (\mathbf{k} - \mathbf{k}_0)^2 \right) \delta_{kk'} \delta_{\nu\nu'} \quad (3.21)$$

$$\langle \nu' \mathbf{k}' | H_1 | \nu \mathbf{k} \rangle = \frac{\hbar}{m} (\mathbf{k} - \mathbf{k}_0) \cdot \mathbf{p}_{\nu'\nu} \delta_{kk'} (1 - \delta_{\nu\nu'}). \quad (3.22)$$

Here $\mathbf{p}_{\nu'\nu}$ is given by equation (3.7). We eliminate H_1 to first order by making the unitary transformation $\exp(-iS)$ where S is a Hermitian operator to be determined. The transformed Hamiltonian is

$$K = \exp(-iS) H \exp(iS) = H + i[H, S] - \frac{1}{2}[[H, S], S] + \dots \quad (3.23)$$

The elimination of H_1 to first order is accomplished by requiring S to satisfy

$$i[H_0, S] + H_1 = 0. \quad (3.24)$$

Thus

$$K = H_0 + U_i + i/2[H_1, S] + i[U_1, S] - \frac{1}{2}[[H_1, S], S] - \frac{1}{2}[[U_1, S], S] + \dots \quad (3.25)$$

Taking matrix elements of both sides of equation (3.24) we obtain

$$\langle \nu' \mathbf{k}' | S | \nu \mathbf{k} \rangle = \frac{i}{m\omega_{\nu'\nu}} (\mathbf{k} - \mathbf{k}_0) \cdot \mathbf{p}_{\nu'\nu} \delta_{kk'} (1 - \delta_{\nu\nu'}) \quad (3.26)$$

where

$$\hbar\omega_{\nu'\nu} = E_{\nu'}(\mathbf{k}_0) - E_\nu(\mathbf{k}_0). \quad (3.27)$$

For $E_{\nu'}(\mathbf{k}_0) = E_\nu(\mathbf{k}_0)$, the matrix element of S can be selected arbitrarily and set equal to zero.

The matrix elements of the third term in equation (3.25) are

$$\frac{1}{2} \langle \nu' \mathbf{k}' | i[H_1, S] | \nu \mathbf{k} \rangle = \frac{\hbar \delta_{kk'}}{2m^2} (\mathbf{k} - \mathbf{k}_0) \cdot \sum'_{\nu''} \left[\left(\frac{1}{\omega_{\nu'\nu''}} + \frac{1}{\omega_{\nu\nu''}} \right) \mathbf{p}_{\nu'\nu''} \mathbf{p}_{\nu''\nu} \right] \cdot (\mathbf{k} - \mathbf{k}_0) \quad (3.28)$$

where the sum over ν'' extends over all states other than those for which $E_{\nu''}(\mathbf{k}_0)$ equals either $E_{\nu'}(\mathbf{k}_0)$ or $E_\nu(\mathbf{k}_0)$. This is indicated by the prime on the summation sign.

The matrix elements of the fourth term in equation (3.25) are

$$\langle \nu' \mathbf{k}' | i[U_i, S] | \nu \mathbf{k} \rangle = \frac{1}{m} \sum'_{\nu''} \left(\frac{(\mathbf{k}' - \mathbf{k}_0) \cdot \mathbf{p}_{\nu' \nu''}}{\omega_{\nu' \nu''}} \langle \nu'' \mathbf{k}' | U_i | \nu \mathbf{k} \rangle + \frac{(\mathbf{k} - \mathbf{k}_0) \cdot \mathbf{p}_{\nu'' \nu}}{\omega_{\nu'' \nu}} \langle \nu' \mathbf{k}' | U_i | \nu'' \mathbf{k} \rangle \right). \quad (3.29)$$

The remaining terms in equation (3.25) are negligible because the fifth term is proportional to $(\mathbf{k} - \mathbf{k}_0)^3$ and the sixth to $(\mathbf{k} - \mathbf{k}_0)^2 U_i$. Further terms behave as even higher powers of these quantities. For shallow donors and acceptors in semiconductors $U_i(r)$ is slowly varying and its spatial extension has a diameter a_i large compared to that of the primitive cell. The matrix element of U_i can be rewritten in the form

$$\langle \nu' \mathbf{k}' | U_i | \nu \mathbf{k} \rangle \approx \frac{1}{N_c} \sum_{\mathbf{n}} \exp[i(\mathbf{k}' - \mathbf{k}) \cdot \mathbf{n}] U_i(\mathbf{n}) \int_{(v_0)} \exp[i(\mathbf{k}' - \mathbf{k}) \cdot \mathbf{r}] u_{\nu' k_0}^*(\mathbf{r}) u_{\nu k_0}(\mathbf{r}) d\mathbf{r}. \quad (3.30)$$

Here we have assumed that $U_i(r)$ does not vary appreciably across a primitive cell and replaced its value by that at each lattice point \mathbf{n} . The sum over \mathbf{n} is over all N_c primitive cells of the crystal. The integral extends over the volume of the primitive cell, v_0 . The sum over \mathbf{n} is approximately the Fourier transform of the impurity potential

$$U_i(\mathbf{k}' - \mathbf{k}) \approx \frac{1}{N_c} \sum_{\mathbf{n}} \exp[i(\mathbf{k}' - \mathbf{k}) \cdot \mathbf{n}] U_i(\mathbf{n}). \quad (3.31)$$

These Fourier components are small if $|\mathbf{k}' - \mathbf{k}| > 1/a_i$ so that in evaluating the integral over v_0 , in equation (3.30) it is enough to restrict the discussion to $|\mathbf{k}' - \mathbf{k}| < 1/a_i$. However, the exponent $(\mathbf{k}' - \mathbf{k}) \cdot \mathbf{r}$ has, then, a maximum value $\sim a/a_i$ where a is the lattice parameter. If $a \ll a_i$, $\exp[i(\mathbf{k}' - \mathbf{k}) \cdot \mathbf{r}]$ can be approximated to unity and the integral reduces simply to $\delta_{\nu \nu'}$ by virtue of the orthogonality of the $u_{\nu k_0}(\mathbf{r})$ over the volume v_0 . Thus, equation (3.29) reduces to

$$\langle \nu' \mathbf{k}' | i[U_i, S] | \nu \mathbf{k} \rangle = \frac{1}{m} U_i(\mathbf{k}' - \mathbf{k}) \frac{(\mathbf{k}' - \mathbf{k}) \cdot \mathbf{p}_{\nu' \nu}}{\omega_{\nu' \nu}} \quad (3.32)$$

which is negligible compared to

$$\langle \nu' \mathbf{k}' | U_i | \nu \mathbf{k} \rangle = U_i(\mathbf{k}' - \mathbf{k}) \delta_{\nu \nu'}. \quad (3.33)$$

The matrix elements of K in this approximation are

$$\begin{aligned} \langle \nu' \mathbf{k}' | K | \nu \mathbf{k} \rangle &= \left(E_\nu(\mathbf{k}_0) + \frac{\hbar^2}{2m} (\mathbf{k} - \mathbf{k}_0)^2 \right) \delta_{\nu \nu'} \delta_{kk'} \\ &+ \frac{\hbar}{2m^2} \delta_{kk'} (\mathbf{k} - \mathbf{k}_0) \cdot \sum'_{\nu''} \left[\left(\frac{1}{\omega_{\nu' \nu''}} + \frac{1}{\omega_{\nu'' \nu}} \right) \mathbf{p}_{\nu' \nu''} \mathbf{p}_{\nu'' \nu} \right] \cdot (\mathbf{k} - \mathbf{k}_0) \\ &+ U_i(\mathbf{k}' - \mathbf{k}) \delta_{\nu \nu'}. \end{aligned} \quad (3.34)$$

We consider the case in which $E_\nu(\mathbf{k}_0)$ is non-degenerate. From equation (3.10) we have

$$\begin{aligned} \langle \nu \mathbf{k}' | K | \nu \mathbf{k} \rangle &= \left(E_\nu(\mathbf{k}_0) + \frac{\hbar^2}{2m} (\mathbf{k} - \mathbf{k}_0) \cdot \boldsymbol{\alpha} \cdot (\mathbf{k} - \mathbf{k}_0) \right) \delta_{kk'} + U_i(\mathbf{k}' - \mathbf{k}) \\ &= E_\nu(\mathbf{k}) \delta_{kk'} + U_i(\mathbf{k}' - \mathbf{k}). \end{aligned} \quad (3.35)$$

The eigenvalue problem associated with the Hamiltonian matrix in equation (3.35) is

$$E_\nu(\mathbf{k}) B_\nu(\mathbf{k}) + \sum_{\mathbf{k}'} U_i(\mathbf{k}' - \mathbf{k}) B_\nu(\mathbf{k}') = E B_\nu(\mathbf{k}). \quad (3.36)$$

We notice that, in this approximation, contributions arising from different bands are separated and the integral equation (3.36), giving the wavefunction in \mathbf{k} space, must be solved for each band independently. In the coordinate representation the wavefunction is

$$F_\nu(\mathbf{r}) = \sum_{\mathbf{k}} \exp[i(\mathbf{k} - \mathbf{k}_0) \cdot \mathbf{r}] B_\nu(\mathbf{k}) \quad (3.37)$$

with

$$B_\nu(\mathbf{k}) = \frac{1}{V} \int F_\nu(\mathbf{r}) \exp[-i(\mathbf{k} - \mathbf{k}_0) \cdot \mathbf{r}] d\mathbf{r}. \quad (3.38)$$

$F_\nu(\mathbf{r})$ is called the envelope wavefunction. Equation (3.36) is equivalent to the differential equation

$$[E_\nu(\mathbf{k}_0 - i\nabla) + U_i(\mathbf{r})] F_\nu(\mathbf{r}) = \left(E_\nu(\mathbf{k}_0) - \frac{\hbar^2}{2m} \nabla \cdot \alpha \cdot \nabla + U_i(\mathbf{r}) \right) F_\nu(\mathbf{r}) = E F_\nu(\mathbf{r}). \quad (3.39)$$

The wavefunction of the bound carrier in the representation diagonalising H in equation (3.18) is

$$\psi(\mathbf{r}) = \exp(iS) \sum_{\mathbf{k}} B_\nu(\mathbf{k}) \chi_{\nu\mathbf{k}}(\mathbf{r}) \cong \sum_{\mathbf{k}} B_\nu(\mathbf{k}) \chi_{\nu\mathbf{k}}(\mathbf{r})$$

or

$$\psi(\mathbf{r}) = \sum_{\mathbf{k}} \frac{1}{V} \int F_\nu(\mathbf{r}') \exp[-i(\mathbf{k} - \mathbf{k}_0) \cdot \mathbf{r}'] \chi_{\nu\mathbf{k}}(\mathbf{r}') d\mathbf{r}' = F_\nu(\mathbf{r}) \psi_{\nu\mathbf{k}_0}(\mathbf{r}). \quad (3.40)$$

In a cubic crystal with a non-degenerate conduction band minimum at $\mathbf{k}_0=0$ (e.g. the Γ_6 conduction band minimum of GaAs) $E(\mathbf{k})=\hbar^2 k^2/2m^*$ and the differential equation for $F(\mathbf{r})$ is

$$-\frac{\hbar^2}{2m^*} \nabla^2 F + U_i(\mathbf{r}) F = E F. \quad (3.41)$$

For a shallow donor $U_i(r) = -fe^2/r$ where, for r large compared to a , $f = \Delta Z/\kappa$, κ is the dielectric constant and ΔZ is the difference in valence between the substitutional donor and the atom it replaces. For small r the value of f depends on the incomplete screening of the extra electron by the core states of the donor. For $r \gtrsim a$ and $\Delta Z=1$, equation (3.41) is

$$\left(-\frac{\hbar^2}{2m^*} \nabla^2 - \frac{e^2}{\kappa r} \right) F = E F. \quad (3.42)$$

Its ground-state wavefunction is

$$F = (1/\pi a_1^3)^{1/2} \exp(-r/a_1) \quad (3.43)$$

where $a_1 = \hbar^2 \kappa / m^* e^2$. The eigenvalues of equation (3.42) are $E_n = -(m^* e^4 / 2\hbar^2 n^2 \kappa^2)$ where n is a positive integer. The ground and excited states have the same symmetry as those of the corresponding levels of the hydrogen atom. We thus see that this theory confirms the intuitive picture outlined in §1.

If $\mathbf{k}_0 \neq 0$ we can always find a set of orthogonal axes, called the principal axes, such that

$$E_\nu(\mathbf{k}) = E_\nu(\mathbf{k}_0) + \sum_{i=1}^3 \frac{\hbar^2}{2m_i^*} (k_i - k_{0i})^2 + \dots \quad (3.44)$$

Equation (3.39) applied to this case is now no longer separable, and approximate solutions can be found using the variational principle. In Si there are six equivalent Δ_1 minima along the $\langle 100 \rangle$ directions while in Ge there are four such L_1 minima at the Brillouin zone (BZ) boundary along the $\langle 111 \rangle$ directions. The expansion in equation (3.44) for these cases can be rewritten in the vicinity of each conduction band minimum as

$$E_\nu(\mathbf{k}) = E_\nu(k_0) + \frac{\hbar^2}{2m_t} (k_x^2 + k_y^2) + \frac{\hbar^2}{2m_l} (k_z - k_0)^2 \quad (3.45)$$

where the z axis is along a $\langle 100 \rangle$ direction in the case of Si and along a $\langle 111 \rangle$ direction for Ge. The equation for $F_\nu(\mathbf{r})$ thus becomes

$$-\frac{\hbar^2}{2m_t} \left(\frac{\partial^2 F_\nu}{\partial x^2} + \frac{\partial^2 F_\nu}{\partial y^2} \right) - \frac{\hbar^2}{2m_l} \frac{\partial^2 F_\nu}{\partial z^2} + U_i F_\nu = (E - E_\nu(k_0)) F_\nu. \quad (3.46)$$

Equation (3.46) has axial symmetry about the z axis rather than spherical symmetry. Hence the effective Hamiltonian commutes with the z component of the angular momentum, L_z , but not with the other components. Thus the eigenfunctions of equation (3.46) are of the form $R_{km}(r, \theta) \exp(im\varphi)$ where r, θ, φ are the polar coordinates of the electron. The states with magnetic quantum numbers m and $-m$ are degenerate because of time-reversal invariance. Thus, for a p state, the levels, which when $m_t = m_l$ are degenerate, now split into a singlet p_0 with $m=0$ and a doublet p_\pm with $m=\pm 1$.

In Si(Ge) as already stated there are six (four) equivalent positions in the Brillouin zone for which $E_\nu(\mathbf{k})$ is a minimum. We designate these by $\mathbf{k}_j (|\mathbf{k}_j| = k_0)$. For each of these positions we must solve equation (3.46), bearing in mind that, while the structure of the differential equation remains the same, the z direction is different for each minimum. Arising from these considerations the donor states exhibit a six-fold (four-fold) degeneracy for Si(Ge). In principle this degeneracy is removed by the crystal potential. As will be seen in the experimental section, the splitting turns out to be significant only for the ground state. This effect is called the 'chemical splitting' because it depends on the chemical nature of the impurity atom. The ground-state wavefunctions can be written as

$$\Phi_i(\mathbf{r}) = \sum_{j=1}^N \alpha_{ij} F_j(\mathbf{r}) \psi_{\nu k_j}(\mathbf{r}) \quad (3.47)$$

where $N=6$ or 4 , depending on whether we are considering Si or Ge. Irrespective of the nature of the correction to the impurity potential used in equation (3.46) it must conform to the T_d site symmetry of the impurity. It is thus necessary to characterise the energy states of the donor in terms of the irreducible representations of T_d . Kohn and Luttinger (1955) have given such a description for donors in silicon using a standard group theoretical technique. We give below a different procedure in which the Frobenius reciprocity theorem (Ramdas *et al* 1963) is used; this technique is particularly useful when perturbation effects are considered.

The envelope wavefunction $F_j(\mathbf{r})$ in equation (3.47) belongs to one of the irreducible representations of the axially symmetric group $D_{\infty h}$. The Bloch functions, $\psi_j(\mathbf{r})$, conform to the symmetry of the bottom of the conduction band, i.e. C_{4v} for silicon and D_{3d} for germanium (Koster 1957, Callaway 1958). However, the energy levels are classified according to T_d , the site symmetry of the impurity; hence, the appropriate symmetry of these conduction band minima is C_{2v} and C_{3v} for silicon and germanium, respectively. Thus, the symmetry group under which the product functions $F_j(\mathbf{r}) \psi_j(\mathbf{r})$ transform is

defined by the elements of symmetry common to $D_{\infty h}$ and $C_{2v}(C_{3v})$ for silicon (germanium). This common group is C_{2v} for silicon and C_{3v} for germanium. The irreducible representations of C_{2v} and C_{3v} according to which $\psi_j(\mathbf{r})$ transforms are totally symmetric since this is the case for the pure crystal. From a knowledge of the irreducible representations of C_{2v} or C_{3v} generated by $F_j(\mathbf{r}) \psi_j(\mathbf{r})$ the irreducible representations of T_d generated by $\Phi_i(\mathbf{r})$ can be constructed using Frobenius' theorem. The results of such an analysis for silicon and germanium are given in table 1.

Table 1. Irreducible representations[†] of s- and p-like states of group V donors in silicon and germanium.

Crystal	State	$\Gamma(O_3)$	$\Gamma(D_{\infty h})$	$\Gamma(H)$	$\Gamma(T_d)$
Si	s-like	D_0^+	Σ_g^+	A_1	$A_1 + E + T_2$
	p-like	D_1^-	$\Sigma_u^+(m=0)$ $\Pi_u(m=\pm 1)$	A_1 $B_1 + B_2$	$A_1 + E + T_2$ $2T_1 + 2T_2$
Ge	s-like	D_0^+	Σ_g^+	A_1	$A_1 + T_2$
	p-like	D_1^-	$\Sigma_u^+(m=0)$ $\Pi_u(m=\pm 1)$	A_1 E	$A_1 + T_2$ $E + T_1 + T_2$

[†] In this table, O_3 denotes the full three-dimensional orthogonal group; its representations are labelled using the notation of Elliot and Dawber (1979). For silicon and germanium H is C_{2v} and C_{3v} , respectively. The nomenclature of columns 4–6 is that of Wilson *et al* (1955).

From table 1 it can be seen that the N -fold degeneracy of the effective-mass states is, in principle, lifted. As mentioned above, this effect need be considered only for the s states. Thus, one expects for silicon a singlet $1s(A_1)$, a doublet $1s(E)$ and a triplet $1s(T_2)$, and a singlet $1s(A_1)$ and a triplet $1s(T_2)$ for germanium. Here we use the group theoretical notation used by Wilson *et al* (1955) with $T_1 \equiv F_1$ and $T_2 \equiv F_2$. (In the paper of Kohn and Luttinger (1955), T_1 and T_2 are interchanged.) The reduction of the N -dimensional representation generated by the states (3.47) for the $1s$ ground-state multiplet is accomplished for Si with the following coefficients:

$$\alpha_{A_{1,j}} = \frac{1}{\sqrt{6}} (1, 1, 1, 1, 1, 1) \quad (3.48)$$

$$\alpha_{E,j} = \begin{cases} \frac{1}{\sqrt{12}} (-1, -1, -1, -1, 2, 2) \\ \frac{1}{2} (1, 1, -1, -1, 0, 0) \end{cases} \quad (3.49)$$

$$\alpha_{T_{2,j}} = \begin{cases} \frac{1}{\sqrt{2}} (1, -1, 0, 0, 0, 0) \\ \frac{1}{\sqrt{2}} (0, 0, 1, -1, 0, 0) \\ \frac{1}{\sqrt{2}} (0, 0, 0, 0, 1, -1) \end{cases} \quad (3.50)$$

For Ge the corresponding reduction is achieved by

$$\alpha_{A_1,j} = \frac{1}{2} (1, 1, 1, 1) \quad (3.51)$$

$$\alpha_{T_2,j} = \begin{cases} \frac{1}{2} (1, 1, -1, -1) \\ \frac{1}{2} (1, -1, -1, 1) \\ \frac{1}{2} (1, -1, 1, -1). \end{cases} \quad (3.52)$$

From the nature of the linear combinations of the wavefunctions it is clear (Kohn 1957) that the 1s(A_1) state in both silicon and germanium has the largest amplitude at the donor site and hence should be most affected by species-dependent effects. The p-like states must, in principle, also split in a manner shown in table 1. However, such states give a small probability density near the nucleus of the donor, and consequently the splittings are too small to be observed experimentally, except for Mg^+ which we will discuss in the experimental section. The energy separations of the different components of the 1s manifold are called the 'valley-orbit' splittings.

In contrast to equation (3.42) the eigenvalue problem represented by equation (3.46) cannot be solved exactly and one must resort to the variational principle to obtain approximate eigenvalues and eigenfunctions. Such studies were carried out by Kittel and Mitchell (1954) and Kohn and Luttinger (1955). Kittel and Mitchell calculated the ground-state energy of donors in Si and Ge using a wavefunction of the form

$$\left(\frac{1}{\pi a^2 b} \right)^{1/2} \exp \left[- \left(\frac{x^2 + y^2}{a^2} + \frac{z^2}{b^2} \right)^{1/2} \right]$$

where a and b are variational parameters. Kohn and Luttinger, besides calculating the ground-state energy, computed the binding energies of the 2s, 2p₀, 2p_± and 3p₀ states. In their procedure equation (3.46) is written in the form

$$-\frac{\partial^2 F}{\partial x^2} - \frac{\partial^2 F}{\partial y^2} - \gamma \frac{\partial^2 F}{\partial z^2} - \frac{2}{r} F = (E - E(k_0)) F \quad (3.53)$$

where

$$\gamma = m_t/m_1$$

the units of energy and length being $(m_t e^4 / 2 \hbar^2 \kappa^2)$ and $(\hbar^2 \kappa / m_t e^2)$, respectively. Exact solutions can be found for $\gamma=1$ (scaled-down hydrogen atom) and for $\gamma=0$. The latter limit is similar to the adiabatic approximation in molecular physics. The exact eigenvalue for $\gamma=0$ is -4 in the units just defined. In addition, using the Feynman-Hellman theorem one shows that the binding energy is a monotonically decreasing function of γ going from 4 for $\gamma=0$ to 1 for $\gamma=1$. More recently, Faulkner (1969) has used the Ritz method to find the binding energies of a large number of donor states in Si and Ge. His results are compared with experiments in the following section.

We now turn our attention to the study of acceptor states. We note that in Si and Ge, the extremum of the valence band occurs at $k=0$ and that there is a degeneracy at this point, necessitating the use of degenerate perturbation theory. To second order in the components of the wavevector we must diagonalise the sub-matrix obtained from equation (3.34) between states which are degenerate at $k_0=0$. Let ν and ν' be any two such states. Then, the elements of the sub-matrix of the effective Hamiltonian K are

$$\langle \nu' \mathbf{k}' | K | \nu \mathbf{k} \rangle = \mathcal{D}_{\nu' \nu}(\mathbf{k}) \delta_{\mathbf{k} \mathbf{k}'} + U_i(\mathbf{k}' - \mathbf{k}) \delta_{\nu' \nu} \quad (3.54)$$

where

$$\mathcal{D}_{\nu'\nu}(\mathbf{k}) = \left(E(0) + \frac{\hbar^2 k^2}{2m} \right) \delta_{\nu\nu'} + \frac{\hbar}{m^2} \mathbf{k} \cdot \sum'_{\nu''} \frac{\mathbf{p}_{\nu'\nu''} \mathbf{p}_{\nu''\nu}}{\omega_{\nu\nu''}} \cdot \mathbf{k}. \quad (3.55)$$

We now notice that $\mathcal{D}_{\nu'\nu}(\mathbf{k})$ is identical to the Hamiltonian sub-matrix given in equation (3.11). The energy eigenvalue problem following the methods of degenerate perturbation theory requires the solution of the coupled integral equations

$$\sum_{\nu'} \mathcal{D}_{\nu'\nu}(\mathbf{k}) B_{\nu'}(\mathbf{k}) + \sum_{k'} U_1(\mathbf{k}' - \mathbf{k}) B_{\nu}(\mathbf{k}') = E B_{\nu}(\mathbf{k}) \quad (3.56)$$

in the subspace of states ν, ν' degenerate at $\mathbf{k}_0 = 0$. By a Fourier transformation similar to that used for the non-degenerate case, this is equivalent to finding the solutions of the coupled differential equations

$$\sum_{\nu'} \mathcal{D}_{\nu'\nu}(-i\nabla) F_{\nu'}(\mathbf{r}) + U_1(\mathbf{r}) F_{\nu}(\mathbf{r}) = E F_{\nu}(\mathbf{r}). \quad (3.57)$$

When spin-orbit interaction is included, equations (3.57) correspond to an eigenvalue problem associated with the 6×6 matrix operator

$$\mathcal{D}(\mathbf{k}) = \begin{bmatrix} Ak^2 - P & R & -S & 0 & -\frac{1}{\sqrt{2}}R & \sqrt{2}S \\ R^* & Ak^2 + P & 0 & -S & -\sqrt{2}P & \frac{\sqrt{3}}{\sqrt{2}}R \\ -S^* & 0 & Ak^2 + P & -R & \frac{\sqrt{3}}{\sqrt{2}}R^* & \sqrt{2}P \\ 0 & -S^* & -R^* & Ak^2 - P & -\sqrt{2}S^* - \frac{R^*}{\sqrt{2}} & \\ -\frac{1}{\sqrt{2}}R^* & -\sqrt{2}P & \frac{\sqrt{3}}{\sqrt{2}}R & -\sqrt{2}S & Ak^2 - \lambda & 0 \\ \sqrt{2}S^* & \frac{\sqrt{3}}{\sqrt{2}}R^* & \sqrt{2}P & -\frac{R}{\sqrt{2}} & 0 & Ak^2 - \lambda \end{bmatrix} \quad (3.58)$$

where

$$\begin{aligned} P &= \frac{1}{2}B(2k_z^2 - k_x^2 - k_y^2) \\ R &= -Dk_z(k_x - ik_y) \\ S &= \frac{1}{2}\sqrt{3}B(k_x^2 - k_y^2) - \frac{iD}{\sqrt{3}}k_xk_y \end{aligned} \quad (3.59)$$

and \mathbf{k} is replaced by $-i\nabla$. In the limit of large spin-orbit splitting, λ , we can decouple the 2×2 eigenvalue problem corresponding to $J = \frac{1}{2}$ from the 4×4 problem corresponding to $J = \frac{3}{2}$ by neglecting the off-diagonal terms connecting these multiplets in equation (3.58). We denote the states associated with $J = \frac{3}{2}$ by the symbol $p_{3/2}$ and those of $J = \frac{1}{2}$ by $p_{1/2}$. This model is expected to be more appropriate for germanium than for silicon, because λ is much larger than the binding energies of the acceptor states for germanium whereas they are comparable to λ in the case of silicon.

The impurity states can be characterised according to the symmetry deduced from the transformation properties of the products $\Psi_\nu(r) = F_\nu(r) \Psi_{\nu 0}(r)$ of equation (3.40). Both F_ν and $\psi_{\nu 0}$ form bases for the irreducible representations of \bar{O}_h . Hence the symmetry properties of the $\Psi_\nu(r)$ are obtained by forming the direct product of the irreducible representations of \bar{O}_h to which F_ν and $\psi_{\nu 0}$ belong. In the effective-mass theory, the envelope functions, F_ν , may be approximated by the s, p, d, . . ., hydrogen functions, which belong to the irreducible representations D_0^+ , D_1^- , D_2^+ , . . ., respectively, of the orthogonal group in three dimensions; under \bar{O}_h , these reduce to Γ_1^+ , Γ_4^- , $\Gamma_3^+ + \Gamma_5^+$, . . ., respectively. Hence, the symmetries of the $p_{3/2}$ impurity states are given by direct products of the irreducible representation of the envelope function and Γ_8^+ , the representation of Bloch states at the top of the valence band. They are $\Gamma_1^+ \times \Gamma_8^+$, $\Gamma_4^- \times \Gamma_8^+$, $(\Gamma_3^+ + \Gamma_5^+) \times \Gamma_8^+$, . . ., for the hydrogenic s, p, d, . . ., states, respectively. This classification scheme was given by Schechter (1962). However, the impurity potential is not in reality spherically symmetric, but must possess the symmetry of the impurity site, T_d . Thus, the acceptor wavefunctions must transform according to the operations of the double group \bar{T}_d . The reduction of the representations of \bar{O}_h to those of \bar{T}_d yield additional splittings due to the deviations of the impurity potential from e^2/kr . For example, the p-like hydrogenic states which, in the effective-mass theory yield states of symmetry $\Gamma_4^- \times \Gamma_8^+$, reduce to four levels of symmetry Γ_8 , Γ_8 , Γ_7 , Γ_6 as shown in table 2. Schechter (1962) and Kohn (1957) labelled the 2p states as $2p^{(1)}$, $2p^{(2)}$, $2p^{(3)}$ and $2p^{(4)}$, in order of increasing energy. A different and more comprehensive notation was introduced by Mendelson and James (1964).

Table 2. Symmetry of group III acceptor states associated with the $p_{3/2}$ and $p_{1/2}$ valence band edges of silicon and germanium.

Band	Hydrogenic state	Symmetry under O_3	Symmetry under \bar{O}_h	$\Gamma(F_j) \times \Gamma(\psi_j)$ ^a	Acceptor state ^b	Symmetry under \bar{T}_d
$p_{3/2}$	S	D_0^+	Γ_1^+	Γ_8^+	$S_{3/2}$ $P_{1/2}$	Γ_8
	P	D_1^-	Γ_4^-	$\Gamma_7^- + \Gamma_8^- + 2\Gamma_8^-$	$P_{3/2}$ $P_{5/2}$	Γ_6 Γ_8 $\Gamma_7 + \Gamma_8$
	S	D_0^+	Γ_1^+	Γ_7^+	$S_{1/2}$	Γ_7
	P	D_1^-	Γ_4^-	$\Gamma_7^- + \Gamma_8^-$	$P_{1/2}$ $P_{3/2}$	Γ_6 Γ_8

^a The symmetries of the Bloch functions, ψ_j , under \bar{O}_h are $\Gamma_8^+(p_{3/2})$ and $\Gamma_7^+(p_{1/2})$.

^b S, P, . . ., refer to the hydrogenic state and sub-index to the quantum number F defined by equation (3.71).

A new approach to the classification of the acceptor states, introduced by Baldereschi and Lipari (1973), has the additional advantage of providing a convenient algorithm for numerical calculation of the energies. Their procedure consists in rewriting equations (3.57) by separating the contributions having spherical symmetry from those having only cubic symmetry. This programme is carried out introducing the tensors

$$k_{ij} = 3k_i k_j - \delta_{ij} k^2 \quad (3.60)$$

and

$$J_{ij} = 3\{J_i J_j\} - \delta_{ij} J^2. \quad (3.61)$$

The Hamiltonian matrix (3.16) is most conveniently expressed in the form

$$\mathcal{D}_{3/2}(\mathbf{k}) = A k^2 - \frac{1}{9} \sum_{ij} \left[\frac{D}{\sqrt{3}} + \left(B - \frac{D}{\sqrt{3}} \right) \delta_{ij} \right] k_{ij} J_{ij}. \quad (3.62)$$

The second-rank tensors (3.60) and (3.61) can be written in terms of their irreducible components, i.e. components that transform under the operations of the rotation group as the spherical harmonics with $l=0, 1, 2$. We note that these tensors are symmetric and have a zero trace; thus the only non-vanishing components are those corresponding to $l=2$. We denote them by the symbols $k_\kappa^{(2)}$ and $J_\kappa^{(2)}$ ($\kappa=0, \pm 1, \pm 2$). The only combination of products of components of these tensors which remain invariant under rotations is the scalar product

$$\mathbf{k}^{(2)} \cdot \mathbf{J}^{(2)} = \sum_{\kappa} (-1)^\kappa k_\kappa^{(2)} J_{-\kappa}^{(2)}. \quad (3.63)$$

The remaining contributions to $\mathcal{D}_{3/2}$ can be expressed in terms of the products

$$[\mathbf{k}^{(2)} \times \mathbf{J}^{(2)}]_{\kappa}^{(k)} = (-1)^\kappa (2k+1)^{1/2} \sum_{\kappa_1 \kappa_2} \begin{pmatrix} 2 & 2 & k \\ \kappa_1 & \kappa_2 - \kappa & \end{pmatrix} k_{\kappa_1}^{(2)} J_{\kappa_2}^{(2)} \quad (3.64)$$

where the symbol in parenthesis on the right-hand side is the familiar $3j$ symbol of the theory of angular momentum operators (Messiah 1966). With this notation we write

$$\begin{aligned} \mathcal{D}_{3/2}(\mathbf{k}) = A(k^2 - (\mu/9)) \mathbf{k}^{(2)} \cdot \mathbf{J}^{(2)} + \frac{1}{9} \delta \{ & [\mathbf{k}^{(2)} \times \mathbf{J}^{(2)}]_4^{(4)} + (14/5)^{1/2} [\mathbf{k}^{(2)} \times \mathbf{J}^{(2)}]_0^{(4)} \\ & + [\mathbf{k}^{(2)} \times \mathbf{J}^{(2)}]_{-4}^{(4)} \} \end{aligned} \quad (3.65)$$

where

$$\mu = \frac{2B + D\sqrt{3}}{5A} \quad (3.66)$$

and

$$\delta = \frac{D - B\sqrt{3}}{2A\sqrt{3}}. \quad (3.67)$$

The quantities A, B, D, μ and δ are given in table 3 for a number of semiconductors. We notice that, except for silicon, $\delta \ll \mu$; this justifies setting $\delta=0$ as a satisfactory initial approximation and is referred to as the spherical approximation. The shape of the electron energy bands in the spherical approximation is

$$E_{\pm} = A(1 \pm \mu) k^2. \quad (3.68)$$

The acceptor states, neglecting δ , are obtained by solving

$$\left[A \left(k^2 - \frac{\mu}{9} \mathbf{k}^{(2)} \cdot \mathbf{J}^{(2)} \right) + \frac{e^2}{\kappa r} \right] F_\nu = E F_\nu \quad (3.69)$$

in which \mathbf{k} is replaced by the operator $-i\nabla$. Equation (3.69) can be rewritten as

$$\left(A \{ k^2 - \mu[(\mathbf{k} \cdot \mathbf{J})^2 - \frac{1}{3} k^2 J^2] \} + \frac{e^2}{\kappa r} \right) F_\nu = E F_\nu \quad (3.70)$$

and is identical to that of the H atom if $\mu=0$ except that, since $A<0$, the bound states have positive energies. Now, the term $(\mu/9)\mathbf{k}^{(2)} \cdot \mathbf{J}^{(2)}$ introduces a coupling of the states with angular momentum \mathbf{L} with an ‘angular momentum’ \mathbf{J} with $J=\frac{3}{2}$. A total angular momentum \mathbf{F} is defined by

$$\mathbf{F} = \mathbf{L} + \mathbf{J}. \quad (3.71)$$

Table 3. Values of the static dielectric constant ϵ_0 and of the valence band parameters γ_1 , γ_2 and γ_3 used by Baldereschi and Lipari (1973). The valence band parameters μ and δ are also given together with the energy and length units R_0 and a_0 . $\gamma_1 = -2m A/\hbar^2$, $\gamma_2 = -mB/\hbar^2$, $\gamma_3 = -mD/\sqrt{3}\hbar^2$.

	ϵ_0	γ_1^a	γ_2^a	γ_3^a	μ	δ	R_0 (meV)	a_0 (Å)
Si	11.40 ^b	4.22	0.39	1.44	0.483	0.249	24.8	25.5
Ge	15.36 ^b	13.35	4.25	5.69	0.766	0.108	4.3	108.5
AlSb	12.0 ^e	4.15	1.01	1.75	0.701	0.178	22.8	26.4
GaP	10.75 ^d	4.20	0.98	1.66	0.661	0.162	28.0	23.9
GaAs	12.56 ^e	7.65	2.41	3.28	0.767	0.114	11.3	50.8
GaSb	15.7 ^c	11.80	4.03	5.26	0.808	0.104	4.7	98.0
InP	12.4 ^f	6.28	2.08	2.76	0.792	0.108	14.1	41.2
InAs	14.6 ^g	19.67	8.37	9.29	0.907	0.047	3.2	152.0
InSb	17.9 ^c	35.08	15.64	16.91	0.935	0.036	1.2	332.3
ZnS	8.1 ^h	2.54	0.75	1.09	0.751	0.134	81.6	10.9
ZnSe	9.1 ^h	3.77	1.24	1.67	0.795	0.114	43.6	18.2
ZnTe	10.1 ^h	3.74	1.07	1.64	0.755	0.152	35.7	20.0
CdTe	9.7 ^h	5.29	1.89	2.46	0.844	0.108	27.3	27.2

^a Valence band parameters are given by Lawaetz (1971).

^b Faulkner (1969).

^c Hass and Henvis (1962).

^d Patrick and Dean (1969).

^e Stillman *et al* (1971).

^f Hilsum *et al* (1969).

^g Lorimor and Spitzer (1965).

^h Berlincourt *et al* (1963).

F^2 and F_z are constants of the motion within the spherical approximation. Using the rules for the composition of angular momenta we classify the energy levels according to the quantum number F . For example, for $L=0$ (S states) we have $F=\frac{0}{2}$, whereas for $L=1$ (P states) F can take the values $\frac{1}{2}, \frac{2}{2}, \frac{3}{2}$. The solutions of equation (3.69) reduce to those of two coupled differential equations involving radial wavefunctions since the term $\mathbf{k}^{(2)} \cdot \mathbf{J}^{(2)}$ mixes only states for which $\Delta L=0, \pm 2$.

The acceptor levels associated with the $p_{1/2}$ valence band are obtained in the ' $\lambda=\infty$ ' approximation using equation (3.17). They are the 'hydrogenic' levels given by

$$E_n = -\lambda - \frac{e^4}{4A\kappa^2 n^2} = -\lambda + \frac{e^4}{4|A|\kappa^2 n^2} \quad (3.72)$$

where $n=1, 2, 3, \dots$. Corrections to E_n in equation (3.71) arise from the coupling of the $p_{3/2}$ and the $p_{1/2}$ valence bands to the extent λ is finite and the matrix elements of $\mathcal{D}(\mathbf{k})$ connecting these multiplets in equation (3.58) are not neglected. Such corrections have been studied by Zwerdling *et al* (1960b).

To summarise, we classify the energy levels of a shallow acceptor specifying the principal hydrogenic quantum number n , L and F . Thus the states with $L=0$ are denoted by $nS_{3/2}$ where the sub-index denotes F . The states with $L=1$ are $nP_{1/2}$, $nP_{3/2}$, $nP_{5/2}$. This classification scheme is exhibited in the sixth column in table 2 for the $p_{3/2}$ and $p_{1/2}$ states arising from the S and P hydrogenic levels. In view of the term $(\mathbf{k} \cdot \mathbf{J})^2$ in equation (3.70), L is not a good quantum number; thus the states $nS_{3/2}$, $nP_{3/2}$, $nP_{5/2}$, \dots , are admixtures consistent with $\Delta L=0, \pm 2$. The states $nP_{1/2}$ have, however, P character and eigenvalues given by $[e^4/4|A|\kappa^2(1+\mu)n^2]$.

The above discussion explicitly deals with the case in which the spin-orbit coupling λ is large compared to the binding energies of the acceptor. If λ is negligible, we use

$\mathcal{D}(\mathbf{k})$ given by equation (3.11) and a similar classification is possible with

$$\mathbf{F} = \mathbf{L} + \mathbf{I} \quad (3.73)$$

where $I=1$.

Baldereschi and Lipari (1974) consider the cubic terms in equation (3.65) as perturbations to the Hamiltonian of equation (3.69). They notice that the S states are not affected by this perturbation and of the P states, those classified as $P_{5/2}$ split into states of symmetry Γ_7^- and Γ_8^- . In two subsequent papers, Lipari and Baldereschi (1978) and Baldereschi and Lipari (1976) have extended this work to include the effect of the split-off band (λ finite) and a more accurate dielectric screening. Their calculations will be compared with experimental results in the next section.

4. Experimental results in the absence of external fields

4.1. Group V donors in silicon (Si) and germanium (Ge)

Figure 6 shows the excitation spectrum of phosphorus donors introduced by neutron transmutation of ^{30}Si in a pure Si sample exposed to a thermal neutron flux of 2.5×10^{13} neutrons $\text{cm}^{-2} \text{s}^{-1}$ for 7.8 h, yielding a phosphorus concentration of $\sim 1.2 \times 10^{14} \text{ cm}^{-3}$. The sample was annealed at 800°C to remove the damage caused by the irradiation. A Fourier transform spectrometer was used and measurements were made with the sample cooled to liquid helium temperature (Jagannath *et al* 1979, 1981). A series of sharp excitation lines is observed in the range 32–45 meV. The occurrence of the spectrum clearly demonstrates the existence of the bound states expected on the basis of equation (3.46); they are due to electric dipole transitions from the 1s ground state to

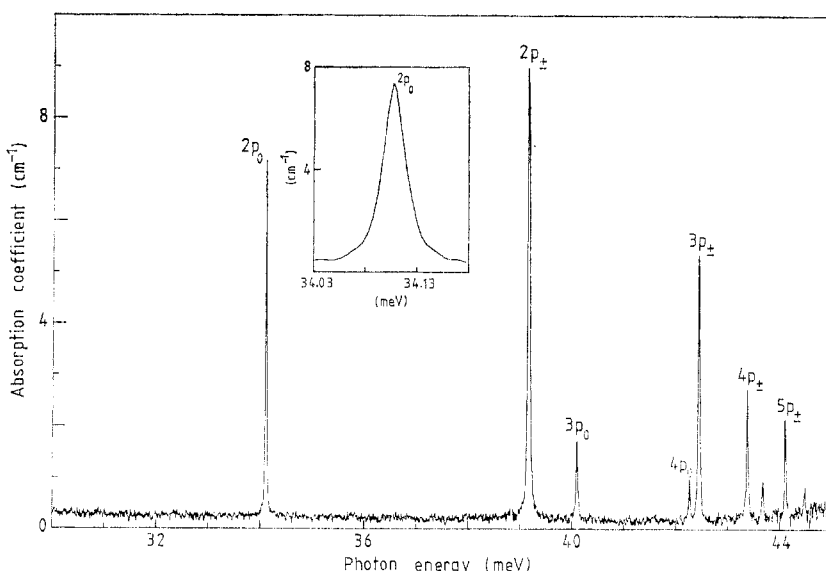


Figure 6. Excitation spectrum of phosphorus donors in neutron-transmutation-doped silicon. Liquid helium is used as a coolant. Phosphorus donor concentration, $n \sim 1.2 \times 10^{14} \text{ cm}^{-3}$. The instrumental resolution with and without apodisation is 0.09 and 0.06 cm^{-1} , respectively. The $2p_0$ line with an expanded horizontal scale is shown in the inset. The $2p_{\pm}$ line has been truncated because, with the thickness of the sample used, the transmission approaches zero at the peak (from Jagannath *et al* 1981).

the excited p states, i.e. they are the Lyman transitions $1s \rightarrow np$, $n=2, 3, 4, \dots$. Since equation (3.46) rather than equation (3.42) is applicable to the case of Si and Ge, a consequence of the effective-mass tensor characterising the conduction band minimum, the transitions show an inherent splitting due to np_0 not being degenerate with np_{\pm} . The labelling of the lines denotes the final state of the transition involved and the assignment is based on a comparison of the experimentally observed spacing of the lines with those deduced from the binding energies of the p states calculated by Faulkner (1969) using the Ritz method to solve equation (3.46) (see table 4). It should be pointed out here that Faulkner's calculations yield an ionisation energy for a group V donor in Si of 31.27 meV whereas even the lowest energy excitation line of Si(P) occurs at 34.11 meV. In this context it is useful to compare the excitation spectrum of Si(P) with that of another group V impurity in Si. Figure 7 shows such a spectrum for Si(As) (Jagannath *et al* 1981). We notice a striking similarity between the excitation spectra of Si(P) and Si(As); the relative intensities of the lines are very similar and their spacings are identical within experimental errors. In table 4 the binding energies of the states are deduced from the experimentally observed transition energies; they are computed assuming that the theory accurately gives the binding energy of the $3p_{\pm}$ state as 3.12 meV. It is clear that the theory is remarkably successful in accounting for the spacings of the excitation lines. We ascribe this to the validity of the screened Coulomb potential in equation (1.1) for the calculation of p states. As expected on the basis of the theoretical considerations outlined in the previous section, the binding energies of the p states ought to be independent of the chemical nature of the donor. In contrast, the shift of the entire spectrum of a given donor from that of another must arise from the chemical-species-dependent binding energy of one or more components of the 1s multiplet.

As was pointed out in the previous section, the 1s multiplet of a group V donor in Si resolves into a singlet $1s(A_1)$, a doublet $1s(E)$ and a triplet $1s(T_2)$ component consistent with the T_d site symmetry of the donor. From equations (3.48)–(3.50) it is clear that the $1s(A_1)$ wavefunction has a large concentration at the donor site, in contrast to the $1s(E)$ and $1s(T_2)$ wavefunctions. Electron paramagnetic resonance experiments by Fletcher *et al* (1954a, b) and Feher (1959a, b) show that the hyperfine interaction of the donor

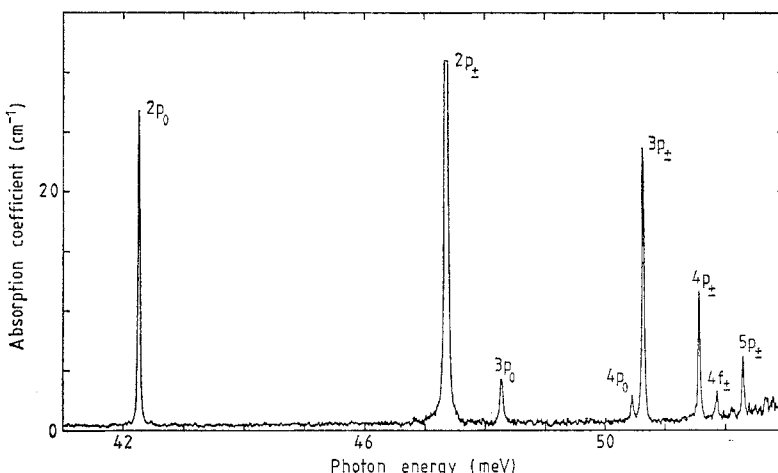


Figure 7. Excitation spectrum of arsenic donors in silicon. Liquid helium used as a coolant. Instrumental resolution 0.06 cm^{-1} . Room-temperature resistivity of the sample $\sim 6 \Omega \text{ cm}$ ($n \sim 7 \times 10^{14} \text{ cm}^{-3}$). The $2p_{\pm}$ line is truncated (after Jagannath *et al* 1981).

Table 4. Binding energies of the energy levels of donors in silicon (meV).

Level	P^a	A^s	Sb^b	Bi^c	Li^d	$Li-O^e$	Mg^{+d}	S^e	Theory ^f
1s(A ₁)	45.59	53.76	42.74	70.98	31.24	39.67	256.47	107.50	186.42
1s(E)	32.58 ^{b,g,h}	31.26 ^{b,g,h}	30.47 ^{b,h}						31.27
1s(E+T ₂)									
1s(T ₂)	33.89	32.67 ^b	{32.89 32.91}	32.89 ⁱ 31.89 ^j	33.02	32.00			
2p ₀	11.48	11.50	11.51	11.44	11.51	11.57	47.84	11.70	11.4
2s		9.11 ^k		8.78 ^k					11.51 8.83
2p _±	6.40	6.40	6.38	6.37	6.40	6.40	{26.25 26.05}	6.38	6.2
3p ₀	5.47	5.49	5.50 ^j	5.48	5.49	5.51	22.60	5.55	5.5
3s	{3.83 ^j 3.73 }			4.70					5.48 4.75
3d ₀		3.88 ^k		3.80					3.75
4p ₀	3.31	3.31	3.33 ^j	3.30	3.32	3.33	13.47	3.33	3.33
3p _±	3.12	3.12	3.12	3.12	3.12	3.12	12.48	3.12	3.12
4s				2.89					2.85
4f ₀	2.33			2.36					2.33
4p _z , 5p ₀	2.19	2.19	2.20	2.18	2.20	2.20	8.55	2.17	2.19, 2.23
4f _±	1.90	1.90	1.94 ^j	1.91	1.90	1.90			1.89
5f ₀	1.65		1.71 ^j	1.67	1.64	1.66			1.62
5p _±	1.46	1.46	1.48 ^j	1.46	1.47	1.47			1.44
5f _±	1.26				1.25	1.29			1.27
6p _±	1.09	1.07 ^b	1.10 ^j	1.08	1.07	1.09			1.04

^a Jagannath *et al.* (1981). The binding energies given for Li-O are for the A series; the binding energy for 1s(E+T₂) for that series is from Aggarwal *et al.* (1965).

^b Aggarwal and Ramdas (1965b, c).

^c Butler *et al.* (1975).

^d Ho and Ramdas (1972). The binding energies for the excited states of Mg⁺ have to be divided by four in order to compare them with theory.

^e Krag and Zeiger (1962).

^f Faulkner (1969).

^g Wright and Mooradian (1967).

^h Jain *et al.* (1976).

ⁱ Krag *et al.* (1970).

^j Pajot *et al.* (1979).

^k Kleiner and Krag (1970).

nucleus with the electron is consistent with a $1s(A_1)$ wavefunction for the latter. Theoretical considerations also suggest that the $1s(E)$ and $1s(T_2)$ levels have binding energies close to those calculated for the $1s$ level in the effective-mass approximation. Figure 8 shows the energy level scheme based on these considerations. The shift of the $1s(A_1)$ level *below* the theoretical value represents the failure of the screened Coulomb potential to account for its binding energy entirely; this depression can be expected to differ for the different group V impurities. At liquid helium temperatures one thus observes the $1s(A_1) \rightarrow np_0, np_{\pm}$ series. The decomposition of the $1s$ multiplet into its components is referred to in the literature as 'valley-orbit' or 'chemical' splitting.

In figure 9 we show the Lyman spectrum of Ge(As) recorded by Reuszer and Fisher (1965). The experimental binding energies of the donor states deduced from the positions of the excitation lines in the Lyman spectra of Ge(As), Ge(P), Ge(Bi) and Ge(Sb) are

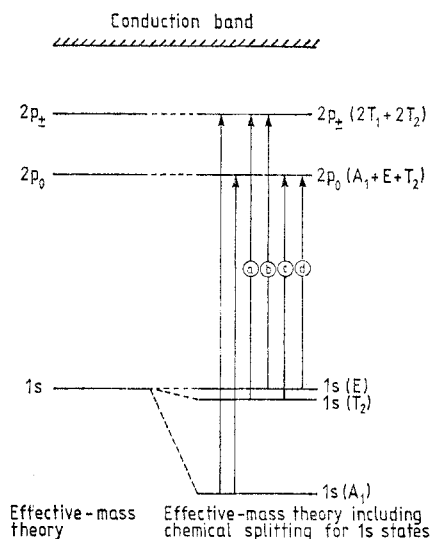


Figure 8. Energy level scheme (not to scale) of group V impurities in silicon for transitions from the $1s$ states to the $2p_0, 2p_{\pm}$ states. The letters next to a level indicate the irreducible representations of T_d ; the energy separation between $1s(E)$ and $1s(A_1)$ is usually designated by $6\Delta_c$.

given in table 5 and compared with those predicted by Faulkner (1969). Once again one notices the remarkable success of the theory in predicting the binding energies of the p states. As in Si, the spectra of the various group V donors in Ge, though identical in spacing, are shifted from one another. The ground-state $1s$ multiplet resolves into a singlet $1s(A_1)$ and a triplet $1s(T_2)$, with $1s(A_1)$ depressed below the $1s(T_2)$ which is expected to lie close to the theoretically calculated position. Figure 10 shows schematically the energy levels for donors in Ge. The excitation lines in figure 9 are then due to the $1s(A_1) \rightarrow np_0, np_{\pm}$ transitions.

Fisher (1962) and Reuszer and Fisher (1964) gave a convincing demonstration of the splitting of the $1s(A_1 + T_2)$ into $1s(A_1)$ and $1s(T_2)$ in the case of donors in Ge. By thermally populating the $1s(T_2)$ level, they observed the $1s(T_2) \rightarrow np_0, np_{\pm}$ transitions as can be seen in figure 11. Aggarwal (1964) and Aggarwal and Ramdas (1965b) reported the $1s(E), 1s(T_2) \rightarrow np_0, np_{\pm}$ transitions for donors in Si by thermally populating the $1s(E)$ and $1s(T_2)$ levels; figure 12 shows their results for Si(P). These measurements revealed

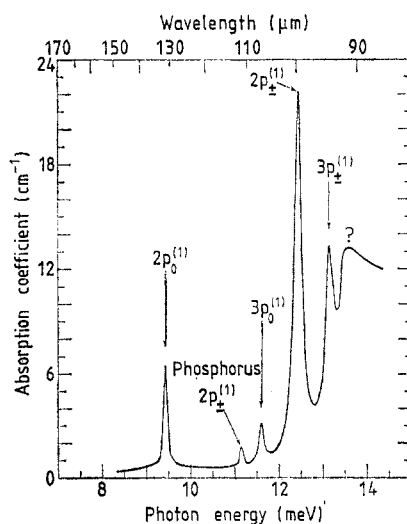


Figure 9. The excitation spectrum of Ge(As) at ~ 7 K. $n(\text{As}) \approx 1.2 \times 10^{15} \text{ cm}^{-3}$. Ge(As)–326 A (no 4) (after Reuszer and Fisher 1965).

even the small energy separation between the $1s(E)$ and $1s(T_2)$ levels and showed that the $1s(E)$ lies above the $1s(T_2)$ level as shown in figure 8.

Tables 4 and 5 give the ionisation energies of donors in Si and Ge as well as the binding energies of the $1s(E)$ and $1s(T_2)$ levels in Si and that of the $1s(T_2)$ level in Ge. The binding energies of the $2s$, $3s$, $3d_0$ and $4s$ states of donors in Si have been deduced experimentally from the transitions originating from the $1s(A_1)$ ground state and terminating at these states (Kleiner and Krag 1970). These photoexcitations, though allowed by general symmetry considerations as dipole transitions, are forbidden in the effective-mass approximation; a breakdown of the effective-mass approximation is invoked to account

Table 5. Binding energies of the energy levels of donors in germanium (meV).

Level	P ^b	As ^a	Sb ^b	Bi ^a	Li ^b	Theory ^c
$1s(A_1)$	12.88, 12.87 ^a	14.18	10.45, 10.32 ^a	12.75	8.1 ^d	9.81
$1s(T_2)$	10.06 ^a	9.94 ^a	9.99 ^a	9.90 ^a	10	9.81
$2p_0$	4.72 ^a	4.74	4.74 ^a	4.75		4.74
$3p_0$	2.54 ^a	2.57	2.57 ^a	2.55		2.56
$2p_{\pm}$	1.72	1.74	1.71	1.67	1.72	1.73
$4p_0$						1.67
$3p_{\pm}$	1.03		1.03	1.03	1.03	1.03
$5p_0$						0.84
$4p_{\pm}$	0.75		0.75		0.74	0.73
$4f_{\pm}$	0.62		0.59			0.61
$5p_{\pm}$	0.47		0.46			0.53
$5f_{\pm}$	0.39		0.39			0.41
$6p_{\pm}$	0.32		0.32			0.38
$6f_{\pm}$			0.30			0.32

^a Reuszer and Fisher (1964).

^b Seccombe and Korn (1972).

^c Faulkner (1969).

^d Buzdin *et al* (1973).

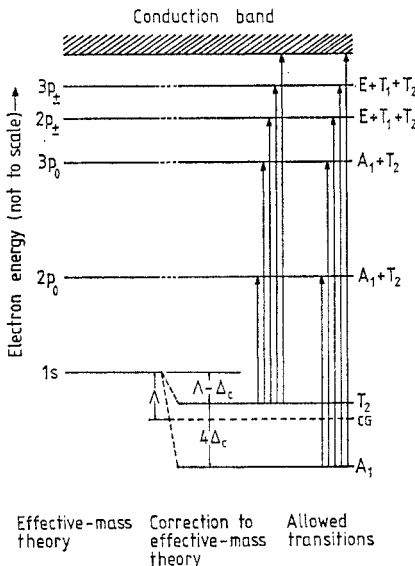


Figure 10. The energy level scheme (not to scale) of a group V impurity in germanium showing the $1s(A_1)$ and $1s(T_2)$ ground states and the p states. The energy separation between $1s(T_2)$ and $1s(A_1)$ is usually designated by $4\Delta_c$.

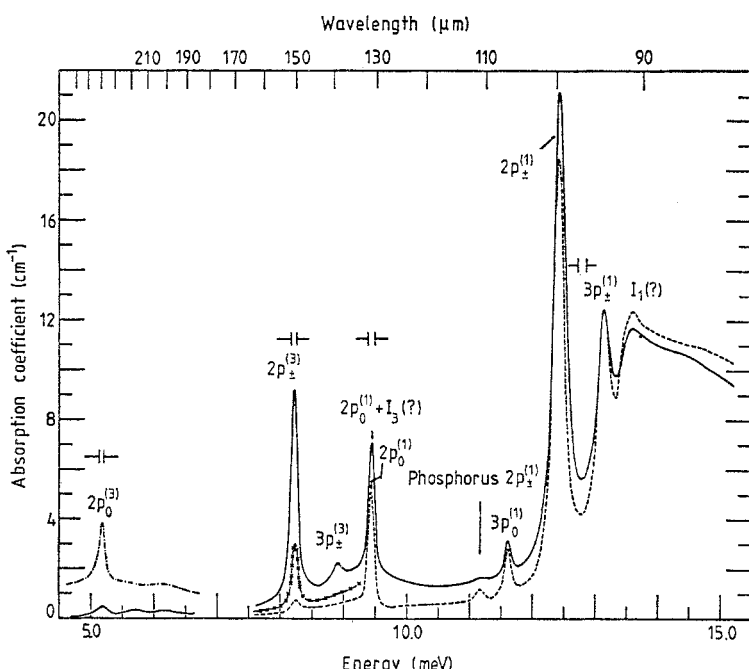


Figure 11. The excitation spectrum of Ge(As) for different sample temperatures: —, ~ 20 K; —, ~ 12 K; —×—, ~ 11 K; ---, ~ 8 K. $n \approx 1 \times 10^{15} cm^{-3}$. The superscripts (1) and (3) refer to the $1s(A_1)$ singlet and $1s(T_2)$ triplet ground states from which the transitions originated. Ge(As)-127B no 2 (after Reuszer and Fisher 1964).

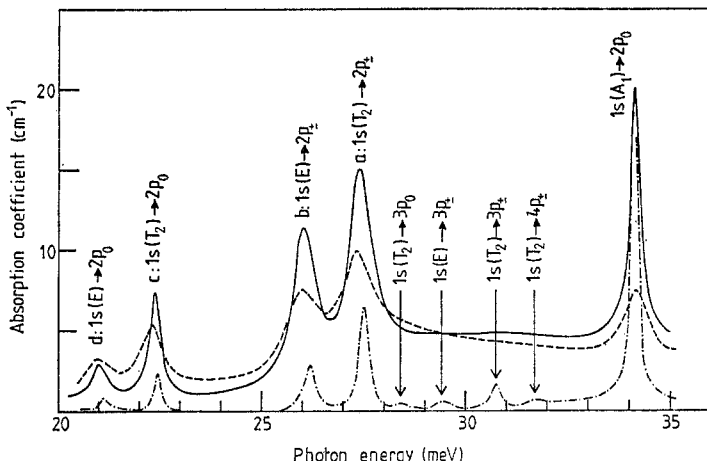


Figure 12. Excitation spectrum of Si(P) at different temperatures (---, ~ 80 K; —, ~ 59 K; -·-, ~ 30 K), showing transitions originating from the $1s(A_1)$ singlet, $1s(E)$ doublet and $1s(T_2)$ triplet ground states. $n \approx 5.2 \times 10^{15} \text{ cm}^{-3}$ (after Aggarwal and Ramdas 1965b).

for the observation of these weak transitions. Krag *et al* (1970) reported the $1s(A_1) \rightarrow 1s(T_2)$ transition in Si(Bi); they observed a doublet structure in this line and ascribed it to a spin-orbit splitting of the $1s(T_2)$ level. Buzdin *et al* (1973) have reported the $1s(A_1) \rightarrow 1s(T_2)$ transitions for Ge(P), Ge(As) and Ge(Li); their values of 2.8 and 4.2 meV for the transition in P and As compare very well with those deduced by Reuszer and Fisher (1964) for the $1s(T_2)$ - $1s(A_1)$ separation. Gershenson *et al* (1973, 1977) have investigated the submillimetre spectra of donors in Ge using backward-wave tubes; in the course of this study they have observed transitions like $3d_0 \rightarrow 4p_{\pm}$, $3s \rightarrow 4p_{\pm}$, $2s \rightarrow 2p_{\pm}$, $2p_0 \rightarrow 2p_{\pm}$, . . . , in Ge(Sb), Ge(P) and Ge(As). Similar work has been carried out by Nisida and Muro (1975).

The electronic Raman effect associated with donors in Si has been observed by Wright and Mooradian (1967). They reported the $1s(A_1) \rightarrow 1s(E)$ transition for Si(P) at 13.1 meV shown in figure 13. This is in excellent agreement with the $1s(A_1)$ - $1s(E)$ separation determined by Aggarwal and Ramdas (1965b). Though both the $1s(A_1) \rightarrow 1s(E)$ and the $1s(A_1) \rightarrow 1s(T_2)$ transitions are Raman-active, Wright and Mooradian showed, using effective-mass wavefunctions, that the $1s(A_1) \rightarrow 1s(T_2)$ transition vanishes in the Raman

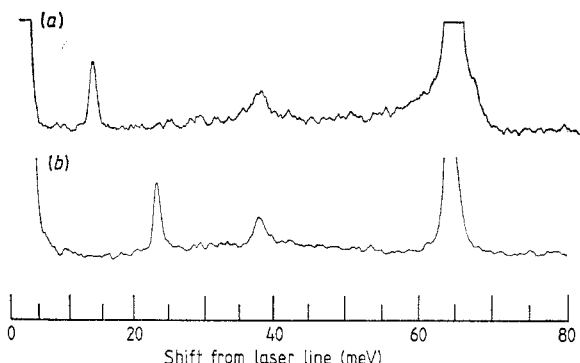


Figure 13. Electronic Raman spectra of impurities in silicon at 4.2 K. (a) Phosphorus donors, $n = 1.6 \times 10^{16} \text{ cm}^{-3}$, (b) boron acceptors, $p = 1.2 \times 10^{16} \text{ cm}^{-3}$ (after Wright and Mooradian 1967).

effect. The 22.32 meV line observed by Jain *et al* (1976) in the Raman spectrum of Si(As) is consistent with its being a $1s(A_1) \rightarrow 1s(E)$ transition.

Wood *et al* (1977) and Aggarwal *et al* (1980) have studied the third-order non-linear optical susceptibility, $\chi^{(3)}$, of Ge(P) and Ge(As). They investigated the generation of a combination frequency $2\omega_2 - \omega_1$ induced by $\chi^{(3)}$ when two separately tunable CO₂ lasers with frequencies ω_1 and ω_2 ($\omega_1 > \omega_2$) illuminate the n-type Ge. A sharp resonance is observed for $\omega_1 - \omega_2 = 4\Delta_c$, the valley-orbit splitting of the ground state of the donor. In figure 14 we show their results for the two donors they studied. Their values of 4.17 and 2.8 meV for As and P, respectively, are in excellent agreement with the measurements of Reuszer and Fisher (1964) obtained from the $1s(A_1) \rightarrow np$ and $1s(T_2) \rightarrow np$ Lyman

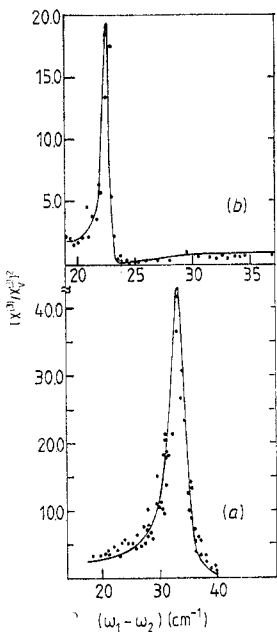


Figure 14. The third-order non-linear optical susceptibility, $\chi^{(3)}$, of Ge(P) (b) and Ge(As) (a) deduced from the power P generated at $2\omega_2 - \omega_1$; $\chi_v^{(3)}$ is the contribution due to the valence electrons and the total $\chi^{(3)}$ is the sum of $\chi_v^{(3)}$ and $\chi_D^{(3)}$, the contribution due to donors. $\chi_D^{(3)}$ shows a resonance for $\omega_1 - \omega_2 = 4\Delta_c$, the valley-orbit splitting of the ground state of the donor (after Wood *et al* 1977).

series. The above experiment exploits the resonance in the third-order susceptibility of the group V donors corresponding to the $1s(A_1) \rightarrow 1s(T_2)$ transition. Doehler *et al* (1974, 1975) have reported an electronic Raman line corresponding to this transition in Ge(As). Indeed the same selection rules govern the cross section in the Raman scattering and the resonance in $\chi^{(3)}$.

The theories of the origin of the valley-orbit splitting are beyond the scope of this review. We refer the reader to the book by Bassani and Pastori Parravicini (1975) and the review article by Pantelides (1978).

An extraordinarily sensitive technique for the study of the excitation spectra of impurities in semiconductors has been developed by Lifshits and Nad (1965) and reviewed by Kogan and Lifshits (1977). In this technique the photoconductivity of the doped semiconductor is measured as a function of photon energy ($\hbar\omega$); for $\hbar\omega \geq E_I$, the neutral

impurity is ionised by the photon and the appearance of free carriers results in increased conductivity—this is the usual photoconductivity. At absolute zero temperature, photons with $\hbar\omega < E_1$ will not produce photoconductivity even if, for some photon energies, optical transitions to an excited state can occur, e.g. for $\hbar\omega$ corresponding to the $1s(A_1) \rightarrow np$ transition in a donor. At finite temperatures, however, such an excitation can be followed by a thermal ionisation of the impurity, the additional energy for the ionisation being supplied by phonons in the appropriate energy range. As a result of such a two-step process, a photoconductive peak is recorded. The entire photoexcitation spectrum is thus recorded as peaks in the photoconductivity spectrum, the sample under investigation itself serving the role of the detector in the spectrometer. Such a spectrum is referred to as the photothermal ionisation spectrum. It is clear that at a given temperature the states with lesser binding energies will be more easily ionised and hence optical transitions to such states will be favoured in this technique. Figure 15 shows the photoconductivity

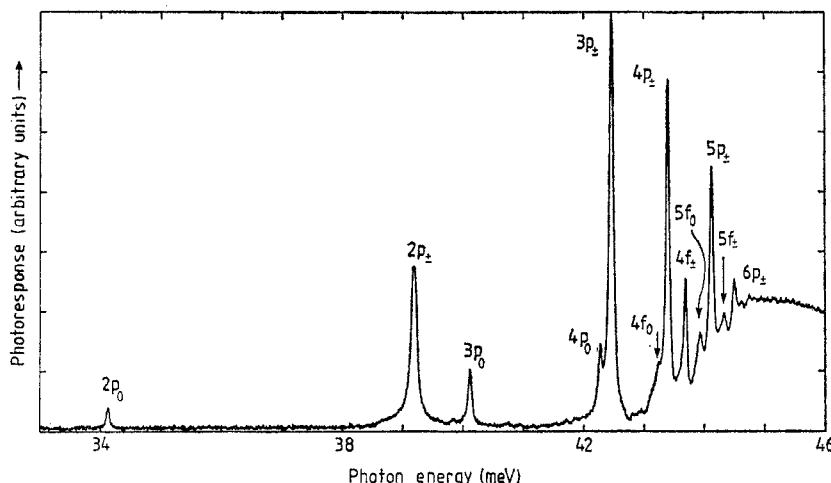


Figure 15. Photothermal ionisation spectrum of phosphorus donors in silicon. Phosphorus donor concentration is estimated to be $\sim 2 \times 10^{14} \text{ cm}^{-3}$. Instrumental resolution $\sim 0.06 \text{ cm}^{-1}$ without apodisation (after Jagannath *et al* 1981).

of Si(P) recorded by Jagannath *et al* (1981) in the spectral range where the excitation lines of phosphorus donors occur. A comparison of figures 6 and 15 clearly demonstrates how the intensities of the peaks in the photothermal ionisation spectrum reflect the product of the transition probability for the transition to the excited state and the factor controlling the thermal ionisation from the excited state to the conduction band; many of the optical transitions close to the conduction band thus appear prominently in figure 15. The photothermal ionisation technique has been exploited by Seccombe and Korn (1972) for a number of donors in Ge. One of the remarkable aspects of the photothermal ionisation technique is its extraordinary sensitivity—impurity concentrations as small as 10^8 cm^{-3} can be detected with it!

4.2. Other donors in Si and Ge

It is expected that the substitutional group VI impurities like S, Se and Te should behave as double donors in Si and Ge. From considerations of chemical bonds with the nearest-neighbour host atoms it is easy to see that the two electrons not needed in the bonding

scheme are bound to the doubly charged positive impurity centre, resulting in a solid-state analogue of the neutral helium atom. Krag and Zeiger (1962) reported the excitation spectra of both neutral and singly ionised sulphur centres in Si. In a further publication, Krag *et al* (1966) identified four different sulphur centres, two neutral and two singly ionised. The ground states in all cases are $1s(A_1)$. For some of the centres they observed the $1s(A_1) \rightarrow 1s(T_2)$ transitions. The binding energies and ionisation energy for one of them are given in table 4. Swartz *et al* (1980) have recently reported the excitation spectrum of Si(Se) and Si(Se⁺) with results similar to those for Si(S).

When an impurity is in an interstitial rather than a substitutional position, it may behave as a donor rather than as an acceptor. Interstitial aluminium has been reported in electron-irradiated aluminium-doped silicon where interstitial silicon and substitutional aluminium are believed to exchange their roles (Watkins 1965); it has been shown that these interstitial aluminium impurities are then donors. The group II element magnesium, when diffused into silicon, behaves like a double donor rather than a double acceptor (Franks and Robertson 1967, Ho and Ramdas 1970, 1972). This behaviour can be understood only if magnesium is interstitial rather than substitutional. The donor electrons are the two 3s electrons of magnesium. The excitation spectrum of Si(Mg⁰) recorded by Ho and Ramdas is shown in figure 16. When one of the two donor electrons is excited, the screening of the nuclear charge by the remaining electron and the other core electrons should result in group V donor-like excitation states. The remarkable similarity of the spacings between the excited states of Mg⁰ and those of the group V donors is thus explained. If Mg⁰ is introduced into Si-containing acceptors like B, one of the two donor electrons may be captured by the acceptor, leaving the magnesium donors as singly ionised Mg⁺. We thus have the analogue of He⁺. In figure 16 the excitation spectrum of Si(Mg⁺) is also shown. The comparison of the excitation spectra of Si(Mg⁰) and Si(Mg⁺) shows that the spacings of the corresponding excitation lines are close to four times larger for the latter as is to be expected. The binding energies of the

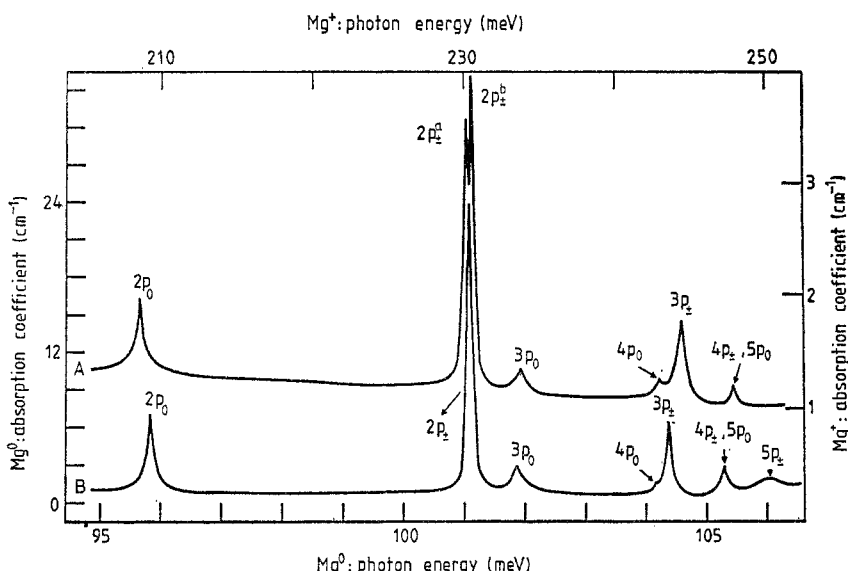


Figure 16. Excitation spectra of Si(Mg⁰) (B) and Si(Mg⁺) (A). Liquid helium used as coolant. Mg⁺ was produced by compensating Mg⁰ with boron acceptors. Note that the energy scale for Mg⁺ is four times larger than that for Mg⁰ (after Ho and Ramdas 1972).

donor states are given in table 4. The ionisation energies strongly suggest that in both cases the ground state is $1s(A_1)$. A noteworthy feature in the Mg^+ spectrum is the doublet nature of the $2p_{\pm}$ line, $2p_{\pm}^a$ and $2p_{\pm}^b$. This has been ascribed to the chemical splitting of the excited state.

Lithium as an impurity in the elemental semiconductors, silicon and germanium, and the III-V compound semiconductors has attracted considerable attention as a consequence of its remarkable diffusion properties (Reiss and Fuller 1960) and its ability to complex with other chemical impurities which may be present in the crystals (Fuller 1960). The diffusion coefficient of Li in Si at 800 K is eight orders of magnitude larger than that of P in the same host (see Wolf 1969). Lithium is known to complex with dispersed oxygen in Si and Ge. Both Li and Li-O complexes in Si and Ge are shallow donors.

Consider interstitial lithium in Si and Ge; its $2s$ valence electron is presumably the donor electron. Aggarwal *et al* (1965) observed the excitation spectrum associated with Si(Li) (see also Gilmer *et al* 1965). The excitation spectrum of lithium diffused into high-purity floating-zone silicon recorded under high resolution using a Fourier transform spectrometer, with the sample cooled to liquid helium temperature, is shown in figure 17 (Jagannath *et al* 1981). Identifying the lowest energy line at 21.50 meV as a $1s \rightarrow 2p_0$ transition, all the other lines can be assigned according to the final-state labels given in the figure. The spacings agree in an excellent manner with those predicted by Faulkner's calculations and with those of group V impurities already discussed in §4.1. The relative intensities of the excitation lines in Si(Li) bear a striking resemblance to those of group V donors in Si. The particularly close agreement of the ionisation energy of Li (33.02 meV) with the theoretical value of Faulkner, 31.27 meV, is remarkable. The lowest ground state is clearly effective-mass-like. Measurements at a slightly elevated temperature revealed the existence of a line (1.76 ± 0.04) meV to the low-energy side of the transition labelled $2p_{\pm}$ (Aggarwal *et al* 1965, Jagannath *et al* 1981). Since the $1s(E)$ and $1s(T_2)$ levels are expected to be close to the effective-mass position of the $1s$ state, the lower

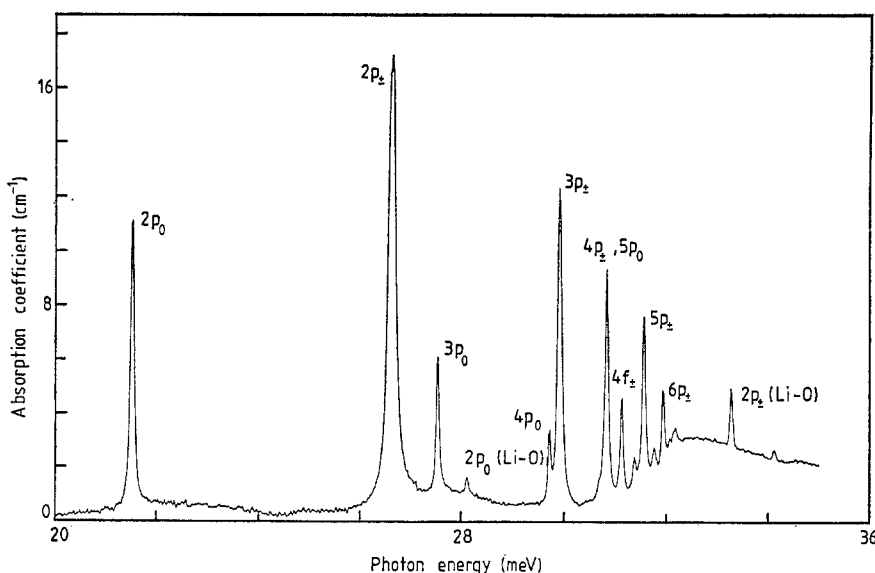


Figure 17. The excitation spectrum of lithium donors introduced into a high-purity float-zone silicon sample. Lithium donor concentration $\sim 1.1 \times 10^{15} \text{ cm}^{-3}$. Liquid helium used as coolant. Instrumental resolution $\sim 0.28 \text{ cm}^{-1}$ (after Jagannath *et al* 1981).

ground state has been attributed to $1s(E + T_2)$ and the upper ground state to $1s(A_1)$. Thus the ground-state complex of interstitial lithium has an 'inverted' arrangement in comparison to that observed for the group V donors, the $1s(A_1)$ lying above rather than below $1s(E)$, $1s(T_2)$. The interstitial nature of Li appears to be the underlying cause. Nara and Morita (1967) have made theoretical calculations partly explaining this experimental observation. In a later section we will see how observations of the excitation spectrum under uniaxial stress provide a convincing demonstration of this assignment. The electron paramagnetic resonance experiments by Watkins and Ham (1970) confirm that interstitial lithium donors in Si have a degenerate $1s(E + T_2)$ ground state, with $1s(A_1)$ lying (1.8 ± 0.3) meV above it.

Lithium diffused into high-resistivity crucible-grown Si forms Li-O donor complexes with the oxygen which enters into Si from the quartz crucible during crystal growth (Pell 1960). Aggarwal *et al* (1965) and Jagannath *et al* (1981) showed that such samples exhibit a characteristic donor excitation spectrum at liquid helium temperature, similar to that of group V donors in Si. They observed a prominent series with an ionisation energy of (39.67 ± 0.04) meV, i.e. with a chemical shift of 8.4 meV below the effective-mass 1s level. Measurements at liquid hydrogen temperatures produced a new line at 25.6 meV, (7.7 ± 0.1) meV to the low-energy side of the prominent transition at 33.27 meV; the latter is assigned to the $1s(A_1) \rightarrow 2p_{\pm}$ and the former to $1s(E + T_2) \rightarrow 2p_{\pm}$ transitions. Uniaxial stress experiments confirm the identification of the 33.27 meV with the $1s(A_1) \rightarrow 2p_{\pm}$ transition. Thus the ground states of this Li-O centre have the same structure as that of the group V donors. In addition to the prominent series (Aggarwal *et al* 1965) several additional lines, labelled 'x', have been observed. Gilmer *et al* (1965) presented evidence that more than one species of Li-O donor complexes are produced, each with its characteristic chemical splitting. The prominence of a given type appears to depend on the sample history. In figure 18 we show the excitation spectrum of Si(Li) and Si(Li-O) in a sample cooled to liquid helium temperature and the spectrum recorded by Jagannath and Ramdas (1980). From the intensities of the Li-O spectrum they estimate an oxygen concentration of $\sim 10^{14} \text{ cm}^{-3}$. It appears that the excitation spectrum of oxygen 'decorated' by lithium is a very sensitive means for determining oxygen concentrations in silicon as was first pointed out by Aggarwal *et al* (1965).

The excitation spectrum of Ge(Li) was also reported by Aggarwal *et al* (1965). The excitation lines occur very close to the positions predicted for the $1s(T_2) \rightarrow np$ transitions with an ionisation energy of (9.89 ± 0.05) meV; this is to be compared to the 9.81 meV

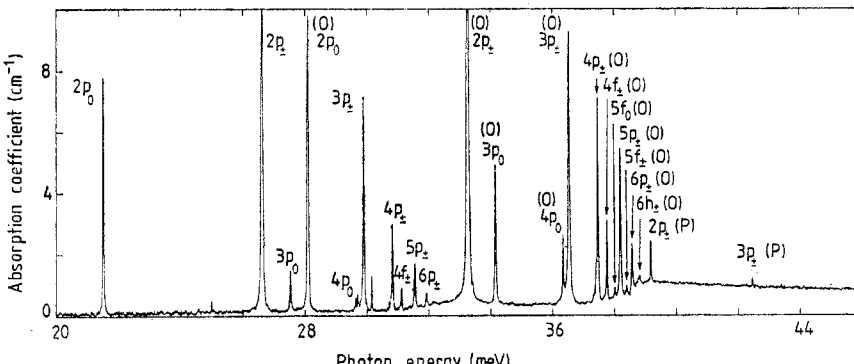


Figure 18. Excitation spectra of Si(Li) and Si(Li-O). The transitions corresponding to Si(Li-O) are labelled 'O' in parenthesis. Coolant: liquid helium (after Jagannath and Ramdas 1980).

calculated by Faulkner (1969); measurements of Seccombe and Korn (1972) gave an ionisation energy of 10 meV. Buzzdin *et al* (1973) observed a line at 1.9 meV for Ge(Li) which they assigned to a $1s(T_2) \rightarrow 1s(A_1)$ transition, suggesting that in germanium too lithium interstitial donors have an ‘inverted’ ground-state structure. Additional lines belonging to one or more centres different from interstitial lithium have been reported (Aggarwal *et al* 1965) and ascribed to Li-O complexes by Bykova *et al* (1976) and Darken (1977). On the basis of electron paramagnetic and piezospectroscopic data Haller and Falicov (1978) have deduced that these centres have $\langle 111 \rangle$ symmetry; the details of their interpretation are based on tunnelling between the equivalent $\langle 111 \rangle$ orientations, resulting in a multiple ground state with binding energies of 9.63, 9.72 and 10.34 meV. Once again the low level of oxygen concentration ($\sim 10^{13} \text{ cm}^{-3}$) established on the basis of such spectra is impressive.

We conclude this section by drawing attention to two very interesting cases of donor complexes, viz. donor centres in silicon consisting of group V donors and defects produced by electron irradiation (Chen *et al* 1972) and heat treatment centres in Si and Ge which are donors (Morin *et al* 1954, Kaiser *et al* 1958, Kaiser 1962). Electronic excitation spectra have been reported for such centres in Si (Hrostowski and Kaiser 1958, Aggarwal 1965, Chen *et al* 1972).

4.3. Group III acceptors in Si and Ge

The far-infrared absorption spectra of Ge(B) and Ge(T1) at liquid helium temperature obtained by Soepangkat and Fisher (1973) are shown in figures 19 and 20. The sharp lines clearly reveal the existence of the bound states of the acceptors; the spectra of these acceptors as well as those of Al, Ga and In are strikingly similar in that they exhibit lines with similar relative intensities and the spacings between the corresponding lines are the same within experimental errors. In table 6 we compare the binding energies of the final state for each excitation line; also given are the ionisation energies. In constructing this table, it is assumed that the effective-mass theory as employed by Baldereschi and Lipari (1976) correctly gives the binding energy of the final state of line

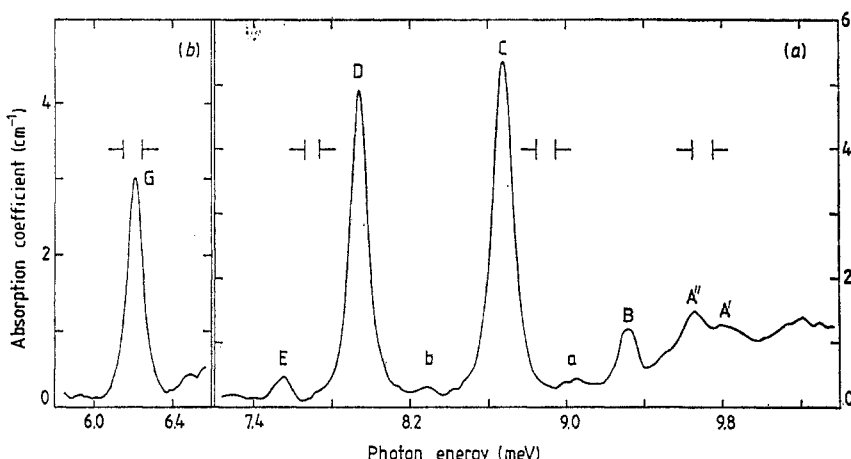


Figure 19. Excitation spectrum of Ge(B). The acceptor concentration p of Ge(B)-150 A no 1 (a) was $\sim 2 \times 10^{14} \text{ cm}^{-3}$ while that of Ge(B)-180 A no 5(b) was $\sim 8 \times 10^{14} \text{ cm}^{-3}$. Liquid helium used as coolant (after Soepangkat and Fisher 1973).

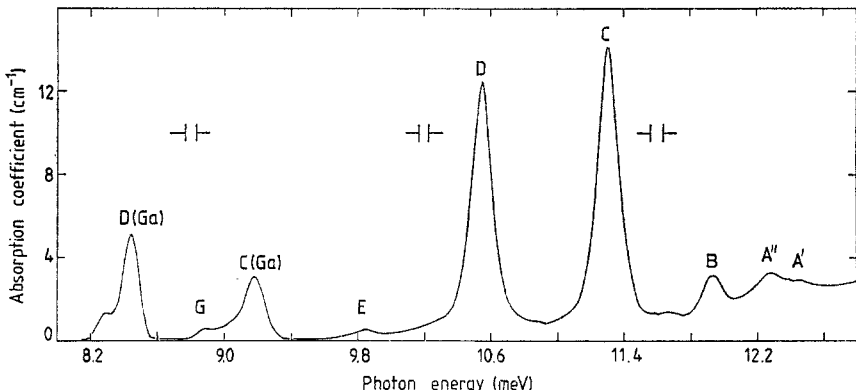


Figure 20. Excitation spectrum of Ge(Tl). $p \approx 2 \times 10^{14} \text{ cm}^{-3}$. Liquid helium used as coolant. Ge(Tl)-368B no 1 (after Soepangkat and Fisher 1973).

D. In figure 21 we show the photothermal ionisation spectrum of a germanium sample containing Al, B and Ga recorded by Haller and Hansen (1974).

The excellent agreement between the observed and calculated binding energies in table 6 is indicative of the success of the effective-mass theory for the excited states of odd parity. On the other hand, the ground states for these acceptors have suffered chemical shifts by differing amounts, placing the excitation spectra in different spectral regions. In figure 22 we show schematically the transitions from the Γ_8 ground state to the excited

Table 6. Binding energies[†] of the final states of the excitation lines of group III acceptors in germanium (meV).

Line	B ^a	Al ^b	Ga ^b	In ^b	Tl ^a	Theory
G	4.61	4.56	4.58	4.57	4.52	4.58 ($1\Gamma_8^-$)
E	3.27		3.30	3.54	3.57	
D	2.88	2.88	2.88	2.88	2.88	2.88 ($2\Gamma_8^-$)
C	2.14	2.13	2.13	2.10	2.13	2.13 ($1\Gamma_7^-$) 2.11 ($3\Gamma_8^-$)
a	1.76 ^b			1.76	1.78 ^b	
B	1.49	1.48	1.48	1.48	1.50	1.48 ($4\Gamma_8^-$) 1.22 ($5\Gamma_8^-$)
A''	1.16	1.13	1.15	1.15	1.14	1.14 ($2\Gamma_7^-$)
A'	1.03	1.00	1.01	1.00	1.01	1.14 ($1\Gamma_6^-$) 1.13 ($6\Gamma_8^-$)
E_I	10.82	11.15	11.32	11.96	13.43	

[†] The ionisation energy E_I is calculated assuming a binding energy of 2.88 meV for the final state of line D (Baldereschi and Lipari 1976). Within the framework of the effective-mass approximation, and taking $U_I = -e^2/\kappa r$, the symmetry of acceptor states is that of O_h . For this reason the last column in this table gives the representations appropriate to this point group.

^a Soepangkat and Fisher (1973).

^b Jones and Fisher (1965).

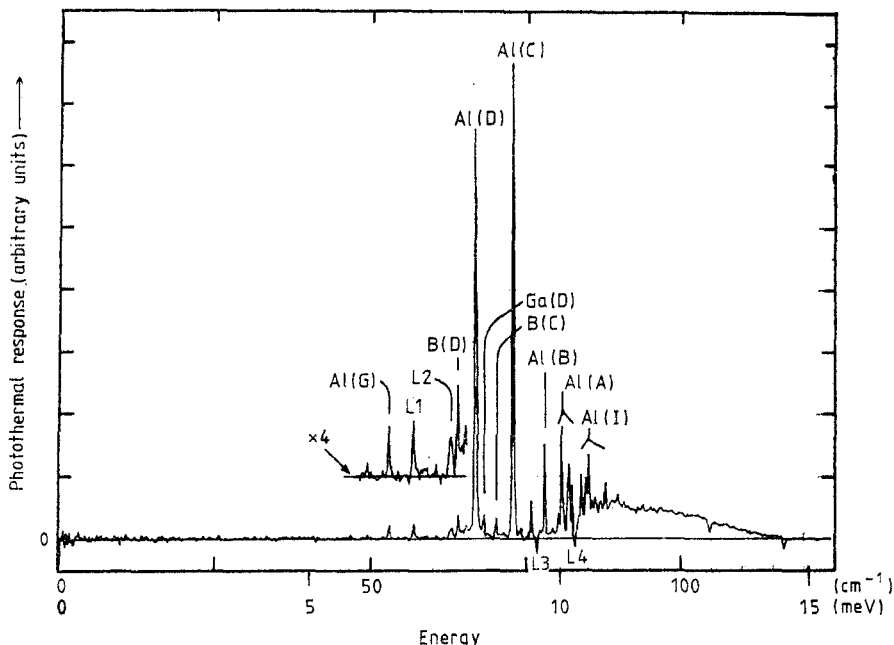


Figure 21. Photothermal ionisation spectra of group III acceptors in germanium (after Haller and Hansen 1974).

states associated with the $p_{3/2}$ and the $p_{1/2}$ valence bands and refer to them as the ' $p_{3/2}$ ' and the ' $p_{1/2}$ ' series, respectively. In germanium no $p_{1/2}$ transitions have been observed. For B, Al and Ga Haller and Hansen have reported more structure in the transitions A' and A'' and have observed eight more transitions closer to the photoionisation limit labelled by them as I₁, I₂, . . . , I₈; for In they observe the additional transitions in the

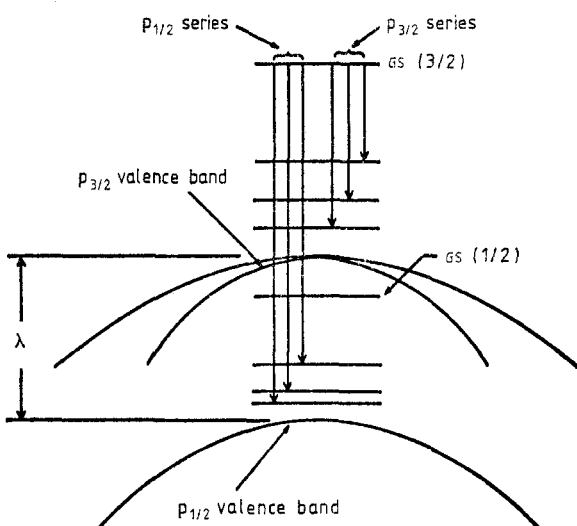


Figure 22. The spin-orbit-split valence band of silicon with associated acceptor states. Here GS is the ground state and λ is the spin-orbit splitting at $k=0$.

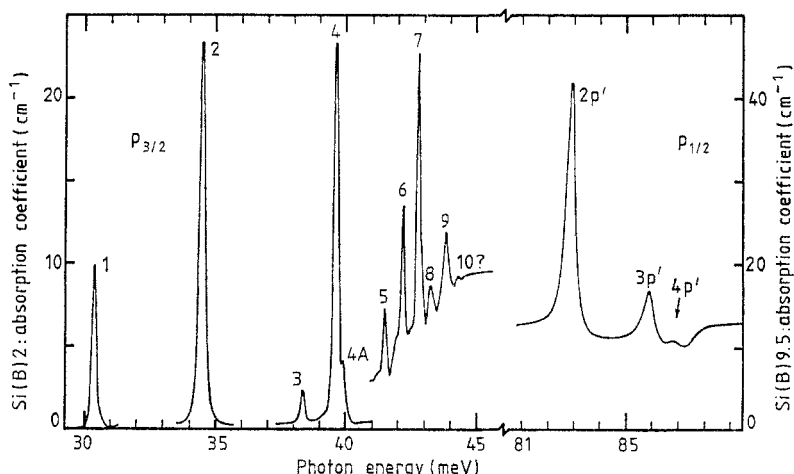


Figure 23. The excitation spectrum of Si(B). Lines 1–4A were measured with sample Si(B) no 2, p (carrier concentration at 300 K)= $1.5 \times 10^{15} \text{ cm}^{-3}$. Lines 5–4p' were measured with sample Si(B) no 9.5, p (300 K)= $2.2 \times 10^{16} \text{ cm}^{-3}$. Liquid helium used as coolant (after Onton *et al* 1967a).

vicinity of A' and A'' . The extraordinary sensitivity of the photothermal ionisation technique has enabled them to discover two shallow acceptors of undetermined origin.

The excitation spectrum of Si(B) recorded by Onton *et al* (1967a) is shown in figure 23. A consistent interpretation can be given if lines 1–10 are assigned to the $p_{3/2}$ series and lines 2p', 3p' and 4p' to the $p_{1/2}$ series as shown in figure 22. The $p_{1/2}$ series in Si was first observed by Zwerdling *et al* (1960b). In figures 24 and 25 we show the recent high-resolution Si(B) spectrum recorded by Jagannath *et al* (1981) using a Fourier transform spectrometer; the line 4 complex shows additional structure under this resolution. In figure 26 we give a sketch of the group III acceptor excitation spectra in Si with the same energy scale but with the relative shifts such that the 2p' lines of the various

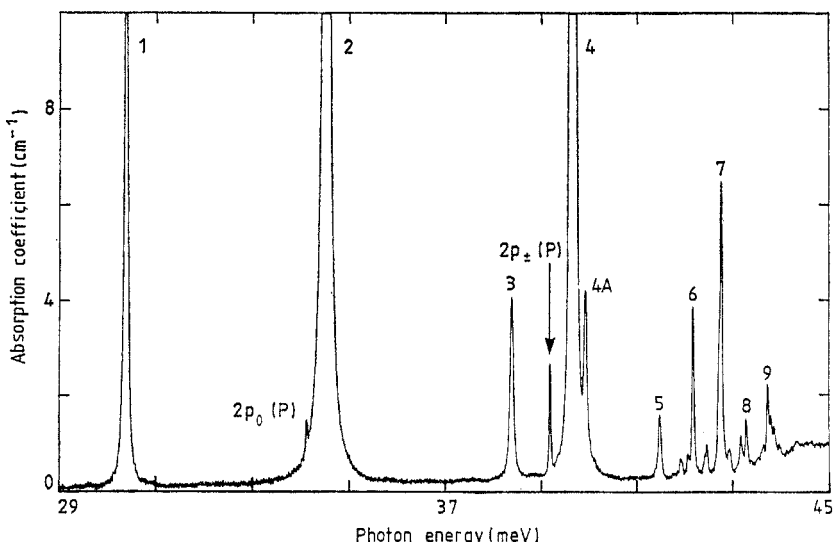


Figure 24. Excitation spectrum of Si(B), p (300 K)= $8.5 \times 10^{14} \text{ cm}^{-3}$. The Si(P) lines are labelled 'P' in parenthesis. Liquid helium used as coolant (after Jagannath *et al* 1981).

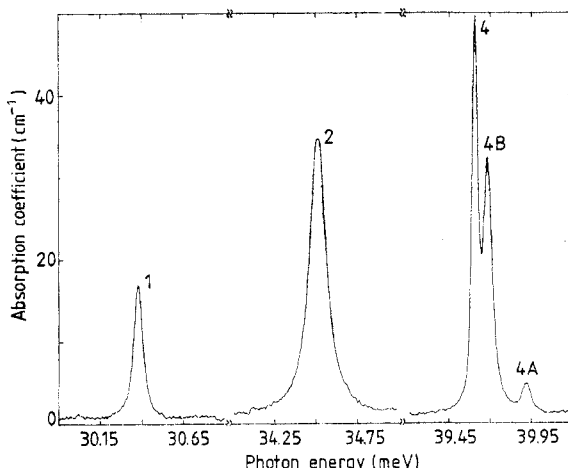


Figure 25. Lines 1, 2, 4, 4A of Si(B) on an expanded horizontal scale. The sample used is the same as that in figure 24 but with reduced thickness. Liquid helium used as coolant (after Jagannath *et al* 1981).

spectra have been brought into coincidence. The ground states of the various acceptors have clearly suffered significant chemical shifts with respect to one another. The intensities of the corresponding excitation lines for the different acceptors do not resemble one another as closely as they do for acceptors in germanium. Onton *et al* (1967a, b) showed that the chemical shifts bring the $p_{3/2}$ excitation spectra of Al and Ga into the energy range of the optical phonons in Si. A resonant interaction occurs between the electronic and phonon excitations of the crystal, resulting in the broadening of the excitation line. This phenomenon also occurs for the $1s(A_1) \rightarrow 2p_0$ excitation line of Si(Bi) (Onton *et al*

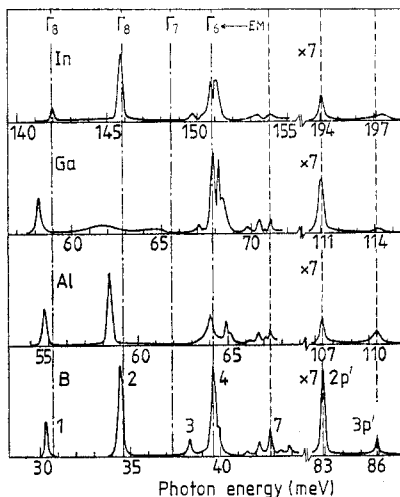


Figure 26. Sketch of the group III acceptor excitation spectra in silicon. The sketch shows the positions of the lines accurately. The relative intensities of the lines within a given spectrum are representative; the intensities of the $p_{1/2}$ lines compared to those of the $p_{3/2}$ lines have been scaled up by a factor of 7. The $2p'$ lines of the various spectra have been brought into coincidence and the discontinuities in the horizontal scales have the same magnitude (after Onton *et al* 1967a).

1967b, Butler *et al* 1975). The absence of line 2 in Si(Ga) and line 3 in Si(Al) can be traced to this resonant interaction. We describe further details of this resonant interaction in §6. In table 7 we compare the binding energies of the group III acceptor excited states with those calculated by Baldereschi and Lipari (1976) and Lipari and Baldereschi (1978); we have assumed that the theory accurately gives the binding energy of the final state of the line 4 transition as 6.1 meV. As can be seen, the binding energies of many excited states are reproduced by the theory with fair success and we deduce an ionisation energy, E_I , for the $p_{3/2}$ series to be 45.71, 70.18, 74.05 and 156.90 meV for B, Al, Ga and In, respectively. Zwerdling *et al* (1960b) showed that the ionisation energy E_I^* for the $p_{1/2}$ series can be deduced by assuming the Rydberg formula; E_I^* thus calculated should equal $E_I + \lambda$, where λ is the spin-orbit splitting of the valence band. From E_I^* of 88.35, 112.93, 116.74 and 200.16 meV for B, Al, Ga and In, respectively (Onton *et al* 1967a)

Table 7. Binding energies[†] of the final states of the excitation lines of group III acceptors^a in silicon (meV).

Line	B	Al	Ga	In	Theory ^c
1	15.33	15.30	15.82	14.91	15.5 ($1\Gamma_8^-$)
2	11.18	11.69		11.11	11.4 ($2\Gamma_8^-$)
3	7.36		6.93	7.16	7.3 ($3\Gamma_8^-$)
4	6.1 ^b	6.1	6.1	6.1	6.1 ($1\Gamma_7^-$)
4A	5.79 ^b	5.22	5.80	5.82	5.8 ($1\Gamma_6^-$)
4B	6.03 ^b	5.02	5.62		5.8 ($4\Gamma_8^-$)
5	4.19	3.9	4.20	4.1	4.1 ($5\Gamma_8^-$)
6	3.52	3.43	3.56	3.63	3.6, 3.5 ($2\Gamma_6^-$, $6\Gamma_8^-$)
7	2.92	3.08	3.25		
8	2.44	2.79	2.94	2.93	
9	1.85	2.28			
10	1.39	1.78			
E_I	45.71	70.18	74.05	156.90	

[†] The ionisation energy E_I is calculated assuming a binding energy of 6.1 meV for the final state of line 4.

^a Onton *et al* (1967a).

^b Jagannath *et al* (1981).

^c Baldereschi and Lipari (1976).

we deduce a λ of (42.84 ± 0.29) meV. This represents the best experimental value for the spin-orbit splitting of the valence band of Si. Bhatia (1971) and Watkins and Fowler (1977) have reported phonon-assisted transitions in the excitation spectra of acceptors in Si; they have observed the interference effects which are characteristic of absorption via two channels, one of which is a discrete transition whereas the other lies in a continuum (Breit and Wigner 1936, Fano 1961).

In the electronic Raman spectrum of Si(B) recorded by Wright and Mooradian (1967) a single sharp line at 23 meV is seen (figure 13). It is due to a transition from the Γ_8^+ ground state to an excited state of even parity, using the notation consistent with the O_h symmetry of the host crystal; Cherlow *et al* (1973) and Chandrasekhar *et al* (1975) attributed this to the transition from the four-fold Γ_8^+ acceptor ground state to its spin-orbit-split Γ_7^+ two-fold partner state. Experimental results involving uniaxial stress were utilised to support this interpretation. Lipari and Baldereschi (1978) have also put forward this interpretation for the 23 meV Raman line in Si(B) based on their

theoretical calculations. A weak 22.7 meV peak in the infrared absorption spectrum of Si(B) has been attributed to the same transition by Chandrasekhar *et al* (1975).

4.4. Other acceptors in Si and Ge

The excitation spectra of several group II acceptors and of the group I acceptor Cu have been observed in Ge: neutral beryllium, Be⁰ (Shenker *et al* 1967, Moore 1971), Zn⁰ (Fisher and Fan 1960, Moore 1965, Fisher *et al* 1966, Jones 1968), Hg⁰ (Chapman and Hutchinson 1965, 1967a, Moore 1965, Pajot and Darviot 1966), singly ionised Zn⁻ (Fisher and Fan 1960, Barra *et al* 1973, Butler and Fisher 1976) and Cu⁰ (Fisher and Fan 1960, Moore 1965). The excitation spectra of Zn⁰ and Zn⁻ are shown in figures 27 and 28. The spectra of the neutral impurities closely resemble one another in the relative intensities and the spacings of the corresponding lines. In table 8 we list the binding energies of the excited states assuming that the final state of line D has a binding energy of 2.88 meV calculated for the $2\Gamma_8^-$ state of the group III acceptors. Implicit in this identification is the assumption that these multi-hole acceptors are characterised by excited states essentially the same as those of group III acceptors; a comparison of tables 6 and 8 shows the validity of this assumption. The excitation lines are due to one-particle excitation, the hole(s) remaining in the closer orbit screening the 'nuclear charge' very effectively. The binding energies of Zn⁻ are ~ 4 times those of the corresponding lines of Zn⁰, thus showing that the former is analogous to singly ionised helium and the latter to neutral helium. We note that line G in Ge(Zn⁻) is very weak and its position has been deduced by Butler and Fisher (1976) on the basis of uniaxial stress measurements.

The onset of impurity photoconductivity determines the ionisation energies of the impurities and an interesting application of photoconductivity has been made by Moore (1965). Minima are observed in the photoconductive response of a sample containing two species of acceptor impurities; the photoconductivity in the region of the minima arises from the photoionisation of the shallower impurity whereas the minima themselves are due to competing excitations associated with the deeper acceptor. Moore

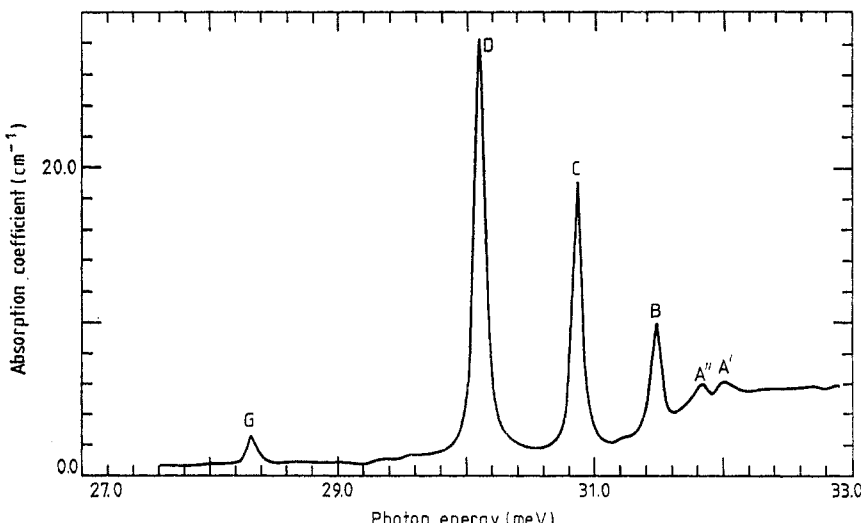


Figure 27. The excitation spectrum of Ge(Zn⁰). Liquid helium used as coolant. Room-temperature resistivity = 2.04 Ω cm. Ge(Zn) 431A.1 (after Jones 1968).

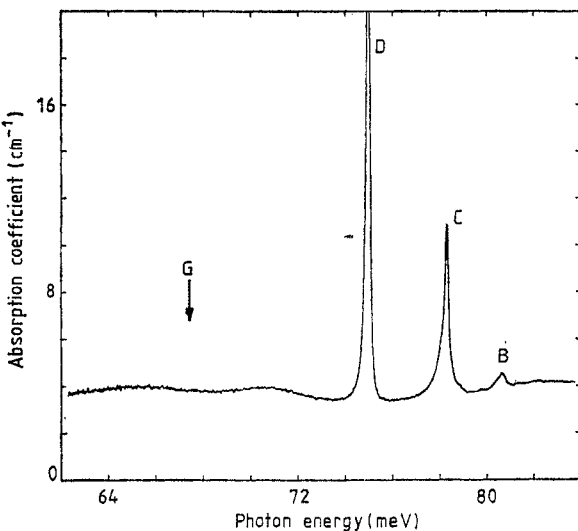


Figure 28. The excitation spectrum of $\text{Ge}(\text{Zn}^-)$, Zn^0 being partially compensated by Sb donors. Liquid helium used as coolant. $\text{Ge}(\text{Zn}, \text{Sb})$ 437B-3 (after Butler and Fisher 1976).

studied $\text{Ge}(\text{Ga}, \text{Zn})$, $\text{Ge}(\text{Zn}, \text{Cu})$ and $\text{Ge}(\text{Cu}, \text{Hg})$ using this technique. Butler and Fisher (1974) have reported photothermal ionisation spectra of $\text{Ge}(\text{Cu}^0)$. A number of extremely sensitive infrared detectors are based on the photoionisation of group II acceptors for photon energies $\hbar\omega \geq E_I$; $\text{Ge}(\text{Zn}^0)$, $\text{Ge}(\text{Cu}^0)$ and $\text{Ge}(\text{Hg}^0)$ photoconductive

Table 8. Binding energies of the final states of the excitation lines of group II and group I acceptors in germanium (meV).

Line	Be^{0a}	Zn^{0b}	Hg^{0d}	Cu^{0c}	Zn^{-e}
G	4.99 4.81	4.66 4.68	5.38 4.68	4.60 ^f	4.68×4
E			3.55 ^f		
D	2.88	2.88	2.88	2.88	2.88×4
					$2.08 \times 4 (\text{C}')$
C	2.10	2.12	2.18	2.14	$2.047 \times 4 (\text{C})$
					$1.93 \times 4 (\text{C}'')$
a					1.684×4
B	1.41	1.50	1.58	1.52	1.454×4
A'''					1.261×4
A''	1.14	1.15		1.19	1.08×4
A'		0.98	1.08	1.00	0.931×4
A		0.80 ^f			
E_I	24.81	32.98	91.88	43.21	86.514

^a Shenker *et al* (1967).

^b Jones (1968).

^c Butler and Fisher (1974).

^d Chapman and Hutchinson (1967a).

^e Butler and Fisher (1976).

^f Moore (1965). Note from Moore's data, $E_I = 43.21$ meV for $\text{Ge}(\text{Cu}^0)$, 33.03 meV for $\text{Ge}(\text{Zn}^0)$ and 91.69 meV for $\text{Ge}(\text{Hg}^0)$.

detectors provide an excellent coverage of the spectral range 40–15, 30–10 and 12–8 μm , respectively.

In the case of Si, Crouch *et al* (1972) reported excitation spectra of Si(Be) and Si(Be-Li). The spectra reveal excited states similar in binding energy to those of the group III acceptors. Other than this investigation, all the work reported in the literature deal with photoconductivity in Si(Cu), Si(Fe), Si(Zn) and Si(Au) (Collins and Carlson 1957, Carlson 1957, Collins *et al* 1957). Sclar (1976, 1977) has surveyed the dopants in Si with special reference to infrared detection.

4.5. Acceptors in diamond

Though diamond is clearly of great interest in the context of impurity states in group IV semiconductors, only a limited amount of work has been done on controlled doping. Custers (1952) reported that some natural type II diamonds are semiconducting; they have resistivities of $\sim 300 \Omega \text{ cm}$ as compared to $\sim 10^{14} \Omega \text{ cm}$ for the majority of diamonds. Acceptor centres in the concentration range of $5 \times 10^{16} \text{ cm}^{-3}$ are responsible for this behaviour (Austin and Wolfe 1956, Wedepohl 1957). Synthetic diamonds have been produced with boron, aluminium and beryllium as dopants (Wentorf and Bovenkerk 1962, Huggins and Cannon 1962). Semiconducting diamonds are referred to as type IIb diamonds. Austin and Wolfe (1956) reported excitation spectra associated with the acceptor centres in the natural IIb diamonds; the thermal activation energy of 380 meV is consistent with the photoionisation limit. The excitation lines have been interpreted as transitions from the ground state of the acceptor to its excited states as well as to one-phonon replicas (Hardy *et al* 1962). Crowther *et al* (1967) and Anastassakis (1969) studied the effect of stress and electric field, respectively, on the excitation spectra of these acceptors. The nature of the acceptor centres in natural IIb diamonds attributed to Al (Brophy 1956, Lightowlers 1962, Dean *et al* 1965) has been questioned by Wedepohl (1968). Collins *et al* (1965) have reported the excitation spectra of acceptors in synthetic diamond. Collins and Lightowlers (1968) have observed the photothermal ionisation spectrum of the acceptors. We show in figure 29 the excitation spectrum of the acceptors in semiconducting diamond recorded by Anastassakis (1969).

As in Si and Ge, the top of the valence band of diamond lies at $k=0$ with Γ_8^+ symmetry. However, the spin-orbit-split Γ_7^+ valence band lies only 6 meV below the Γ_8^+ maximum. Thus the energy levels of the acceptor have to be calculated using the complete 6×6 Hamiltonian matrix corresponding to equation (3.58). Such a calculation for diamond does not appear to have been carried out. We reproduce in figure 30 a schematic correlation between the observed transitions and the acceptor energy levels given by Anastassakis (1969).

4.6. Donors and acceptors in compound semiconductors

The band structures of the tetrahedrally coordinated III-V and II-VI semiconductors are very similar to those of Ge and Si (Chelikowsky and Cohen 1976). Long (1968) has a convenient summary of the band parameters and the symmetry assignments for the band extrema in appendix C of his book. The properties of the conduction electrons and holes, e.g. g factors, mass anisotropies and mobilities of electrons for a given semiconductor, are controlled by the lowest conduction band minimum and the magnitude of the energy gap. For example, InSb, GaSb, InAs, InP, GaAs and CdTe are all characterised by a Γ_8 conduction band minimum whereas GaP and AlSb exhibit a multi-valley

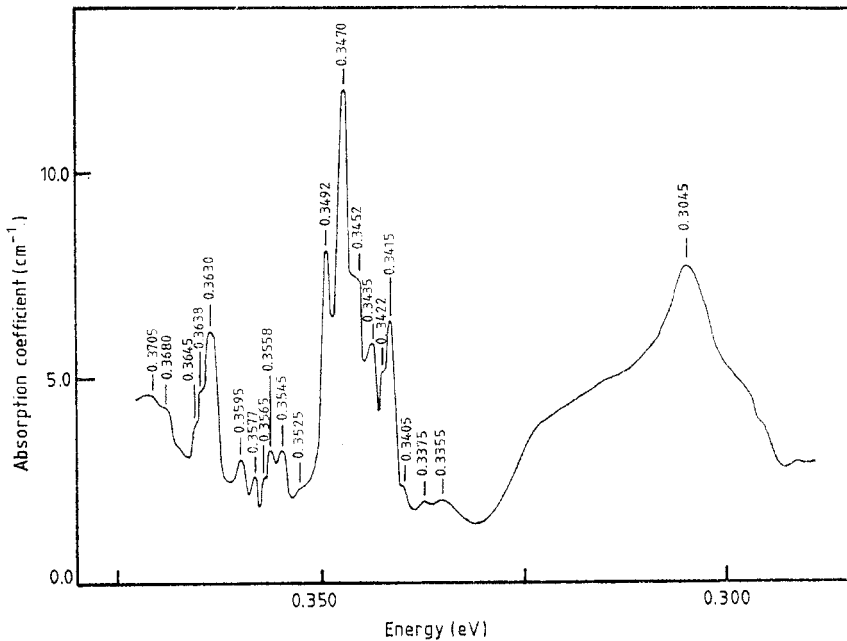


Figure 29. Excitation spectrum of a shallow acceptor in diamond; $T=85\text{ K}$, slit width $70\text{ }\mu\text{m}$ (after Anastassakis 1969).

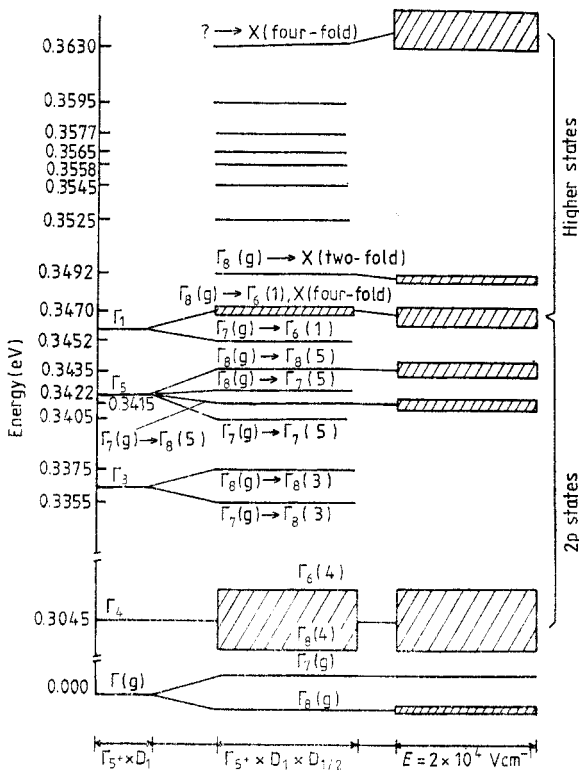


Figure 30. Energy levels of a shallow acceptor in diamond, a schematic correlation with the observed transitions (after Anastassakis 1969).

conduction band along $\langle 100 \rangle$. The small energy gap of InSb results in an isotropic effective mass $\sim (1/100) m$. For GaSb, the Γ_6 minimum is separated from the next higher lying L_6 minimum by only 80 meV (Becker *et al* 1961) resulting in carriers in both Γ_6 and L_6 minima with modest carrier concentrations at room temperature. All of the III-V and II-VI semiconductors have a complex valence band similar to that of Si and Ge except that they exhibit linear k terms in their energy dependence near $k=0$. To the extent the impurity states in the effective-mass approximation reflect the nature of the band extrema with which they are associated, useful insights into the properties of the host can be obtained from the study of the donor and acceptor spectra. A number of compound semiconductors have been studied from this point of view.

As noted above, GaAs, InP, CdTe, InAs and InSb have the absolute conduction band minimum at $k=0$ with Γ_6 symmetry. They all have a small isotropic effective mass. The Lyman spectra of these donors should then be strictly scaled-down versions of the Lyman spectrum of the H atom. The small mass coupled with their large static dielectric constants (Hass 1967, Long 1968) result in very small binding energies for donors in these crystals. Of course, chemical shifts of the 1s ground state are likely to occur in the actual spectra.

(i) *n-GaAs*. Bosomworth *et al* (1968) reported an excitation line in n-GaAs at 4.6 meV. Since then a number of groups have investigated donor spectra in GaAs (Stillman *et al* 1969, 1971, Summers *et al* 1970, Stoelinga *et al* 1978). Fetterman *et al* (1971) determined an effective mass of $(0.06650 \pm 0.00007) m$ for electrons in the Γ_6 conduction band minimum; Stillman *et al* (1969) obtained $(0.0665 \pm 0.0005) m$ from the magnetospectroscopy (Zeeman effect) of the donor spectra which we discuss in §5.2. Using 12.58 for the static dielectric constant, the donor ionisation energy was calculated to be 5.72 meV by Stillman *et al* (1971). Several donor species have been discovered having effective-mass-excited p states but with ground states which have suffered differing chemical shifts. In figure 31 we show the spectra of donors in GaAs recorded by Stillman *et al* (1969) using the photothermal ionisation technique. The excellent agreement between the cyclotron effective mass and that deduced from the excitation spectra indicates that the non-parabolicity of the conduction band of GaAs (see, for example, Chandrasekhar and Ramdas 1980) does not play an essential role in determining the binding energies of the impurity states.

(ii) *n-InP*. Chamberlain *et al* (1971a) observed a $1s \rightarrow 2p$ transition at 5.37 meV for a shallow donor in n-InP. They deduced an effective mass of $(0.085 \pm 0.005) m$ for the electrons in its Γ_6 conduction band, in excellent agreement with $(0.081 \pm 0.0005) m$ obtained from the Zeeman effect of donors as well as the cyclotron resonance value of $(0.0810 \pm 0.0003) m$ (Chamberlain *et al* 1971b). Onton *et al* (1972) have observed zero phonon and phonon-assisted optical transitions from the Γ_6 conduction band to the subsidiary $X_1(X_3)$ conduction band and its donor levels. At sufficiently high concentration of donors (Te or Si), n-InP is degenerate, and at low temperatures the conduction electrons can make optical transitions from states close to the Fermi level in Γ_6 to $X_1(X_3)$ and associated donor levels. They deduced donor binding energies of 106 and 175 meV (± 5 meV) for Te and Si, respectively.

(iii) *n-CdTe*. Cohn *et al* (1970, 1972) have observed the $1s \rightarrow 2p$ transition for a shallow donor in n-CdTe at 10.79 meV; using a static dielectric constant of 9.6 (Berlincourt *et al* 1963) and an effective mass of $(0.096 \pm 0.0008) m$ (Kanazawa and Brown 1964), the energy of this transition is predicted to be 10.66 meV, in good agreement with the experimentally observed position. Simmonds *et al* (1974), Wagner and McCombe (1974) and Golka *et al* (1977) have reported the $1s \rightarrow 3p$ transition. Simmonds *et al* (1974) were

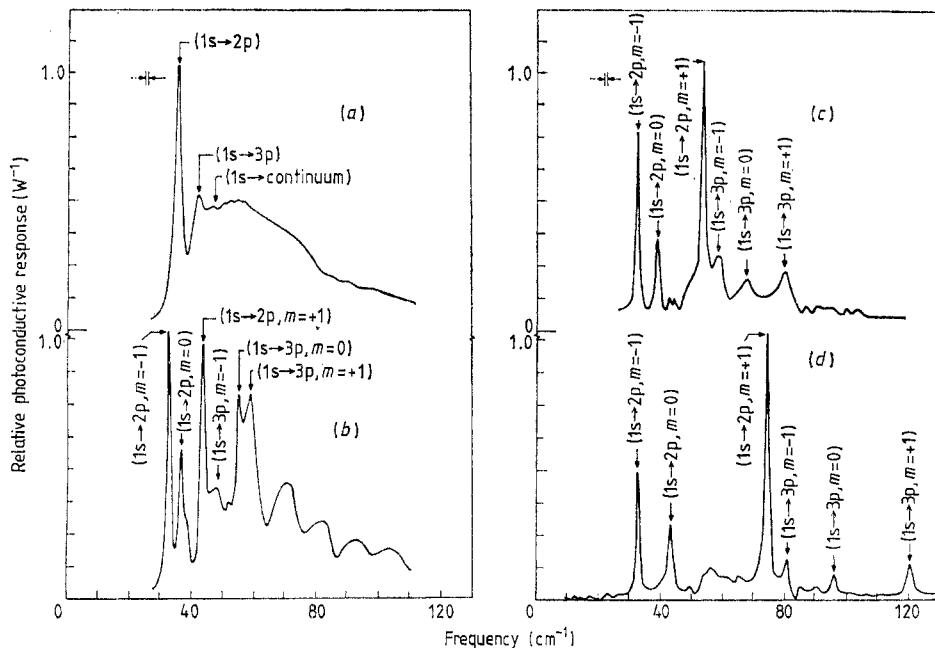


Figure 31. Photothermal ionisation spectrum of donors in high-purity GaAs, with and without magnetic field. $T=1.46\text{ K}$ (after Stillman *et al* 1969). (a) $H=0\text{ kG}$, (b) $H=7.5\text{ kG}$, (c) $H=15\text{ kG}$, (d) $H=29.9\text{ kG}$.

able to detect the chemical shifts associated with the ground states of different species of donors.

(iv) *n-InAs and n-InSb*. The Γ_6 conduction bands of InAs and InSb are characterised by very small effective masses, $(0.024)\text{ }m$ and $(0.0155)\text{ }m$, respectively. Coupled with the large static dielectric constants (14.55 for InAs and 17.88 for InSb), this results in very large Bohr orbits, even for the 1s ground state. Thus, large overlap of wavefunctions occur at even dilute donor concentrations and the ionisation energy vanishes. However, under an applied magnetic field it is possible to eliminate this overlap and allow the localisation of the electronic levels. A magnetically induced de-ionisation of donors in InSb was observed by Keyes and Sladek (1956) and Sladek (1958). Excitation spectra in the far-infrared can thus be observed in the presence of a magnetic field (Kaplan 1969, Litton *et al* 1969). We will discuss some of these results in §5 on the impurity states under external perturbation. Effects associated with donor impurities in a magnetic field are exploited in the photoconductive InSb detectors used in the submillimetre range (Putley 1964).

We now turn our attention to GaP which has conduction band minima along $\langle 100 \rangle$ either at the zone boundary or very close to it. The studies on the absorption edge, especially under uniaxial stress, established the $\langle 100 \rangle$ symmetry of the conduction band minima (Nelson *et al* 1964, Balslev 1966). Leotin *et al* (1975) have deduced a transverse effective mass for conduction electrons, $m_t=(0.25\pm 0.01)\text{ }m$ and $\gamma=m_t/m_1=0.05$. Onton (1969), Onton and Taylor (1970) and Arai *et al* (1972) have reported the photoexcitation spectra of GaP(Si), GaP(S) and GaP(Te). The excitation spectra have been attributed to $1s(A_1) \rightarrow np$ transitions in the case of S and Te donors which substitute for P. However, for Si donors which substitute for Ga, they are ascribed to $1s(T_2) \rightarrow np$ transitions. The difference in the symmetry of the ground state of Si, Ge or C on the one hand and of S,

Se or Te on the other arises as follows (Morgan 1968). The representation X_1 or X_3 to which the conduction band minima at the zone edge belongs depends upon the choice of origin of the coordinate system used to describe the point group of the crystal. With respect to the more attractive (P) site, the lower band has X_1 symmetry, whereas if the centre of symmetry is on the more repulsive (Ga) site, the symmetry is X_3 . Thus, for Si, Ge and C impurities occupying a Ga site the appropriate conduction band symmetry is X_3 and for S, Se and Te occupying a P site it is X_1 . It is straightforward to show that consistent with the multi-valley nature of the conduction band, the 1s state of Si, Ge and C donors belongs to the T_2 representation of the T_d point group whereas the 1s state of S, Se and Te belongs to A_1+E . For the latter $1s(A_1)$ can be expected to be depressed below the effective-mass position by chemical effects. Using piezospectroscopy Scott and Onffroy (1976) have confirmed the differences in the symmetries of the ground and excited states of S on the one hand and Si on the other. Mehran *et al* (1972) showed that Sn donors in GaP, which should be analogous to Si, Ge or C, do exhibit an electronic paramagnetic resonance characteristic of a $1s(T_2)$ ground state. Manchon and Dean (1970) have reported the electronic Raman scattering associated with the $1s(A_1) \rightarrow 1s(E)$ transitions in GaP(Se, S, Te). The binding energies of the excited states of donors in GaP have also been deduced from 'two-electron' spectra first observed and interpreted by Dean *et al* (1967a). The lines in this spectrum arise when the S, Se or Te donor electron is left in an excited state as the exciton bound to the neutral donor recombines. The binding energies of the excited states thus deduced do not agree with those obtained from a photoexcitation spectrum due to $1s(A_1) \rightarrow np$ transitions; the excited states in the 'two-electron' spectrum have been identified as ns states (Onton 1969, Carter *et al* 1977b). Zeeman effect studies support the ns nature of these states (Dean *et al* 1977). A quantitative analysis of the binding energies of the excited states in the context of the Kohn-Luttinger theory (1955) as improved by Faulkner (1969) resulted in values of γ quite different from the cyclotron resonance value (Leotin *et al* 1975). This dilemma has been resolved by recognising that the conduction band minimum does not occur at the X point but is shifted from it along the Δ direction by ~ 0.08 ($2\pi/a$). This results in a 'camel's back' structure which can explain a number of features of the indirect absorption edge (Lawaetz 1975, Dean and Herbert 1976, Humphreys *et al* 1978). The non-parabolicity of the conduction band associated with the 'camel back' structure expressed in terms of the splitting energy δ at X and an additional parameter D can be used to modify the Kohn-Luttinger-Faulkner theory suitably to fit the binding energies of the np and ns states (Kopylov and Pikhtin 1977). An empirical analysis of this problem with a variable γ characterising each excited state has been given by Carter *et al* (1977b). Onton (1971) has reported transitions from the ground states of Si, Te and S donors associated with the lower X conduction band to excited donor states associated with the next-higher lying X band as well as the photoionisation into it. He was able to experimentally deduce the $X_3 - X_1$ interband energy to be (355 ± 3) meV with the conductivity effective mass of the higher band of (0.14 ± 0.02) m .

Ahlburn and Ramdas (1968) have studied the photoexcitation spectra of tellurium and selenium donors in aluminium antimonide which has a multi-valley conduction band with minima along $\langle 100 \rangle$ (Ghanekar and Sladek 1966, Stirn and Becker 1966, Laude *et al* 1970). The observed lines have been ascribed to $1s(A_1) \rightarrow np$ transitions. From these observations the binding energies of the $1s(A_1)$ states in AlSb(Te) and AlSb(Se) have been deduced to be 71.3 and 146.5 meV, respectively. For both donors, a $1s(A_1) \rightarrow 1s(T_2)$ transition has been identified, at 38.31 meV for Te and 117.13 meV for Se. Many of the excitation lines observed in the photoexcitation spectrum of the Te and Se donors

can be interpreted as resulting from electronic excitations accompanied by phonon emission. The spacings of the excitation lines are generally consistent with the effective-mass theory though a detailed comparison must await a more definitive determination of the effective masses using, say, cyclotron resonance. It is important to bear in mind that, as in the case of GaP, the conduction band minima may occur very close to the X points and develop a 'camel's back' structure.

Excitation spectra of acceptors in III-V compound semiconductors have been reported for (i) Zn, Cd, Ag and Ge in InSb (Murzin *et al* 1969, Kaplan 1973), (ii) several species of unknown centres in AlSb (Ahlburn and Ramdas 1969) and (iii) Mn (Chapman and Hutchinson 1967b), C, Mg, Zn and Si (Kirkman *et al* 1978) in GaAs. The electronic Raman effect associated with a transition within the ground-state multiplet and to an excited state has been observed by Henry *et al* (1966) and Manchon and Dean (1970).

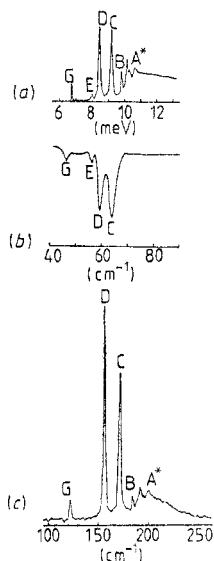


Figure 32. A comparison of acceptor spectra in different semiconductors. (a) Absorption spectrum of Ge(Ga) (Jones and Fisher 1965), (b) absorption spectrum of InSb(Cd) (Kaplan 1973) and (c) photoconductivity spectrum of GaAs(C) at 20 K (Kirkman *et al* 1978).

The similarity in the valence band structure results in an energy level scheme for acceptors which is similar in different hosts like InSb, GaAs and Ge. We reproduce in figure 32 the results for Ge(Ga), InSb(Cd) and GaAs(C) obtained by Jones and Fisher (1965), Kaplan (1973) and Kirkman *et al* (1978), respectively; these results illustrate quite strikingly the general similarity. Kirkman *et al* have compared the energy separations in the excitation lines for different acceptors in GaAs with those calculated by Lipari and Baldereschi (1970, 1972) and Lin-Chung and Henvis (1975, 1976).

We conclude this section by discussing a novel phenomenon described by Street and Senske (1976). One of the spectacular examples of a luminescence spectrum is that associated with donor-acceptor pairs in GaP (Vink and Van Doorn 1962, Hopfield *et al* 1963, Thomas *et al* 1964). A large number of sharp lines are observed near the band gap energy in the photoluminescence spectrum of samples containing one of the donors (S, Te or Se) and one of the acceptors (Zn, Cd or Si); the luminescence energy $\hbar\omega_L$ depends on the pair separation R and is given by $E_{\text{gap}} - (E_A + E_D) + e^2/\kappa R + J(R)$ where

E_D and E_A are the donor (D) and acceptor (A) binding energies and J is the interaction energy of a neutral-donor-acceptor pair. Street and Senske observe the luminescence from a given D-A pair at $\hbar\omega_L$ while exciting the crystal with $\hbar\omega_X$ provided by a tunable dye laser. A peak in the emission intensity at $\hbar\omega_L$ is observed whenever $\hbar\omega_X = E_{\text{gap}} - (E_D + E_A^*) + e^2/\kappa R + J^*(R)$ where E_A^* is the binding energy of a hole in an excited state of the acceptor. The 'excitation spectrum' is studied as a function of R and the binding energies of the acceptor are deduced by choosing R large enough so that both $J(R)$ and $J^*(R)$ are negligible. Street and Senske have deduced the binding energies of s- and p-excited states of C, Mg and Zn acceptors from these experiments. Binding energies of donor-excited states should also be accessible from such measurements.

5. Impurity states under external perturbations

As in atomic spectroscopy external perturbation can be exploited to characterise the energy levels of the impurity. To the extent these states have been described in terms of the properties of the energy bands, such studies yield information about the intrinsic properties of the host. For example, the Zeeman effect of the excitation spectra allows one to obtain g factors and effective-mass parameters whereas uniaxial stress studies yield deformation potential constants characterising the relevant band extrema. From the splittings, shifts and the polarisation characteristics of the components of the spectral lines it is possible to establish level degeneracies and give symmetry assignments. In this section we will discuss the effects of uniaxial stress and magnetic field on the excitation spectra of donors and acceptors in semiconductors.

5.1. Effects of uniaxial stress

Under an external stress, the energy band extrema experience shifts and, when the crystal symmetry is lowered, exhibit splittings. Uniaxial stress as a tool in spectroscopy is unique to solid-state physics. Effects observed under uniaxial stress have been aptly described as 'piezospectroscopic' effects by Kaplyanskii (1964a). Under hydrostatic stress, though the crystal symmetry is preserved, the band extrema shift with respect to one another; thus, the particular band extremum relevant for a given set of impurity states can be altered. Due to experimental limitations, studies under hydrostatic stresses are difficult to carry out and we restrict our discussion to uniaxial stresses.

Under a homogeneous strain the symmetry of a crystal is lowered in general, resulting in the lifting of degeneracies associated with the energy levels of an impurity. However, all one-electron states retain at least a two-fold degeneracy arising from time reversal symmetry, referred to as the Kramers degeneracy (see, for example, Landau and Lifshitz 1977). The point group of the stressed crystal consists of the symmetry operations common to the point group of the unstressed crystal and that of the strain ellipsoid. The strain ellipsoid is defined by the quadratic form $\sum_{\alpha,\beta} \varepsilon_{\alpha\beta} x_\alpha x_\beta$ where $\{\varepsilon_{\alpha\beta}\}$ are the components of the symmetric second-rank tensor

$$\varepsilon_{\alpha\beta} = \frac{1}{2} \left(\frac{\partial u_\alpha}{\partial x_\beta} + \frac{\partial u_\beta}{\partial x_\alpha} \right) \quad (5.1)$$

where $u(x_1, x_2, x_3)$ is the displacement field and x_1, x_2, x_3 are coordinates referred to an arbitrary Cartesian coordinate system. In table 9 we list the reduction of the T_d symmetry under applied force F along crystallographic directions of high symmetry.

Table 9. Reduction of T_d symmetry under uniaxial stress.

Direction of force, \mathbf{F}	Site symmetry
[100]	D_{2d}
[110]	C_{2v}
[111]	C_{3v}

Symmetry arguments, while providing qualitative results, are not sufficient for our discussion. Using perturbation theory, Bardeen and Shockley (1950) developed a phenomenological description of the electron energy levels under elastic strain; in such a theory, referred to as the deformation potential theory, the one-electron Hamiltonian is expanded in a Taylor series in $\epsilon_{\alpha\beta}$:

$$H = H_0 + H' = H_0 + \sum_{\alpha\beta} V_{\alpha\beta} \epsilon_{\alpha\beta} + \dots \quad (5.2)$$

In the experiments we discuss the stresses applied are well within the elastic limit and the stress-strain relations are given by the standard elastic compliance constants, $s_{\alpha\beta\gamma\delta}$ (see, for example, Bhagavantam 1966). We also restrict the expansion in (5.2) to terms linear in $\epsilon_{\alpha\beta}$. The quantities $V_{\alpha\beta}$ are operators satisfying $V_{\alpha\beta} = V_{\beta\alpha}$ and are used in the standard perturbation theory to obtain energy shifts and splittings of specific energy levels.

We now apply the above theory to the case of donors in the multi-valley semiconductors, Si and Ge. We recall that the conduction band extrema occur along Δ for Si and at L for Ge. The shift in the energy of a level at \mathbf{k} in the Brillouin zone can be written, within the framework of the deformation potential theory, as the expectation value of $H' = \sum_{\alpha\beta} V_{\alpha\beta} \epsilon_{\alpha\beta}$ for the state in question. The interaction H' can conveniently be written as a linear combination of terms invariant under the operations of the group of \mathbf{k} , i.e. the subgroup of the point group of the crystal leaving \mathbf{k} invariant. For a level with \mathbf{k} parallel to [001], using x, y, z as the cubic axes, the only invariants are $(\epsilon_{xx} + \epsilon_{yy}) (V_{xx} + V_{yy})$ and $\epsilon_{zz} V_{zz}$ so that the change in energy of the level is

$$\Delta E = \Xi_d (\epsilon_{xx} + \epsilon_{yy}) + (\Xi_d + \Xi_u) \epsilon_{zz} \quad (5.3)$$

where Ξ_d and Ξ_u are constants called the dilatational and shear deformation potential constants, respectively, and depend only on the band state. In a similar fashion, for Ge, in which the conduction band minimum occurs at L , with \mathbf{k} parallel to [111],

$$\Delta E = (\Xi_d + \frac{1}{3}\Xi_u) (\epsilon_{xx} + \epsilon_{yy} + \epsilon_{zz}) + \frac{2}{3}\Xi_u (\epsilon_{yz} + \epsilon_{zx} + \epsilon_{xy}). \quad (5.4)$$

Equations (5.3) and (5.4) can be represented compactly as

$$\Delta E(\mathbf{k}^{(j)}) = \sum_{\alpha\beta} (\Xi_d \delta_{\alpha\beta} + \Xi_u \hat{k}_\alpha^{(j)} \hat{k}_\beta^{(j)}) \epsilon_{\alpha\beta} \quad (5.5)$$

where $\hat{k}^{(j)}$ is a unit vector parallel to $\mathbf{k}^{(j)}$, the position of the j th conduction band minimum in \mathbf{k} space.

In the effective-mass approximation, the dependence of the donor levels on strain is also given by equations (5.5). If it is assumed that both the dielectric constant and the effective masses characterising the conduction band minima are unaltered by a small strain, then the energy level scheme of a group V donor in Si or Ge will be unaffected by the stress since equation (3.46) will be unaltered. However, the energy level schemes bearing different valley labels will be shifted relative to one another by amounts given by equation (5.5). Implicit in this deduction is the assumption that Ξ_d and Ξ_u are the same

for all the donor levels as well as the conduction band extremum. Experimentally, this turns out to be a valid assumption for the p states. The chemical splitting of $1s(A_1 + E + T_2)$ and $1s(A_1 + T_2)$ ground states of donors in Si and Ge, respectively, requires the use of a Hamiltonian which includes both chemical splitting and strain; such a calculation has been given by Price (1956) for Ge and by Wilson and Feher (1961) for Si.

In order to compare experimental results with the theory it is useful to note that the shift of the 'centre of gravity' of the valleys is given by

$$\langle \Delta E^{(j)} \rangle = (\Xi_d + \frac{1}{3} \Xi_u) (\varepsilon_{xx} + \varepsilon_{yy} + \varepsilon_{zz}). \quad (5.6)$$

Figure 33 shows the constant-energy ellipsoids of the conduction band minima of Si along $\langle 100 \rangle$. Let \hat{F} be a unit vector along F and T the magnitude of F divided by the

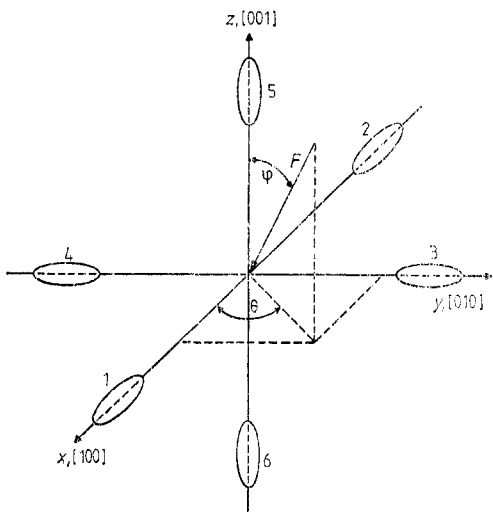


Figure 33. Constant-energy ellipsoids of the conduction band minima of Si along $\langle 100 \rangle$. Also shown, for convenience, are the coordinate axes, the direction of the applied compressive force F and its polar coordinates (after Tekippe *et al* 1972).

cross-sectional area of the sample. It can be shown that the shift of a given valley j with respect to the centre of gravity is given by

$$\delta E^{(j)} = \pm \Xi_u T (s_{11} - s_{12}) [(\hat{k}^{(j)} \cdot \hat{F})^2 - \frac{1}{3}]. \quad (5.7)$$

Similarly for Ge,

$$\delta E^{(j)} = \pm \frac{1}{2} \Xi_u T s_{44} [(\hat{k}^{(j)} \cdot \hat{F})^2 - \frac{1}{3}]. \quad (5.8)$$

Here s_{11} , s_{12} and s_{44} are the elastic compliance constants of the crystal and the + and - signs correspond to tension and compression, respectively. In figure 34 (plate) we show the energy shifts of the conduction band valleys of Si from the centre of gravity for compressive force as a function θ and φ defined in figure 33. It is thus evident that for $F \parallel [100]$, $\delta E^{(1,2)} = -\frac{2}{3} T \Xi_u (s_{11} - s_{12})$ and $\delta E^{(3,4)} = \delta E^{(5,6)} = \frac{1}{3} T \Xi_u (s_{11} - s_{12})$ and the excited p states split into two sublevels, the one of lower energy being shifted twice as much below the centre of gravity as the other is shifted above it. According to Wilson and Feher (1961), the $1s(A_1)$ level shifts from its zero-stress position by

$$\Delta E_{gs} = \Delta_c [3 + \frac{1}{2}x - \frac{2}{3}(x^2 + \frac{4}{3}x + 4)^{1/2}] \quad (5.9)$$

where $6\Delta_c$ is the separation between the $1s(A_1)$ and $1s(E)$ states and

$$x = -[\Xi_u(s_{11} - s_{12}) T]/3\Delta_c \quad (5.10)$$

for compression. Figure 35 gives the energy shifts and splittings of the $1s$ multiplet and an np state for $\mathbf{F} \parallel [100]$, together with their symmetry classification (Aggarwal and Ramdas 1965b).

In figure 36 we show the results of Aggarwal and Ramdas (1965c) for the $1s(A_1) \rightarrow np$ transitions in Si(As) subjected to uniaxial compression along [100]; polarised light was used with the electric vector \mathbf{E} either parallel or perpendicular to \mathbf{F} . As can be seen, each excitation line splits into two components, $np(+)$ and $np(-)$; here + and - signs denote the high- and low-energy components with respect to the zero-stress position. In figure 37 we show the position of the $1s(A_1) \rightarrow 2p_{\pm}(+)$ and $1s(A_1) \rightarrow 2p_{\pm}(-)$ components

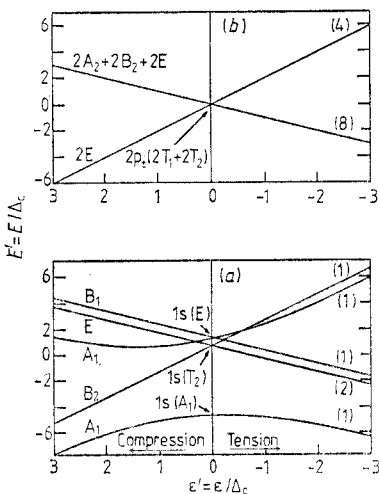


Figure 35. Splitting of the $1s$ ground-state multiplet (a) and the $2p_{\pm}$ state (b) of a group V donor in Si for $\mathbf{F} \parallel [100]$. The numbers in parenthesis indicate the degeneracies of the various states while the letters denote the irreducible representations of D_{2d} , the site symmetry of the donor for $\mathbf{F} \parallel [100]$. $E' = (E/\Delta_c)$ and $e' = (e/\Delta_c)$ where E is the energy of a given state, $\Delta_c = \frac{1}{3}$ (spacing between $1s(E)$ and $1s(A_1)$) and 3ϵ is the energy difference between the $\langle 100 \rangle$ conduction band minima (after Aggarwal and Ramdas 1965b).

of Si(P) as a function of stress (Tekippe *et al* 1972). The full straight lines are energy shifts of the two components of the $2p_{\pm}$ line from the zero-stress position calculated from their energy difference divided in the ratio 2:1. The full curves are due to the shift of the $1s(A_1)$ ground state with stress. The full points are computed by taking the difference between the straight lines and the data points. In figure 38 we display the splitting $\Delta E_{2p_{\pm}} = E_{2p_{\pm}(+)} - E_{2p_{\pm}(-)}$, as a function of stress for Si(Sb), Si(As), Si(P) and Si(Mg). The linear dependence of $\Delta E_{2p_{\pm}}$ with stress has the same slope for all the impurities and yields $\Xi_u = (8.77 \pm 0.07)$ eV. A similar study for Si(Bi) by Butler *et al* (1975) gave $\Xi_u = (8.77 \pm 0.14)$ eV. The value for Ξ_u determined in this manner from the piezospectroscopy of donors equals within experimental error that of the conduction band minimum (Tekippe *et al* 1972). Jagannath and Ramdas (1981) show that the Ξ_u characterising the energy levels of interstitial lithium donors in Si is equal to that of the conduction band. Tekippe *et al* (1972) found that the Ξ_u for the $1s(A_1)$ state is significantly lower than that

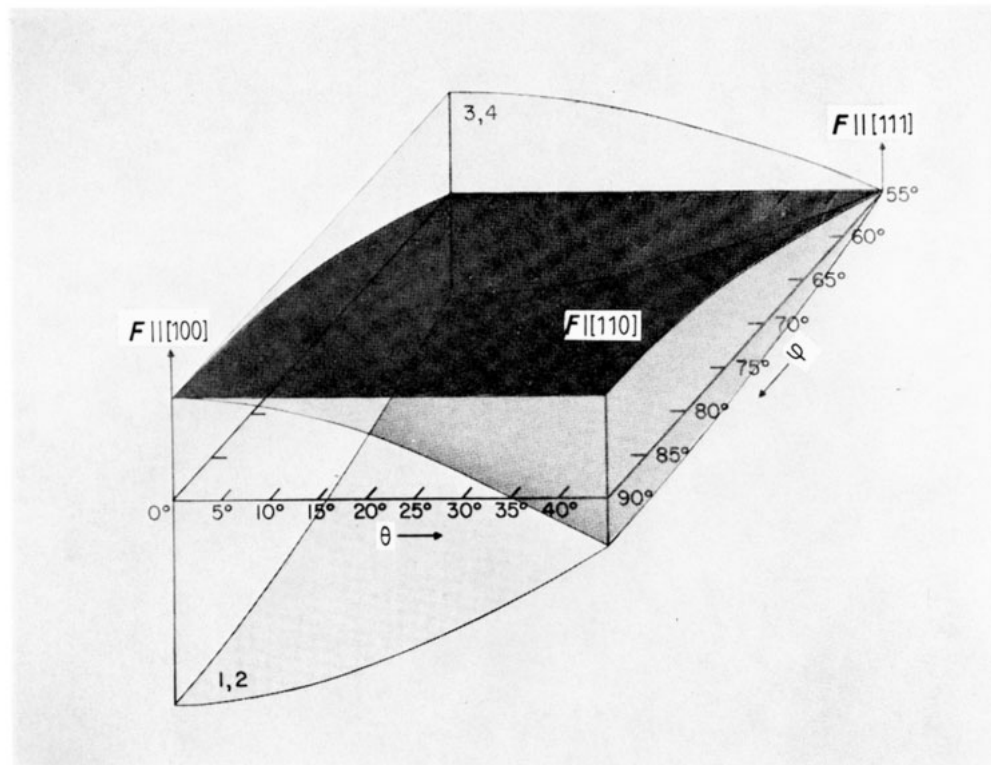


Figure 34. Energy shifts of the conduction band valleys of Si from the centre of gravity as a function of θ and φ defined in figure 33. The horizontal plane corresponds to the centre of gravity of the valleys. The energy sheet labelled '1, 2' corresponds to valleys along [100] and [$\bar{1}00$], the sheet labelled '3, 4' to those along [010] and [0 $\bar{1}0$], and the third sheet corresponds to valleys along [001] and [00 $\bar{1}$] (after Tekippe *et al* 1972).

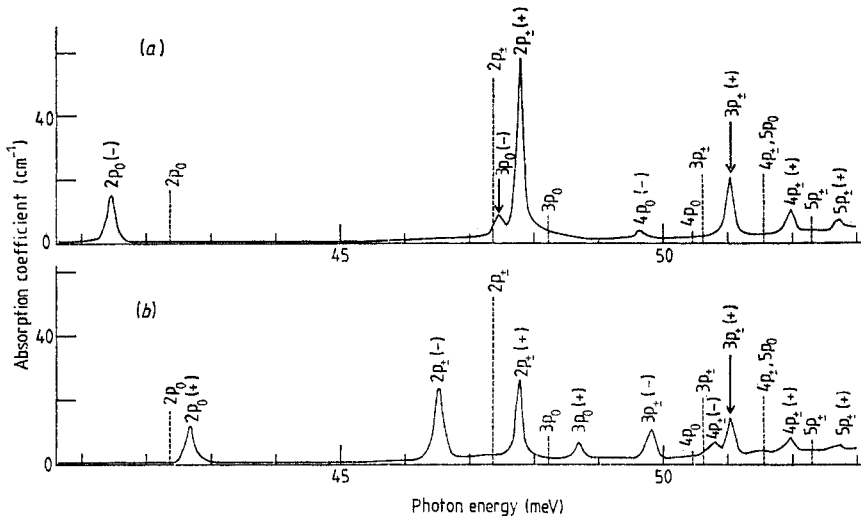


Figure 36. The effect of uniaxial stress on the excitation spectrum of Si (As) for $F \parallel [100]$; \mathbf{q} is the direction of light propagation. Measurements were made using liquid helium as coolant. Donor concentration $n \sim 3 \times 10^{15} \text{ cm}^{-3}$ (after Aggarwal and Ramdas 1965c). (a) $E \parallel F$, $\mathbf{q} \parallel [011]$, (b) $E \perp F$, $\mathbf{q} \parallel [011]$.

for the np states, decreasing with increasing $6\Delta_e$. Jagannath and Ramdas (1981) report that Ξ_u for the $1s(E + T_2)$ state of Si(Li) is identical to that of the np states.

The striking polarisation features of the stress-induced components shown in figure 36 can be explained on the basis of the electric dipole selection rules shown in figure 39. These have been derived within the framework of the effective-mass approximation. In table 10 we show the symmetry classification of the stress-induced sublevels for donors in

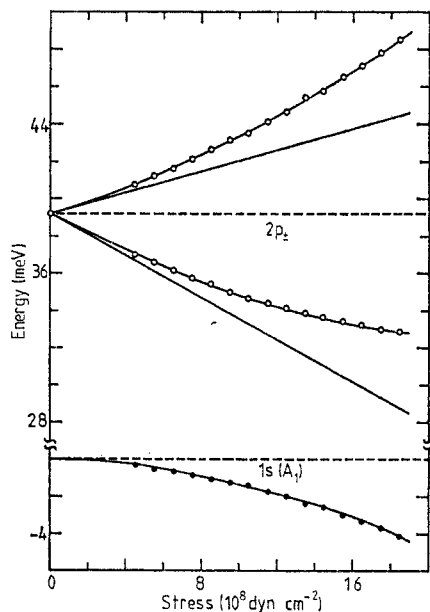


Figure 37. Stress dependence of the energies of the two components of the $1s(A_1) \rightarrow 2p_{\pm}$ line of Si(P) for $F \parallel [100]$ (after Tekippe *et al* 1972).

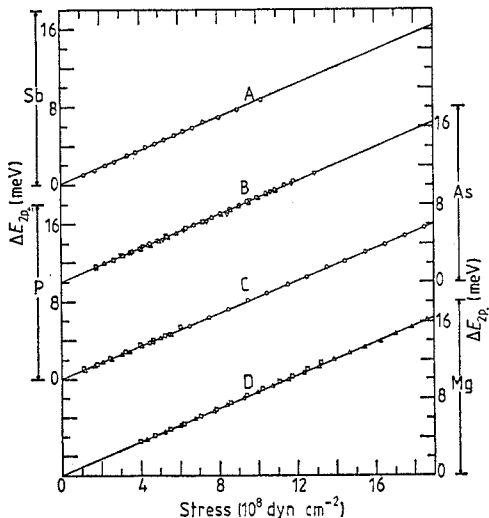


Figure 38. Splitting of the $1s(A_1) \rightarrow 2p_{\pm}$ line with $F \parallel [100]$ as a function of stress for Sb, As, P and Mg donors in Si. The full lines represent least squares fits to all the data points for a given impurity (after Tekippe *et al.* 1972). A, Sb; \circ , sample Si(Sb) no 1.7; B, As, sample Si(As) no 1.2; Δ , run 1, \circ , run 2, \square , run 3, ∇ , run 4; C, P; \circ , sample Si(P) no 1.3, Δ , sample Si(P) no 1.8, run 1, \square , sample Si(P) no 1.8, run 2; D, Mg; Δ , sample Si(Mg) no 13, run 1, \square , sample Si(Mg) no 13, run 2.

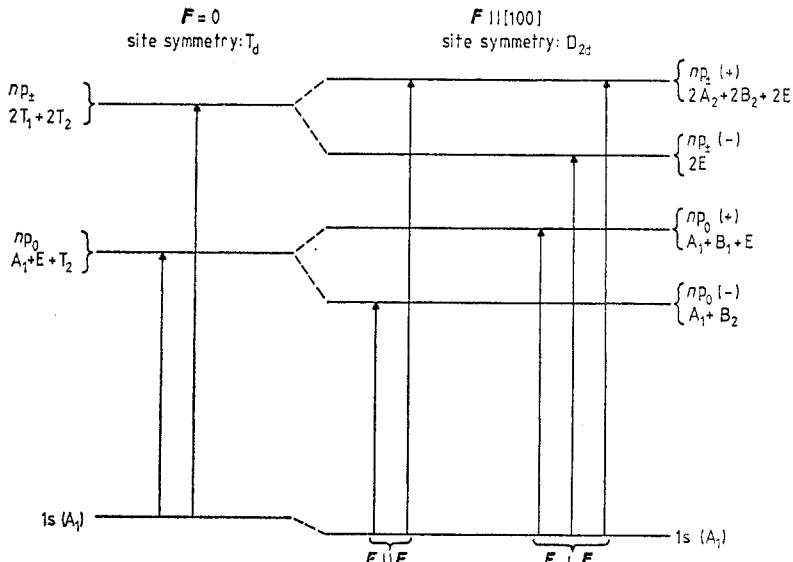


Figure 39. Energy levels of donors in Si (not to scale) for $F=0$ and $F \parallel [100]$. The arrows indicate the allowed transitions with $1s(A_1)$ as the ground state. The letters next to a level denote the irreducible representations of the appropriate site symmetry (after Aggarwal and Ramdas 1965a).

Table 10. Classification of p states of donors in silicon and germanium under uniaxial compression.

Crystal	Direction of compression	Symmetry of impurity valleys†	Symmetry of valleys‡	$\Gamma(D_{2n})$		$\Gamma(\text{valley})$	$\Gamma(\text{impurity})$	Level scheme	
				$F=0$	$F \neq 0$	$F \neq 0$		$F=0$	$F \neq 0$
Si	[100]	D _{2d}	C ₆ (3, 4, 5, 6)	0	Σ_u^+	A ₁	A ₁ +B ₁ +E	A ₁ +B ₁ +E	(3, 4, 5, 6)
			C _{2v} (1, 2)				A ₁ +E+T ₂	A ₁ +B ₂	(1, 2)
			C ₂ (3, 4, 5, 6)		2B	2A ₂ +2B ₂ +2E		2A ₂ +2B ₂ +2E	(3, 4, 5, 6)
				±1	Π_u		2T ₁ +2T ₂		
			C _{2v} (1, 2)			B ₁ +B ₂	2E	2E	(1, 2)
Ge	[111]	C _{3v}	C ₆ (2, 3, 4)	0	Σ_u^+	A'	A ₁ +E	A ₁ +E	(2, 3, 4)
			C _{3v} (1)			A ₁		A ₁	(1)
			C ₆ (2, 3, 4)		A'+A''	A ₁ +A ₂ +2E		A ₁ +A ₂ +2E	(2, 3, 4)
				±1	Π_u		E+T ₁ +T ₂	E	
			C _{3v} (1)			E	E	E	(1)

† The numbers in parentheses label the valleys and indicate to which subgroup a given valley belongs. For silicon the valleys are numbered as follows: 1, [100]; 2, [100]; 3, [010]; 4, [010]; 5, [001] and 6, [001], while for germanium they are: 1, [111]; 2, [111]; 3, [111] and 4, [111].

Si and Ge with $F \parallel [100]$ and [111], respectively. The procedure used is similar to that followed to construct table 3 (Aggarwal and Ramdas 1965a).

The effect of uniaxial compression on the $1s(E) \rightarrow np$ and $1s(T_2) \rightarrow np$ transitions for Si(P) is shown in figure 40. The $1s(E) \rightarrow np$ transitions show low- and high-energy components as well as a component at the zero-stress position. On the other hand, the $1s(T_2) \rightarrow np$ transitions do not split and yield only a zero-stress component. These

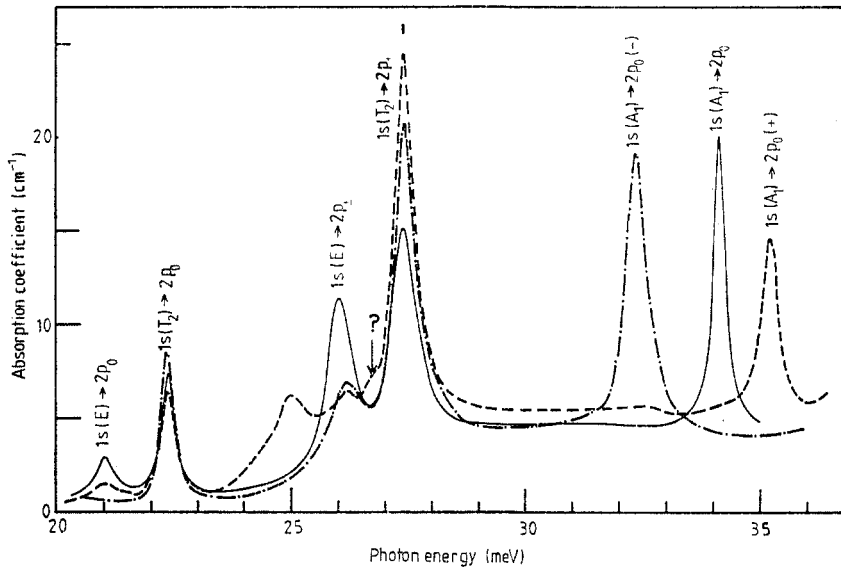


Figure 40. The effect of a [100] compression on the $1s(A_1) \rightarrow 2p_0$, $1s(T_2) \rightarrow 2p_0$, $2p_{\pm}$, $1s(E) \rightarrow 2p_0$, $2p_{\pm}$ transition in Si(P) at 59 K. n , the donor concentration, $\approx 5.2 \times 10^{15} \text{ cm}^{-3}$ (after Aggarwal and Ramdas 1965b). —, $F=0$; - - -, $E \parallel F$, $F \parallel [100]$, $q \parallel [011]$; - · - , $E \perp F$, $F \parallel [100]$, $q \parallel [011]$.

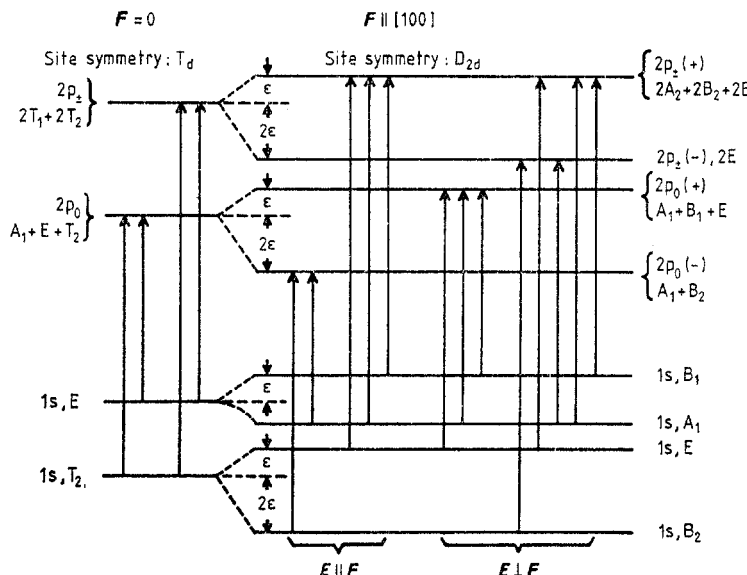


Figure 41. Energy levels (not to scale) of a group V donor for $F=0$ and $F \parallel [100]$. The arrows indicate the allowed transitions. The letters next to a level denote the representations of the appropriate site symmetry.

observations, together with the polarisation characteristics of the stress-induced components, can be deduced from figure 41. We note that it is possible to distinguish transitions originating from the $1s(A_1)$, $1s(E)$ or $1s(T_2)$ ground states by recognising that they give rise to 2, 3 and 1 components, respectively, under uniaxial stress.

As remarked in §4.2, the ground-state multiplet of Si(Li) is inverted, $1s(E+T_2)$ lying below $1s(A_1)$. Under compressive force, say along [001], the $1s(E+T_2) \rightarrow np$ transitions thus show three components, one at the zero-stress position and one each on either side of it, as can be seen in figure 42 (Jagannath and Ramdas 1981). At a slightly elevated temperature, Aggarwal *et al* (1965) observed the $1s(A_1) \rightarrow np$ transition which split into two components, one on either side of the zero-stress position. These observations constitute a convincing demonstration of the inverted nature of the ground-state multiplet.

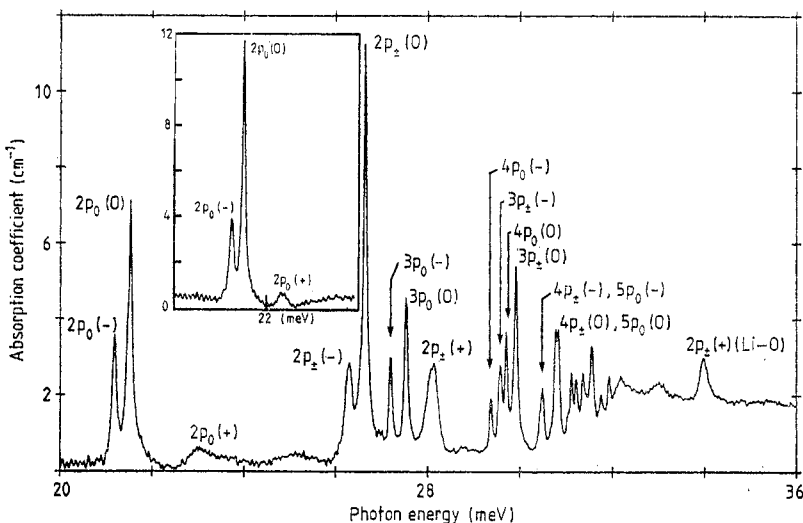


Figure 42. The effect of compressive force F along [001] on the excitation spectrum of Si(Li). T , the force per unit area, is 1.95×10^8 dyn cm $^{-2}$. The inset shows the three components of the $1s(E+T_2) \rightarrow 2p_0$ for $T = 1.12 \times 10^8$ dyn cm $^{-2}$. Measurements made using liquid helium as coolant. Si(Li) no 11 (after Jagannath and Ramdas 1981).

Piezospectroscopy of excitation lines of donors has also been useful in establishing the non-cubic symmetry of sulphur and a species of Li-O donor complexes in Si. Non-cubic centres randomly distributed in the crystal exhibit collectively what has been described by Kaplyanskii (1964b) as ‘orientational degeneracy’. Under uniaxial compression this degeneracy may be lifted; this results in the $1s(A_1)$ ground states for the different sub-groups of centres being shifted by different amounts and additional splittings associated with this behaviour are observed. Such effects have been reported for Si(S) by Krag *et al* (1966) and Jagannath and Ramdas (1981).

Piezospectroscopy of Ge(As) and Ge(Sb) have been studied by Reuszer and Fisher (1965, 1968). Their observations on the stress-induced splittings and their dichroic behaviour are in excellent agreement with symmetry considerations, the deformation potential theory and the stress behaviour of the $1s(A_1)$ and $1s(T_2)$ states separated by chemical splitting. Martin *et al* (1979, 1981) have determined $\Xi_u = (16.4 \pm 0.2)$ eV for the conduction band minimum of Ge from a quantitative study of the $1s(A_1) \rightarrow 2p_0$ line

of Ge(As). Gorman and Solin (1977) have investigated the effect of uniaxial stress in the $1s(A_1) \rightarrow 1s(T_2)$ transition observed in the electronic Raman effect.

Ahlburn and Ramdas (1968) have investigated the excitation spectrum of AlSb(Te) and AlSb(Se) under uniaxial stress. Scott and Onffroy (1976) have reported the results of similar studies in GaP(Si) and GaP(S). The results have been interpreted in a manner analogous to the case of donors in Si. The differences in the symmetries of the ground and excited states of GaP(S) on the one hand and GaP(Si) on the other, discussed in §4.6, have been confirmed by Scott and Onffroy (1976) on the basis of the observed splittings of the lines and their polarisation characteristics.

We now turn our attention to the piezospectroscopy of acceptors in Si and Ge. As we have already noted, the acceptor states reflect the degeneracy of the $\Gamma_8^+(p_{3/2})$ and the $\Gamma_7^+(p_{1/2})$ valence band maxima. For F in an arbitrary direction, the Γ_8^+ state shifts and splits into two Kramers doublets whereas the Γ_7^+ state merely shifts. In order to exploit symmetry arguments to the best advantage, we rewrite the strain-induced Hamiltonian H' as the sum of terms involving the irreducible components of the strain tensor. We note that the components of symmetric second-rank tensor generate the representation

$$[\Gamma_5^- \times \Gamma_5^-] = \Gamma_1^+ + \Gamma_3^+ + \Gamma_5^+. \quad (5.11)$$

The combination $\varepsilon_{xx} + \varepsilon_{yy} + \varepsilon_{zz}$ belongs to Γ_1^+ , $2\varepsilon_{zz} - \varepsilon_{xx} - \varepsilon_{yy}$ and $\sqrt{3}(\varepsilon_{xx} - \varepsilon_{yy})$ generate the irreducible representation Γ_3^+ whereas ε_{yz} , ε_{zx} , ε_{xy} generate Γ_5^+ . This permits us to write

$$\begin{aligned} H' = & \frac{1}{3}(V_{xx} + V_{yy} + V_{zz})(\varepsilon_{xx} + \varepsilon_{yy} + \varepsilon_{zz}) + \frac{1}{6}(2V_{zz} - V_{xx} - V_{yy})(2\varepsilon_{zz} - \varepsilon_{xx} - \varepsilon_{yy}) \\ & + \frac{1}{2}(V_{xx} - V_{yy})(\varepsilon_{xx} - \varepsilon_{yy}) + 2(V_{yz}\varepsilon_{yz} + V_{zx}\varepsilon_{zx} + V_{xy}\varepsilon_{xy}). \end{aligned} \quad (5.12)$$

Within the framework of the first-order degenerate perturbation theory, it is appropriate to express the submatrices for each multiplet in terms of phenomenological constants, called deformation potential constants. For a Γ_8^+ multiplet the interaction submatrix H' is a linear combination of 16 linearly independent Hermitian matrices. These, in turn, can be constructed from J_x , J_y , J_z , the angular momentum matrices for $j=\frac{3}{2}$, by taking their powers and products (Karthäuser *et al* 1974). Using Unsöld's theorem, one can show that the only invariant combinations of such matrices which also satisfy time reversal invariance are $\sum_i \varepsilon_{ii} \sum_j J_j^2$, $(2\varepsilon_{zz} - \varepsilon_{xx} - \varepsilon_{yy})(2J_z^2 - J_x^2 - J_y^2) + 3(\varepsilon_{xx} - \varepsilon_{yy}) \times (J_x^2 - J_y^2) = 2\sum_i \varepsilon_{ii} (3J_i^2 - J^2)$ and $\sum_{i < j} \varepsilon_{ij} \{J_i J_j\}$. Thus we can write

$$H' = -a \sum_i \varepsilon_{ii} - b \sum_i \varepsilon_{ii} (J_i^2 - \frac{1}{3}J^2) - \frac{2d}{\sqrt{3}} \sum_{i < j} \varepsilon_{ij} \{J_i J_j\}. \quad (5.13)$$

Here a , b and d are the deformation potentials for the Γ_8^+ multiplet. If the magnitude of the spin-orbit interaction, λ , is comparable or smaller than the strain energy, it is necessary to consider the Γ_8^+ and Γ_7^+ multiplets as a single entity. Then the $\Gamma_5^+ \times \Gamma_6^+$ states are described by

$$H' + H_{s=0} = -a \sum_i \varepsilon_{ii} - 3b \sum_i \varepsilon_{ii} (I_i^2 - \frac{1}{3}I^2) - 2d \sqrt{3} \sum_{i < j} \varepsilon_{ij} \{I_i I_j\} + \frac{1}{3} \lambda \mathbf{J} \cdot \boldsymbol{\sigma}. \quad (5.14)$$

Here σ_i are the 2×2 Pauli spin matrices and I_i are 3×3 angular momentum matrices. The operator $H' + H_{s=0}$ is to be understood as a 6×6 matrix. If the spin-orbit splitting is large compared to H' it is adequate to use (5.13).

We will consider the energy states of a bound hole in the rest of our discussion and hence all the terms in the right-hand side of equations (5.13) and (5.14) will have the opposite sign. We note that equations (5.13) and (5.14) refer to the valence band of the host crystal and hence has the full symmetry \bar{O}_h . It is clear that the lower \bar{T}_d symmetry appropriate for the bound hole does not introduce any changes in the form of these equations. In principle, of course, the deformation potential constants will be different for different bound states. Bir *et al* (1963) and Suzuki *et al* (1964) have calculated the deformation potential constants of the ground state of the acceptors in the effective-mass approximation. We first consider the case of λ large. It can be shown (Chandrasekhar *et al* 1973, Bir and Pikus 1974) that the centre of gravity of a Γ_8 multiplet of an acceptor is shifted by a $\Sigma \epsilon_{ii}$ whereas it splits into two doublets separated by the energy Δ given by

$$\Delta^2 = 2b^2[(\epsilon_{xx} - \epsilon_{yy})^2 + (\epsilon_{yy} - \epsilon_{zz})^2 + (\epsilon_{zz} - \epsilon_{xx})^2] + 4d^2(\epsilon_{xy}^2 + \epsilon_{yz}^2 + \epsilon_{zx}^2). \quad (5.15)$$

For uniaxial stress with F along an axis with direction cosines α_x , α_y and α_z

$$\Delta^2(\alpha_x, \alpha_y, \alpha_z) = \Delta_{100}^2 + 3(\Delta_{111}^2 - \Delta_{100}^2) K(\alpha_x, \alpha_y, \alpha_z)$$

where $\Delta_{100} = 2b(s_{11} - s_{12})T$, $\Delta_{111} = (d/\sqrt{3})s_{44}T$ and $K(\alpha_x, \alpha_y, \alpha_z) = \alpha_x^2\alpha_y^2 + \alpha_y^2\alpha_z^2 + \alpha_z^2\alpha_x^2$; $|\Delta_{100}|$ and $|\Delta_{111}|$ are the energy separations of the doublets for $F \parallel \langle 100 \rangle$ and $F \parallel \langle 111 \rangle$, respectively. It is interesting to note that if $|\Delta_{100}| = |\Delta_{111}|$, then $\Delta(\alpha_x, \alpha_y, \alpha_z)$ is the same for any direction of F ; we refer to this as 'stress isotropy'. The extrema of K occur for $F \parallel \langle 111 \rangle$, $\langle 110 \rangle$ and $\langle 100 \rangle$, these being $\frac{1}{3}$, $\frac{1}{4}$, and 0, respectively.

In figure 43 the stress-induced splitting of the $\Gamma_8 \rightarrow \Gamma_8$, $\Gamma_8 \rightarrow \Gamma_6$ and $\Gamma_8 \rightarrow \Gamma_7$ transitions for $F \parallel \langle 111 \rangle$ and $F \parallel \langle 100 \rangle$ are shown. The figure also shows the selection rules for electric dipole transitions. In table 11 we give the symmetries and eigenvalues of the stress-induced sublevels of a Γ_8 state for $F \parallel \langle 111 \rangle$ and $\langle 100 \rangle$.

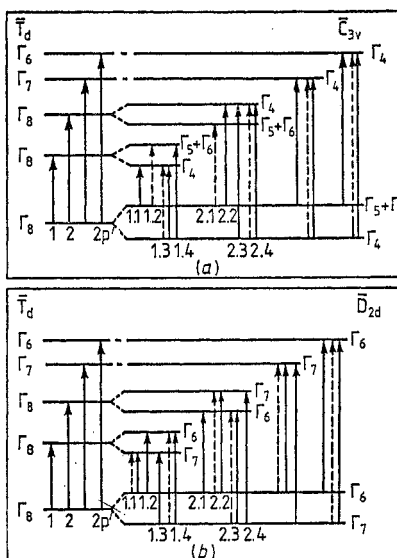


Figure 43. The allowed transitions from a Γ_8 ground state to Γ_6 , Γ_7 and Γ_8 excited states of the double group \bar{T}_d with compressive force F along $\langle 111 \rangle$ (a) or $\langle 100 \rangle$ (b). The site symmetry is C_{3v} and D_{2d} for the $\langle 111 \rangle$ and $\langle 100 \rangle$ compressions, respectively; the designations next to the levels denote the irreducible representations of the appropriate double point group following the notation of Koster *et al* (1963).

Table 11. Symmetries and eigenvalues of stress-induced sublevels of a Γ_8 state for $\mathbf{F} \parallel \langle 111 \rangle$ and $\langle 100 \rangle$.

Direction of \mathbf{F}	State	Eigenvalue ^a
$\langle 111 \rangle$	$\Gamma_5 + \Gamma_6(\bar{\text{C}}_{3v})$	$a(s_{11} + 2s_{12}) T + (d/2\sqrt{3}) s_{44} T$
	$\Gamma_4(\bar{\text{C}}_{3v})$	$a(s_{11} + 2s_{12}) T - (d/2\sqrt{3}) s_{44} T$
$\langle 100 \rangle$	$\Gamma_6(\bar{\text{D}}_{2d})$	$a(s_{11} + 2s_{12}) T + b(s_{11} - s_{12}) T$
	$\Gamma_7(\bar{\text{D}}_{2d})$	$a(s_{11} + 2s_{12}) T - b(s_{11} - s_{12}) T$

^a Following Pikus and Bir (1960), the eigenvalues are those of the bound hole; Kleiner and Roth (1959) use electron energy. The definitions of the deformation potential constants of the latter are related to those of the former by $D_u = -\frac{3}{2}b$ and $D_{u'} = -\frac{1}{2}\sqrt{3}d$.

In figure 44 the excitation spectrum of Si(B) under $\mathbf{F} \parallel \langle 111 \rangle$ is shown (Onton *et al* 1967a). As can be seen lines 1 and 2 split into four components expected for a $\Gamma_8 \rightarrow \Gamma_8$ transition. The 2p' line, on the other hand, splits into two components consistent with a $\Gamma_8 \rightarrow \Gamma_6$ transition. The ordering of the ground-state sublevels has been deduced on the basis of the polarisation and thermal depopulation effects shown in the figure. This, in turn, permitted the ordering of the sublevels of the excited states for lines 1 and 2. The positions of the high- and low-energy components of the 2p' line, 2p'(+) and 2p'(-), are shown in figure 45 for $\mathbf{F} \parallel \langle 110 \rangle$, $\langle 100 \rangle$ and $\langle 111 \rangle$. In figure 46 we show the spacing $2p'(+) - 2p'(-) = \Delta$ as a function of stress (Chandrasekhar *et al* 1973). The slopes of the stress dependence of Δ give b_0 and d_0 , the ground-state deformation potential constants. It is interesting to note that, within experimental error, $|\Delta_{111}| = |\Delta_{100}| = |\Delta_{110}|$ yielding the stress isotropy referred to earlier. The origin of this stress isotropy of the ground state of Si(B) is not yet explained. The positions of the stress-induced com-

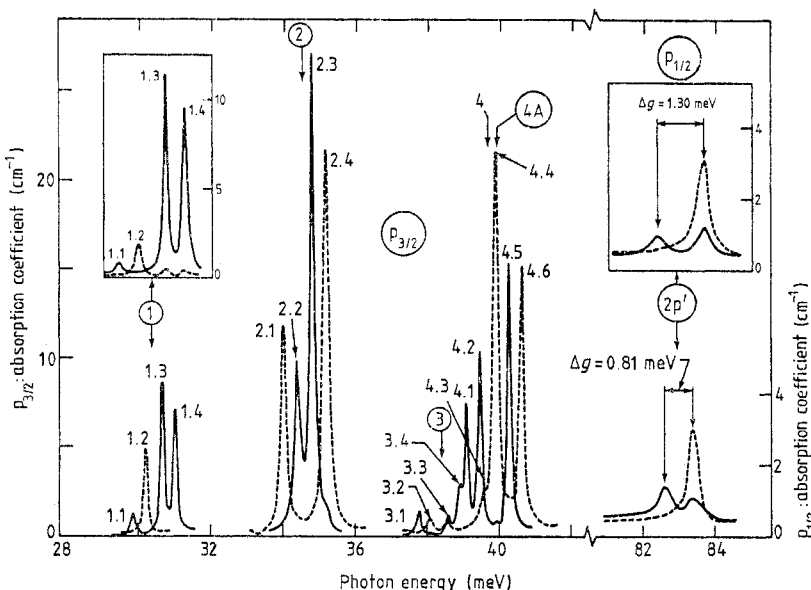


Figure 44. The effect of uniaxial stress on excitation lines 1–4A and 2p' of Si(B) (Si(B) no 5). $\mathbf{F} \parallel \langle 111 \rangle$. The two insets show the effect of a larger stress on lines 1 and 2p'. Liquid helium used as coolant. $p(300 \text{ K}) = 1.5 \times 10^{15} \text{ cm}^{-3}$ (after Onton *et al* 1967a). ---, $\mathbf{E} \parallel \mathbf{F}$; —, $\mathbf{E} \perp \mathbf{F}$.

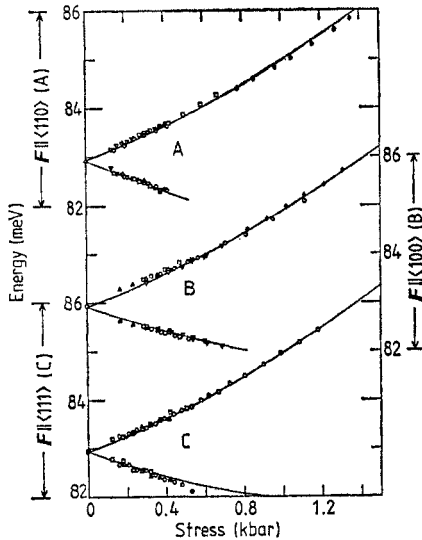


Figure 45. Stress dependence of the components of the 2p' line of Si(B) for $F \parallel \langle 111 \rangle$, $\langle 100 \rangle$ or $\langle 110 \rangle$ (after Chandrasekhar *et al* 1973). A: Si(B) no 8, $F \parallel \langle 110 \rangle$; \triangle run 13, ∇ run 14, \square run 15, \circ run 16, \diamond run 20. B: Si(B) no 7, $F \parallel \langle 100 \rangle$; ∇ run 9, \triangle run 10, \square run 11, \circ run 12, \blacklozenge run 22. C: Si(B) no 4, $F \parallel \langle 111 \rangle$; \square run 5, \circ run 6, \blacktriangle run 7.

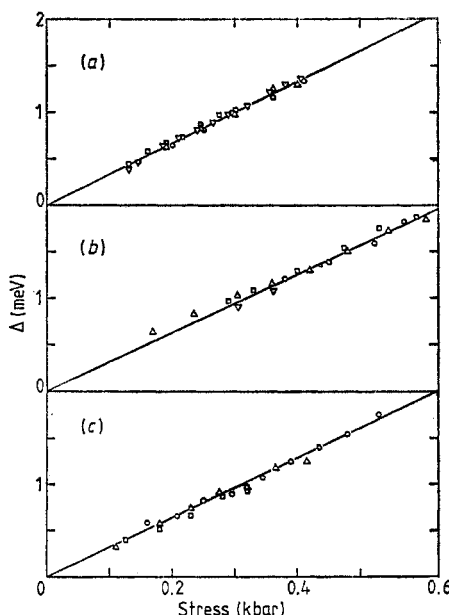


Figure 46. Stress dependence of $\Delta = E[2p'(+) - E[2p'(-)]$ for $F \parallel \langle 111 \rangle$, $\langle 100 \rangle$ or $\langle 110 \rangle$ of Si(B) (after Chandrasekhar *et al* 1973). (a) Si(B) no 8, $F \parallel \langle 110 \rangle$; (b) Si(B) no 7, $F \parallel \langle 100 \rangle$; (c) Si(B) no 4, $F \parallel \langle 111 \rangle$.

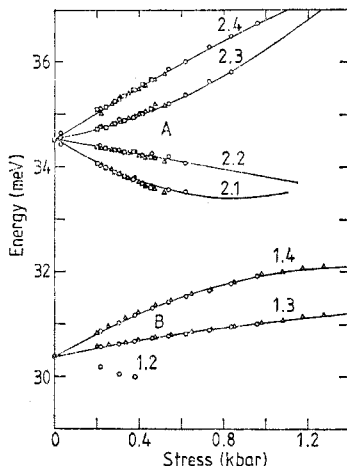


Figure 47. Stress dependence of the energies of the components of line 1 and line 2 in Si(B) for $F \parallel \langle 111 \rangle$ (after Chandrasekhar *et al* 1973). A, Si(B) no 5, $F \parallel \langle 111 \rangle$, \square run 17, \triangle run 18, \circ run 19. B: $F \parallel \langle 111 \rangle$, \triangle run 3, Si(B) no 2; \circ run 19, Si(B) no 5.

ponents of lines 1 and 2 as a function of stress are shown in figure 47. The non-linear stress dependence exhibited in particular by lines 2.1, 2.3 and 1.4 can be explained on the basis of the hybridisation of the $\Gamma_5 + \Gamma_6$ sublevels of the excited states of lines 1 and 2. This hybridisation results in unusual stress dependence of the relative intensities of the components. These aspects of the problem are discussed in detail by Chandrasekhar *et al* (1973).

The piezospectroscopy of acceptors in germanium has been investigated by Jones and Fisher (1964, 1970), Fisher *et al* (1966), Dickey and Dimmock (1967), Rodriguez *et al* (1972) and Barra *et al* (1973). These studies have yielded the symmetry of the ground and excited states of group III acceptors and of the group II acceptors Zn and Zn^- . In the case of Ge(Zn^-), hybridisation effects analogous to those of lines 1 and 2 in Si(B) were observed for lines G and D (Butler and Fisher 1976, Duff *et al* 1980). In figure 48(a) and (b) we show the dramatic increase in the intensity of one of the stress-induced components of line G in Ge(Zn^-) for $F \parallel \langle 111 \rangle$ (Butler and Fisher 1976).

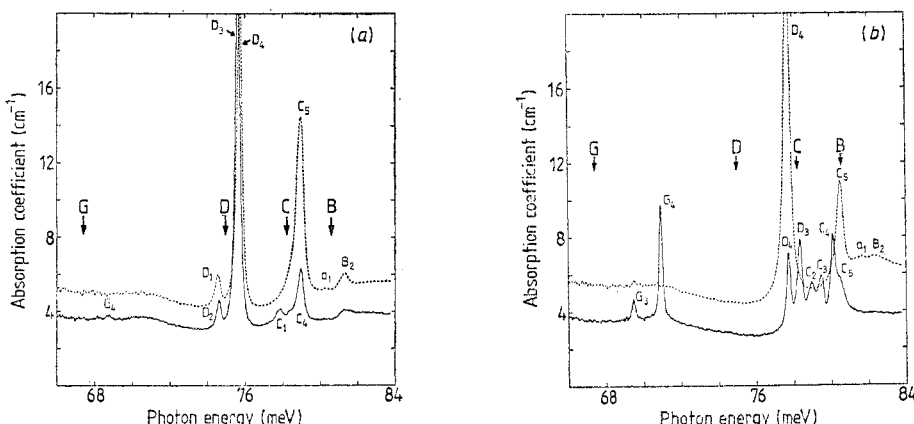


Figure 48. Excitation spectrum of Ge(Zn^-) for $F \parallel \langle 111 \rangle$. (a) stress = 0.55 kbar, (b) stress = 2.21 kbar (after Butler and Fisher 1976). ---, $E \parallel F$; —, $E \perp F$. Ge(Zn, Sb) 436A–4A.

The relative intensities of the stress-induced components of a given transition can be exploited in making symmetry assignments for the sublevels of the initial and final states (Rodriguez *et al* 1972). This proves to be valuable when polarisation features alone do not give a unique assignment. This approach is valid only in the absence of significant hybridisation with adjacent states. In tables 12 and 13 the results of Rodriguez *et al* (1972) for $F \parallel [111]$ and [100] are presented. These results are obtained by calculating the matrix elements of the electric dipole moment operator \mathbf{Q} for the different components

Table 12. Relative intensities for stress-induced components of acceptors in Si and Ge with $F \parallel [111]$.[†]

Zero-stress transition	Stress-induced component	Relative intensity‡	
		E_{\parallel}	E_{\perp}
$\Gamma_8 \rightarrow \Gamma_6$	$\Gamma_4 \rightarrow \Gamma_4$	4	1
	$\Gamma_{5+6} \rightarrow \Gamma_4$	0	3
$\Gamma_8 \rightarrow \Gamma_7$	$\Gamma_4 \rightarrow \Gamma_4$	4	1
	$\Gamma_{5+6} \rightarrow \Gamma_4$	0	3
$\Gamma_8 \rightarrow \Gamma_8$	$\Gamma_4 \rightarrow \Gamma_4$	$\frac{1}{2}(1-u)$	$\frac{1}{2}u$
	$\Gamma_4 \rightarrow \Gamma_{5+6}$	0	$\frac{1}{2}-u/4$
	$\Gamma_{5+6} \rightarrow \Gamma_4$	0	$\frac{1}{2}-u/4$
	$\Gamma_{5+6} \rightarrow \Gamma_{5+6}$	$\frac{1}{2}(1+u)$	0

† E_{\parallel} and E_{\perp} designate radiation polarised parallel and perpendicular to F respectively.

‡ The parameter u ranging between 0 and 1 is defined in terms of ratios of the magnitudes of matrix elements appropriate to the different unperturbed multiplets.

Table 13. Relative intensities for stress-induced components of acceptors in Si and Ge with $F \parallel [001]$.[†]

Zero-stress transition	Stress-induced components	Relative intensity†	
		E_{\parallel}	E_{\perp}
$\Gamma_8 \rightarrow \Gamma_6$	$\Gamma_6 \rightarrow \Gamma_6$	0	3
	$\Gamma_7 \rightarrow \Gamma_6$	4	1
$\Gamma_8 \rightarrow \Gamma_7$	$\Gamma_6 \rightarrow \Gamma_7$	4	1
	$\Gamma_7 \rightarrow \Gamma_7$	0	3
$\Gamma_8 \rightarrow \Gamma_8$	$\Gamma_6 \rightarrow \Gamma_6$	0	$3u/8$
	$\Gamma_6 \rightarrow \Gamma_7$	$\frac{1}{2}-v$	$\frac{1}{2}(1-3u/4+v)$
	$\Gamma_7 \rightarrow \Gamma_6$	$\frac{1}{2}+v$	$\frac{1}{2}(1-3u/4-v)$
	$\Gamma_7 \rightarrow \Gamma_7$	0	$3u/8$

† Here v is defined in a manner similar to u and ranges from $-\frac{1}{2}$ to $\frac{1}{2}$.

of the multiplets. For a transition between two Γ_8 states the matrix elements with respect to states diagonalising J_z are linear combinations of U and V where

$$U_x = \{J_y J_z\} \quad U_y = \{J_z J_x\} \quad U_z = \{J_x J_y\} \quad (5.16)$$

and

$$V_x = \{J_x (J_y^2 - J_z^2)\} \quad V_y = \{J_y (J_z^2 - J_x^2)\} \quad V_z = \{J_z (J_x^2 - J_y^2)\}. \quad (5.17)$$

For transitions from a Γ_8 state to either a Γ_6 or a Γ_7 state, the matrices of \mathbf{Q} in this

representation are proportional to

$$\begin{pmatrix} -\sqrt{3}(\hat{x}+i\hat{y}) & 2\hat{z} & \hat{x}-i\hat{y} & 0 \\ 0 & -(\hat{x}+i\hat{y}) & 2\hat{z} & \sqrt{3}(\hat{x}-i\hat{y}) \end{pmatrix} \quad (5.18)$$

and

$$\begin{pmatrix} (\hat{x}-i\hat{y}) & 0 & \sqrt{3}(\hat{x}+i\hat{y}) & 2\hat{z} \\ 2\hat{z} & -\sqrt{3}(\hat{x}-i\hat{y}) & 0 & -(\hat{x}+i\hat{y}) \end{pmatrix} \quad (5.19)$$

respectively. Here \hat{x} , \hat{y} , \hat{z} are unit vectors along the cubic axes. Thus, in order to obtain the relative intensities of the stress-induced components associated with a $\Gamma_8 \rightarrow \Gamma_8$ transition, it is enough to obtain two independent, non-zero, matrix elements of \mathbf{Q} while for $\Gamma_8 \rightarrow \Gamma_6$ and $\Gamma_8 \rightarrow \Gamma_7$ only one such quantity suffices. Needless to say, one must obtain, in each case, the transformation from the states diagonalising J_z to the eigenfunctions of the stress Hamiltonian. More details can be found in the work of Kartheuser *et al* (1974).

5.2. Effect of a magnetic field on donors and acceptors

As in atomic spectroscopy, the perturbation produced by a magnetic field causes substantial changes in the energy levels of an electron in a crystal. Unlike an elastic strain, the magnetic field breaks the time reversal invariance of the system. This results in the splitting of the otherwise degenerate Kramers doublets of the electron levels. We discuss first the effect of an external magnetic field on the energy levels of an electron in the perfect crystal and then describe the corresponding effect on the energy levels of donors and acceptors.

We approach this question within the framework of the effective-mass approximation. In its simplest form it amounts to regarding the equation of motion of a band electron as being

$$\hbar \frac{dk}{dt} = -\frac{e}{c} \mathbf{v} \times \mathbf{B} \quad (5.20)$$

where \mathbf{k} is the wavevector, $\mathbf{v} = (1/\hbar) \nabla_k E_\nu(\mathbf{k})$ is the group velocity and \mathbf{B} is the magnetic induction.

We can, under some approximations, describe the motion of the electron by Bloch wavefunctions $\psi_{\nu k}(\mathbf{r})$ multiplied by an envelope function $F_\nu(\mathbf{r})$ obeying (Luttinger and Kohn 1955, Wannier 1962)

$$E_\nu \left(-i\nabla + \frac{e}{\hbar c} \mathbf{A} \right) F_\nu(\mathbf{r}) = E F_\nu(\mathbf{r}) \quad (5.21)$$

where \mathbf{A} is the vector potential, i.e. a vector field such that $\mathbf{B} = \nabla \times \mathbf{A}$.

In the case of degenerate levels as those at the top of the valence band in Si and Ge, equation (5.21) is replaced by the set of coupled equations

$$\sum_{\nu'} \mathcal{D}_{\nu\nu'} \left(-i\nabla + \frac{e}{\hbar c} \mathbf{A} \right) F_{\nu'}(\mathbf{r}) = E F_\nu(\mathbf{r}) \quad (5.22)$$

where the matrix elements $\mathcal{D}_{\nu\nu'}$ are given in equations (3.11) or (3.16), as may be appropriate depending on the magnitude of the spin-orbit interaction. In addition, the Zeeman energy $-\mu \cdot \mathbf{B} = g \mu_B \mathbf{s} \cdot \mathbf{B}$ arising from the electron spin must be included. Here μ_B is the Bohr magneton and \mathbf{s} is the spin of the electron.

We note that, in equation (5.22), we replace $-i\nabla$ by the operator

$$\pi = -i\nabla + \frac{e}{\hbar c} A.$$

In writing the effective-mass equation (3.57) in terms of the operator $\mathcal{D}_{3/2}$ defined in equation (3.16) we recall that the three parameters A , B and D were required because there are three independent invariants formed by products of the components of the symmetric tensors $k_i k_j$ and $\{J_i J_j\}$. Terms linear in the angular momentum matrices and in the matrices V_x , V_y , V_z defined in equation (5.17) were ruled out because they do not obey time reversal symmetry. However, in the presence of a magnetic field the tensor $\pi_i \pi_j$ is no longer symmetric but can be separated into symmetric and antisymmetric parts as

$$\pi_i \pi_j = \{\pi_i \pi_j\} + \frac{1}{2} [\pi_i, \pi_j]$$

where

$$[\pi_i, \pi_j] = -\frac{ie}{\hbar c} \left(\frac{\partial A_j}{\partial x_i} - \frac{\partial A_i}{\partial x_j} \right)$$

the commutator of π_i and π_j has off-diagonal elements proportional to the components of the magnetic field. This introduces the two additional invariants

$$\sum_i B_i J_i$$

and

$$\sum_i B_i J_i^3$$

since J_x , J_y , J_z and J_x^3 , J_y^3 , J_z^3 form bases for the representation Γ_4^+ of O_h . Therefore, the matrix \mathcal{D} in equation (5.22) contains the operator

$$\mathcal{D}' = \mu_B g_1 \mathbf{B} \cdot \mathbf{J} + \mu_B g_2 \sum_i B_i J_i^3 \quad (5.23)$$

in addition to $\mathcal{D}_{3/2}$. Furthermore, in writing $\mathcal{D}_{3/2}$ according to equation (3.16) we replace $k_i k_j$ by the symmetric part $\{\pi_i \pi_j\}$ of $\pi_i \pi_j$ (Luttinger 1956). The two additional parameters g_1 and g_2 are called the g factors for the top of the valence band.

With these considerations we can, at least in principle, find the energy levels of the electron. In the simplest case of an isotropic effective mass m^* for a non-degenerate band extremum, say at $\mathbf{k}=0$, the energy eigenstates are the standard Landau levels characterised by

$$E_n(k_z) = \frac{\hbar e B}{m^* c} (n + \frac{1}{2}) + \frac{\hbar^2 k_z^2}{2m} \quad (5.24)$$

where k_z is the component of the wavevector in the direction of the magnetic field. If the effective-mass tensor is anisotropic a more complicated expression arises (Baldereschi and Bassani 1968) for the frequency eB/m^*c but the general structure of equation (5.4) remains the same.

We consider the simple case in which the effective mass m^* is isotropic. The envelope function satisfies the wave equation

$$\left[\frac{1}{2m^*} \left(\mathbf{p} + \frac{e}{c} \mathbf{A} \right)^2 - \frac{e^2}{\kappa r} \right] F = E F. \quad (5.25)$$

Here we have disregarded the Zeeman energy associated with spin as it gives a constant splitting for all energy levels. If we use the symmetric gauge $A = \frac{1}{2}\mathbf{B} \times \mathbf{r}$ and let \mathbf{B} be parallel to the z axis of a Cartesian coordinate system, equation (5.25) becomes

$$\left(\frac{p^2}{2m^*} + \frac{e\hbar B}{2m^*c} L_z + \frac{e^2}{8m^*c^2} B^2 (r^2 - z^2) - \frac{e^2}{\kappa r} \right) F = EF. \quad (5.26)$$

It is immediately seen that L_z is a constant of the motion so that the energy levels can be characterised by quantum numbers associated with the energy E and m , the eigenvalue of L_z . If the magnetic field B is strong enough so that $e^2/\kappa r$ can be regarded as small, we can start with the Landau levels and take the impurity potential as a perturbation. We remark that the wavefunctions of the Landau levels in a uniform magnetic field using the symmetric gauge are

$$\psi_{nmk_z} = R_{nm}(\rho) \exp(i\varphi) \exp(ik_z z) \quad (5.27)$$

where $\rho = (x^2 + y^2)^{1/2}$ and φ are polar coordinates in the plane perpendicular to the magnetic field \mathbf{B} , and the energies are given by equation (5.24). The radial wavefunction R_{nm} is of the form

$$R_{nm}(\rho) = C \exp(-\rho^2/4b^2) \rho^{|m|} F(-n + \frac{1}{2}|m| + \frac{1}{2}m, |m| + 1, \rho^2/2b^2). \quad (5.28)$$

Here $F(\alpha, \beta, z)$ is the confluent hypergeometric function and b is the radius of the cyclotron orbit for an electron of energy $\hbar eB/2m^*c$, i.e.

$$b = (\hbar c/eB)^{1/2}. \quad (5.29)$$

Since F must be a polynomial, $m \leq n$. Clearly, the parameter characterising the validity of the approximation used is

$$\gamma = (a/b)^2 = 4.25 \times 10^{-10} B \kappa^2 (m/m^*)^2 \quad (5.30)$$

where the units of B are in gauss. If $\gamma \gg 1$, we must regard the impurity potential as a perturbation. In the opposite limit, $\gamma \ll 1$, the magnetic field is a small perturbation. While in atomic spectroscopy we are certainly within the second approximation for ordinary values of B , in a semiconductor γ can exceed unity for magnetic fields as low as 10^4 G. Further, for states near the continuum, the requirement for the validity of the Landau level approximation is that the radius of the cyclotron orbit be much less than that of the corresponding atomic-like orbit which is less restrictive than $\gamma > 1$. Several approximation schemes have been used to calculate the energy levels for a range of values of γ . For $\gamma \gg 1$, the ground-state energy shifts below $\hbar eB/2m^*c$ by an amount (Elliot and Loudon 1960)

$$\Delta E = -\frac{m^*c^4}{2\hbar^2\kappa^2} (\ln \gamma)^2. \quad (5.31)$$

The excited states, with approximate double degeneracy, exhibit a hydrogen-like spectrum; their energies are shifted with respect to the lowest Landau level of energy $\hbar eB/2m^*c$ by approximately $-m^*e^4/2\hbar^2\kappa^2 s^2$ ($s = 1, 2, 3, \dots$). In figure 49 we give the results of a comparison of calculations by Lee *et al* (1973) with those of Baldereschi and Bassani (1970). The result is that the Landau states nmk_z yield a set of levels nms for the impurity states. Of these, only those for $n=0$ are true stationary states since for $n>0$ they are degenerate with the continuum associated with $n=0$.

Hasegawa and Howard (1961) have investigated the transition probabilities for the absorption of radiation. They show that, while for $\gamma \ll 1$, the atomic-like approximation

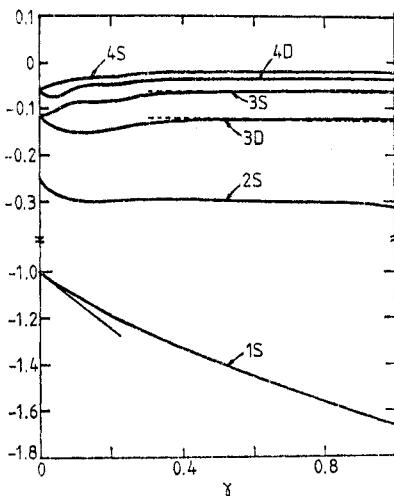


Figure 49. Energies of the lowest bound states with $m=0$ as a function of magnetic field (after Baldereschi and Bassani 1970, Lee *et al* 1973). —, Lee *et al* (1973); ---, Baldereschi and Bassani (1970).

holds and the transition rates are approximately equal to those for the impurity states in the absence of the magnetic field, as B is increased, the transition probabilities to states in the continuum decrease so that for large magnetic fields the observed transitions are to the bound levels alone.

Boyle and Howard (1961) and Baldereschi and Bassani (1970) have proposed a scheme to associate the levels (nms) in the high-field approximation to those in the atomic-like limit as shown in table 14. The selection rules are clearly the following: for light polarised

Table 14. Correspondence of the levels (nms) in the high magnetic-field approximation with the atomic-like levels for the Hamiltonian in equation (3.46). The assignments are based on the restriction $m \leq n$ besides m and parity being good quantum numbers for all intensities of the magnetic field.

Atomic-like levels	(nms)
1s	(0, 0, 0)
2s	(0, 0, 2)
2p ₀	(0, 0, 1)
3p ₀	(0, 0, 3)
2p ₋	(0, -1, 0)
2p ₊	(1, 1, 0)
3p ₋	(0, -1, 2)
3p ₊	(1, 1, 2)
3s; 3d ₀	(0, 0, 4); (0, 0, 6)

parallel to \mathbf{B} , $\Delta m = 0$ and $\Delta s = \pm 1, \pm 3, \dots$, since transitions can be between states of opposite parity. For polarisation perpendicular to \mathbf{B} , they are $\Delta m = \pm 1$, and Δs even; $\Delta m = +1$ is observed for left-circularly polarised light while $\Delta m = -1$ would be observed for right-circular polarisation.

So far we have considered the case in which the effective mass is isotropic. However, for donors in Si and Ge, we must consider that the constant-energy surfaces near the conduction band edge are ellipsoids of revolution characterised by the two parameters

m_1 and m_t . Further, since there are four equivalent minima in Ge and six in Si, the splitting, which will clearly depend on the direction of the magnetic field relative to the axis of rotational symmetry of the constant-energy ellipsoids, will be different for the otherwise degenerate states of the donors. The linear Zeeman effect for donor states in Ge and Si was studied by Haering (1958) and Lax *et al* (1959), respectively. The p_{\pm} levels are shifted by

$$\Delta E_{\pm} = \pm \frac{e\hbar B}{2m_t c} \cos \beta \quad (5.32)$$

where β is the angle formed by B and the principal axis (z axis) of each constant-energy ellipsoid. The Zeeman splitting of these lines is shown in figure 50. Pajot *et al* (1972b) have carried the low-field approximation beyond that studied by Haering to include contributions quadratic in the applied magnetic field.

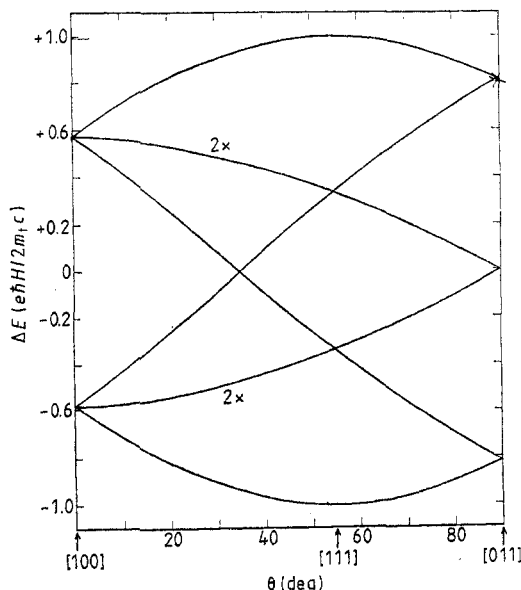


Figure 50. The Zeeman splitting of the $2p_{\pm}$ donor states in Ge as a function of the angle between the magnetic field and the [100] direction, the magnetic field being in the (110) plane. One of the three pairs of lines is doubly degenerate for all angles θ (after Haering 1958).

For acceptors, the effective-mass calculations have been undertaken in the low-magnetic-field limit only. Estimates of some of the energy levels have been given by Bir *et al* (1963), Suzuki *et al* (1964) and Lin-Chung and Wallis (1969).

Bhattacharjee and Rodriguez (1972) have carried out a group theoretical analysis of the Zeeman effect of acceptors in Si and Ge. Their investigation is limited to the low-magnetic-field case which appears to be justified for magnetic fields below 10^4 G, owing to the fact that the effective masses do not differ substantially from the free-electron mass. They also investigate the relative intensities of the Zeeman sublevels approximating the wavefunctions by their zero-magnetic-field values. This is justified as long as the Zeeman multiplets of the excited states do not mix.

The Γ_6 , Γ_7 and Γ_8 levels of an acceptor in Si or Ge are split by the Zeeman energy,

which, according to simple group theoretical considerations, can be written as

$$H_Z^{(i)} = \frac{1}{2} \mu_B g^{(i)} \mathbf{B} \cdot \boldsymbol{\sigma} + q^{(i)} B^2 \quad i=6, 7 \quad (5.33)$$

for a Γ_6 or Γ_7 level where $\boldsymbol{\sigma}$ is the Pauli matrix and

$$H_Z^{(8)} = \mu_B g_1' \mathbf{B} \cdot \mathbf{J} + \mu_B g_2' (B_x J_x^3 + B_y J_y^3 + B_z J_z^3) + q_1 B^2 + q_2 (\mathbf{B} \cdot \mathbf{J})^2 + q_3 (B_x^2 J_x^2 + B_y^2 J_y^2 + B_z^2 J_z^2) \quad (5.34)$$

where \mathbf{J} is the angular momentum operator for $j=\frac{3}{2}$. The linear combinations of the Γ_6 , Γ_7 and Γ_8 eigenstates which diagonalise the Hamiltonian have been determined for magnetic fields \mathbf{B} pointing along one of the higher symmetry directions $\langle 100 \rangle$, $\langle 111 \rangle$ or $\langle 110 \rangle$ of the crystal. The new states allow us to find the matrix elements of the dipole moment operator. We give in tables 15 and 16 the selection rules for the Zeeman components within the dipole approximation of transitions from a Γ_8 ground state to a Γ_6 , Γ_7 or Γ_8 excited state. Defining \mathbf{k} as the direction of propagation of the incident light, the relative intensities in the Faraday ($\mathbf{k} \parallel \mathbf{B}$) and Voigt ($\mathbf{k} \perp \mathbf{B}$) geometries for \mathbf{B} along [001] are given in tables 17 and 18, respectively.

The Zeeman effect of donors in Ge was observed by Fan and Fisher (1959) and Boyle (1959). We show in figure 51 the splitting of the $1s(\text{A}_1) \rightarrow 2p_{\pm}$ line of Ge(As) into a

Table 15. Selection rules for the Zeeman components with $\mathbf{B} \parallel [001]$. ϵ denotes the polarisation of the radiations. ϵ_{\pm} corresponds to $(1/\sqrt{2})(x' \pm iy')$, i.e. to left-circular and right-circular polarisations, respectively. ϵ_{\parallel} corresponds to z' . Here the Cartesian axes x' , y' , z' are selected so that $\mathbf{B} \parallel z'$. $\bar{\mathbf{S}}_4$ is the symmetry group of the crystal in the presence of \mathbf{B} (after Bhattacharjee and Rodriguez 1972).

		Γ_8			
$\bar{\mathbf{T}}_d$	$\bar{\mathbf{S}}_4$	$+3/2(\Gamma_6)$	$+1/2(\Gamma_7)$	$-1/2(\Gamma_8)$	$-3/2(\Gamma_5)$
Γ_6	$+1/2(\Gamma_5)$	ϵ_-	ϵ_{\parallel}	ϵ_+	0
	$-1/2(\Gamma_6)$	0	ϵ_-	ϵ_{\parallel}	ϵ_+
Γ_7	$+1/2(\Gamma_7)$	ϵ_+	0	ϵ_-	ϵ_{\parallel}
	$-1/2(\Gamma_8)$	ϵ_{\parallel}	ϵ_+	0	ϵ_-
Γ_8	$+3/2(\Gamma_6)$	0	ϵ_-	ϵ_{\parallel}	ϵ_+
	$+1/2(\Gamma_7)$	ϵ_+	0	ϵ_-	ϵ_{\parallel}
	$-1/2(\Gamma_8)$	ϵ_{\parallel}	ϵ_+	0	ϵ_-
	$-3/2(\Gamma_5)$	ϵ_-	ϵ_{\parallel}	ϵ_+	0

Table 16. Selection rules for the Zeeman components with $\mathbf{B} \parallel [111]$. The meanings of ϵ_{\pm} , ϵ_{\parallel} are the same as in table 15 but now z' is parallel to [111]. The symmetry group in the presence of \mathbf{B} is $\bar{\mathbf{C}}_3$ (after Bhattacharjee and Rodriguez 1972).

		Γ_8			
$\bar{\mathbf{T}}_d$	$\bar{\mathbf{C}}_3$	$+3/2(\Gamma_6)$	$+1/2(\Gamma_4)$	$-1/2(\Gamma_5)$	$-3/2(\Gamma_6)$
Γ_6	$+1/2(\Gamma_4)$	ϵ_-	ϵ_{\parallel}	ϵ_+	ϵ_-
	$-1/2(\Gamma_5)$	ϵ_+	ϵ_{\parallel}	ϵ_{\parallel}	ϵ_+
Γ_7	$+1/2(\Gamma_4)$	ϵ_-	ϵ_{\parallel}	ϵ_+	ϵ_-
	$-1/2(\Gamma_5)$	ϵ_+	ϵ_{\parallel}	ϵ_{\parallel}	ϵ_+
Γ_8	$+3/2(\Gamma_6)$	ϵ_{\parallel}	ϵ_+	ϵ_-	ϵ_{\parallel}
	$+1/2(\Gamma_4)$	ϵ_-	ϵ_{\parallel}	ϵ_+	ϵ_-
	$-1/2(\Gamma_5)$	ϵ_+	ϵ_{\parallel}	ϵ_{\parallel}	ϵ_+
	$-3/2(\Gamma_6)$	ϵ_{\parallel}	ϵ_{\parallel}	ϵ_-	ϵ_{\parallel}

Table 17. Relative intensities of the Zeeman components in the Faraday configuration with $B \parallel [001]$ (circular polarisation) (after Bhattacharjee and Rodriguez 1972).

Zero-field transition	Components		Relative intensity
	ε_+	ε_-	
$\Gamma_8 \rightarrow \Gamma_6$	$-3/2 \rightarrow -1/2$	$+3/2 \rightarrow +1/2$	$3/4$
	$-1/2 \rightarrow +1/2$	$+1/2 \rightarrow -1/2$	$1/4$
$\Gamma_8 \rightarrow \Gamma_7$	$+3/2 \rightarrow +1/2$	$-3/2 \rightarrow -1/2$	$1/4$
	$+1/2 \rightarrow -1/2$	$-1/2 \rightarrow +1/2$	$3/4$
$\Gamma_8 \rightarrow \Gamma_8$	$+3/2 \rightarrow +1/2$	$-3/2 \rightarrow -1/2$	$1/2 - (3/8)u + (1/2)v$
	$+1/2 \rightarrow -1/2$	$-1/2 \rightarrow +1/2$	$(3/8)u$
	$-1/2 \rightarrow -3/2$	$+1/2 \rightarrow +3/2$	$1/2 - (3/8)u - (1/2)v$
	$-3/2 \rightarrow +3/2$	$+3/2 \rightarrow -3/2$	$(3/8)u$

Table 18. Relative intensities of the Zeeman components in the Voigt configuration with $B \parallel [001]$ (after Bhattacharjee and Rodriguez 1972).

Zero-field transition	Longitudinal polarisation		Transverse polarisation	
	Components	Relative intensity	Components	Relative intensity
$\Gamma_8 \rightarrow \Gamma_6$	$\pm 1/2 \rightarrow \pm 1/2$	$1/2$	$\mp 3/2 \rightarrow \mp 1/2$	$3/8$
			$\mp 1/2 \rightarrow \pm 1/2$	$1/8$
$\Gamma_8 \rightarrow \Gamma_7$	$\pm 3/2 \rightarrow \mp 1/2$	$1/2$	$\pm 3/2 \rightarrow \pm 1/2$	$1/8$
			$\pm 1/2 \rightarrow \mp 1/2$	$3/8$
$\Gamma_8 \rightarrow \Gamma_8$	$\pm 3/2 \rightarrow \mp 1/2$	$1/4 - (1/2)v$	$\pm 3/2 \rightarrow \pm 1/2$	$1/4 - (3/16)u + (1/4)v$
			$\pm 1/2 \rightarrow \mp 1/2$	$(3/16)u$
	$\pm 1/2 \rightarrow \mp 3/2$	$1/4 + (1/2)v$	$\mp 1/2 \rightarrow \mp 3/2$	$1/4 - (3/16)u - (1/4)v$
			$\mp 3/2 \rightarrow \pm 3/2$	$(3/16)u$

doublet when a magnetic field of 16.7 kG is applied along [100] (Fan and Fisher 1959). For this direction of B the donor levels associated with all the $\langle 111 \rangle$ conduction band minima behave identically and the doublet results from the lifting of the $m = \pm 1$ degeneracy as can be deduced from equation (5.32). The splitting increases linearly with B and yields $m_t = (0.077 \pm 0.005) m$ in excellent agreement with the cyclotron resonance value of 0.082 m (Dresselhaus *et al* 1955, Dexter *et al* 1956). Fan and Fisher (1959) as well as Boyle (1959) observed oscillations in the energy range beyond the photoionisation limit. Though initially interpreted as resulting from the large density of states associated with the bottom of Landau levels, Hasegawa and Howard (1961) and Boyle and Howard (1961) showed that they are due to ‘bound states well separated from Landau edges’. They showed the correspondence between low- and high-field states using compatibility on the basis of parity and the magnetic quantum numbers. The energies of the magnetic-field-induced components are expected to exhibit strong non-linear dependence on the field. The energy separation between the $m = +1$ and $m = -1$ states are linear in the field and yield m_t . The intensity of the $1s \rightarrow np_+$ increases with respect to that of $1s \rightarrow np_-$. Also, only the $1s(A_1) \rightarrow 2p_+$ transition survives at the highest fields (Hasegawa and Howard 1961). Nisida and Horii (1971) and Horii and Nisida (1971) have made a comprehensive theoretical and experimental study of the Zeeman effect of Ge(As) and Ge(Sb) and verified the above predictions. In figure 52 we reproduce their data on the energies of the Zeeman components as a function of magnetic field.

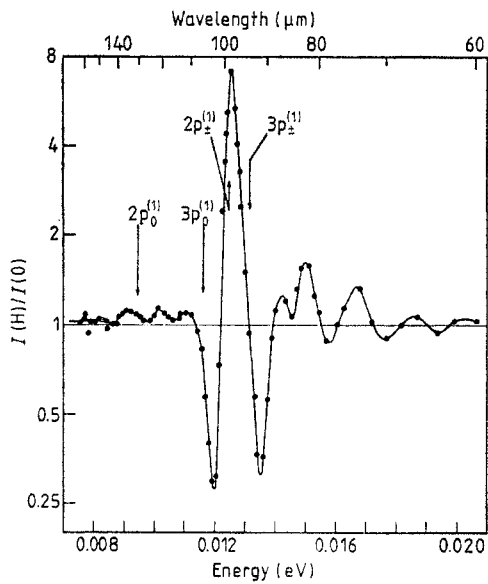


Figure 51. The effect of magnetic field B on the excitation lines of Ge(As). $B = 16.7$ kG. Liquid helium used as coolant. Room-temperature resistivity = $1.7 \Omega \text{ cm}$. Ge(As)-127B (after Fan and Fisher 1959). $B \parallel [100]$.

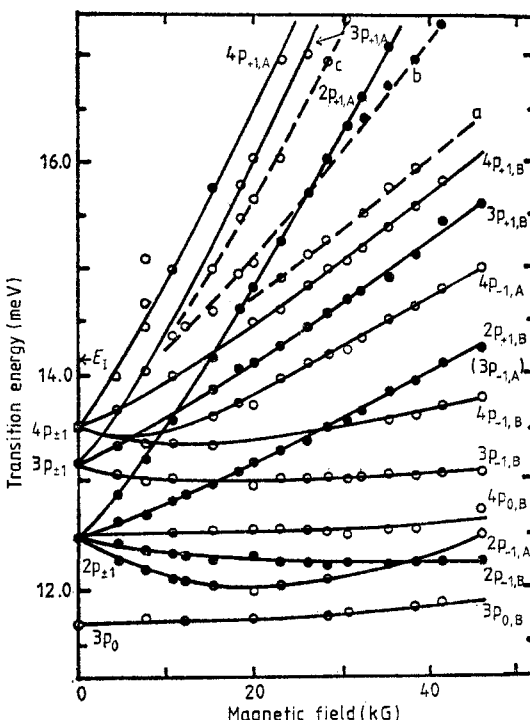


Figure 52. Magnetic-field dependence of the Zeeman components of the excitation lines of Ge(As) (after Horii and Nisida 1971). $H \parallel [111]$, $E \perp H$. ● strong, ○ weak.

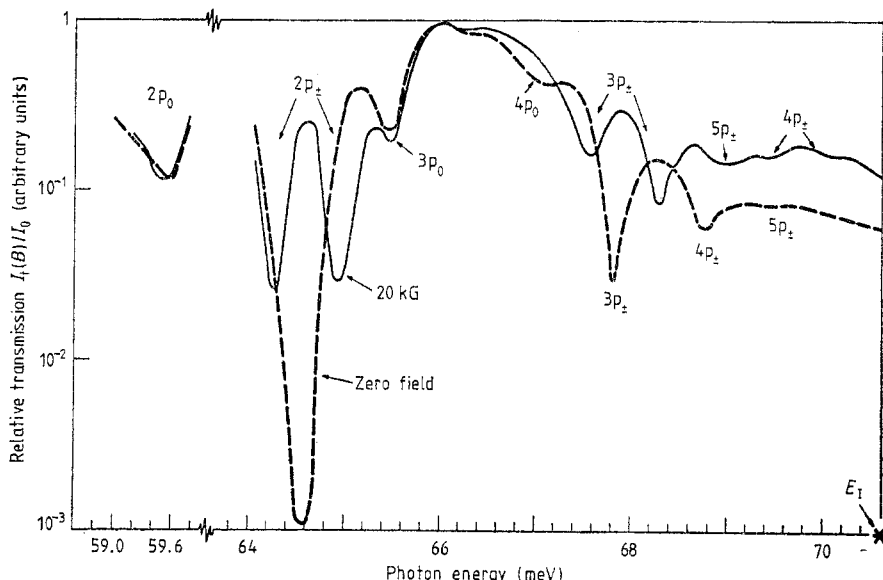


Figure 53. Zeeman effect of the excitation lines of Si(Bi) at 4.2 K (after Zwerdling *et al.* 1960a). $B \parallel [111]$, $E \parallel B$.

The Zeeman effect of donors in Si was investigated by Lax *et al.* (1959) and Zwerdling *et al.* (1960a). Figure 53 shows the splitting of the $1s(A_1) \rightarrow np_{\pm}$ transitions of Si(Bi) with $B \parallel [111]$; as expected for this orientation of the magnetic field these lines split into doublets, the six $\langle 100 \rangle$ conduction band minima being equivalent. From such measurements Zwerdling *et al.* (1960a) obtain $m_t = (0.186 \pm 0.006) m$ in agreement with the cyclotron resonance value of $m_t = (0.192 \pm 0.001) m$ obtained by Rauch *et al.* (1960). More recently Pajot *et al.* (1972a, b) investigated the Zeeman effect of donors in Si including terms quadratic in B using perturbation theory and applied to an experimental investigation of Si(P).

The Zeeman effect of donors in GaAs presents a particularly simple example of a hydrogenic donor in a magnetic field. Figure 31 clearly shows the features expected for donor states characteristic of an isotropic effective mass of the bound electron (Stillman *et al.* 1969); an effective mass $m^* = (0.0665 \pm 0.0005) m$ was deduced from their measurements. They clearly show the tendency of the $1s \rightarrow 2p_+$ line to dominate at the higher fields. Kaplan (1969) has made an extensive study of the Zeeman effect of donors in InSb where the high-field limit is easily reached in view of the extremely small effective mass of conduction electrons. More recently Kuchar *et al.* (1977) reported their investigation on the doping dependence of high-field donor spectra in InSb. The Zeeman effect of GaP(Si), GaP(S) and GaP(Te) has been reported by Carter *et al.* (1976, 1977b); their results give additional evidence for the 'camel's back' nature of the conduction band minimum of GaP.

The Zeeman effect of group III acceptors in Ge first reported by Fisher and Fan (1959) has been investigated more completely by Soepangkat and Fisher (1973) and Broeckx *et al.* (1979). Fisher and Fan (1960) and Moore (1971) have studied the Zeeman effect of the double and triple acceptors, Ge(Zn), Ge(Hg), Ge(Be) and Ge(Cu). In figure 54 we show the Zeeman effect of Ge(B) with $B \parallel [100]$ in the Voigt geometry (Soepangkat and Fisher 1973). From an analysis of the field dependence of the Zeeman components of the D line of Ge(B), their relative intensities and polarisation features, they deduced

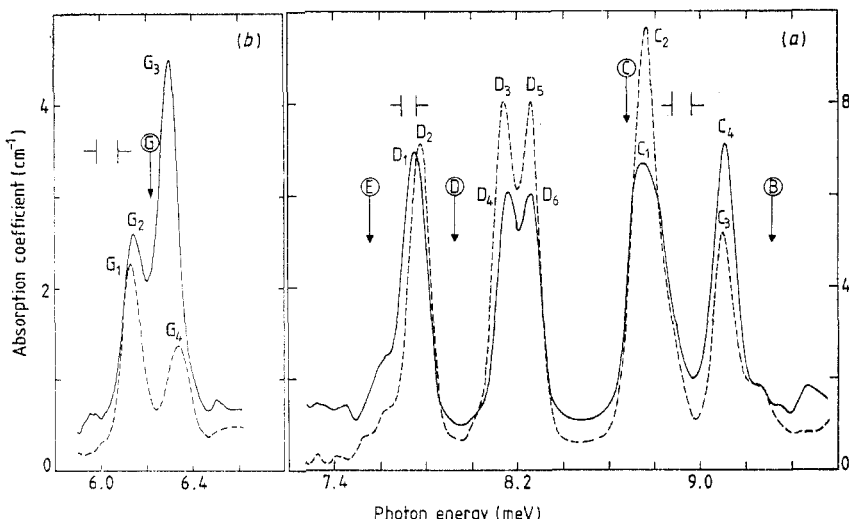


Figure 54. Transverse Zeeman effect of the excitation lines of Ge(B). $p \sim 2.5 \times 10^{14} \text{ cm}^{-3}$ for Ge(B)-150A no 3 (a) and $p \sim 8 \times 10^{14} \text{ cm}^{-3}$ for Ge(B)-180A no 5 (b). Liquid helium used as coolant (after Soepangkat and Fisher 1973). $B \parallel \langle 111 \rangle$; ---, $E \parallel B$; —, $E \perp B$; $B = 18.5 \text{ kG}$.

$g_1' = -1.73 \pm 0.11$, $g_2' = 0.78 \pm 0.07$ for the Γ_8 ground state and $g_1^D = -6.92 \pm 0.16$ and $g_2^D = 3.11 \pm 0.08$ for the final state of this transition. This analysis was based on a fit for the data to equation (5.34) including terms quadratic in B . As stated above this equation is valid for low fields and in the absence of hybridisation. Broeckx *et al* (1979) studied the Zeeman effect of the C and D lines of Ge(Al) and Ge(B) using the photo-thermal ionisation technique and a Fourier transform spectrometer enabled them to resolve the Zeeman components at low fields where the effects of admixture can be expected to be unimportant. Analysing the data in this regime and assuming zero Zeeman splitting for the Γ_8 ground state they obtained $g_1^D = 8.4 \pm 0.4$ and $g_2^D = -4.1 \pm 0.2$. The assumption of zero splitting of the ground state does not allow the absolute signs of g_1^D and g_2^D to be determined even though their relative signs can be deduced. Tokumoto and Ishiguro (1977) studied the magnetoacoustic resonance attenuation in Ge(Ga) and deduced $g_1' = -0.16 \pm 0.08$ and $g_2' = 0.08 \pm 0.04$. These observations do support the assumption of zero-ground-state Zeeman splitting. To date no electron spin resonance experiments for acceptors in Ge appear to have been carried out and would clearly be of interest in view of the discrepancy in the interpretations given on the one hand by Soepangkat and Fisher (1973) and on the other by Broeckx *et al* (1979). For numerical calculations of g factors using effective-mass theory, reference may be made to Bir *et al* (1963), Suzuki *et al* (1964), Lin-Chung and Wallis (1969) and Broeckx and Clauws (1978). In order to interpret the experimental results on the double acceptors (Fisher and Fan 1960, Moore 1971) the nature of the ground state which is $\{\Gamma_8 \times \Gamma_8\}$ for Ge(Zn, Be, ...) should clearly be taken into account. A similar comment is relevant for Ge(Cu).

The Zeeman effect of acceptors in Si was first investigated by Zwerdling *et al* (1960a) for Si(Al). Merlet *et al* (1975) examined the Zeeman effect of Si(B) in the Voigt as well as the Faraday geometries and deduced the g factors for the ground and excited states of lines 1 and 2. They obtained for the ground state $g_1' = 1.03 \pm 0.07$ and $g_2' = 0.04 \pm 0.04$ which are to be compared with $g_1' = 0.84 \pm 0.09$ and $g_2' = 0.13 \pm 0.08$ obtained by Cherlow *et al* (1973) from the Zeeman effect of the 23 meV electronic Raman transition, $\Gamma_8^+ \rightarrow \Gamma_7^+$,

discussed in §4.3. Feher *et al* (1960) studied the electron paramagnetic resonance of Si(B) and deduced $g_1' = 1.21 \pm 0.01$ and $g_2' = 0.00 \pm 0.01$. Though in general qualitative agreement, these sets of values for g_1' and g_2' have yet to be quantitatively reconciled.

6. Linewidths of excitation lines

There is continuing interest in the natural width and shape of the line spectra exhibited by carriers bound to impurities in semiconductors and in the factors which lead to the observed linewidths and shapes. The various mechanisms observed and/or proposed in this context are: (i) interaction of bound carriers and phonons (Lax and Burstein 1955, Kane 1960), (ii) overlap of the wavefunctions of bound carriers (Newman 1956), (iii) random electric fields produced by ionised and neutral impurities causing Stark and quadrupole broadening (Larsen 1973, 1976), and (iv) strains resulting from the presence of impurities, both electrically active and inactive (Kogan and Lifshits 1977). Unusual line broadening can occur due to special circumstances, e.g. in the excitation spectrum of bismuth donors and gallium acceptors in silicon remarkable broadening of specific lines due to a resonant interaction between the electronic excitation and an optical phonon has been reported and theoretically analysed (Onton *et al* 1967a, b, Rodriguez and Schultz 1969, Butler *et al* 1975, Chandrasekhar *et al* 1976). Linewidths and shapes of the various lines of the excitation spectrum can be used as probes to study these broadening phenomena. As a basis for such studies it is essential to establish the 'natural' linewidths of the various lines. Having determined the natural linewidths, changes in the width and shape can be correlated to the broadening mechanism present. In the following we discuss the experimental and theoretical aspects of some of these mechanisms.

6.1. Interaction of bound carriers and phonons

Lax and Burstein (1955) proposed that the interaction of the donor electron and acoustic phonons in the crystal produces a broadening of the 1s, 2p, . . . , levels, the broadening of the 1s ground state accounting for about 90% of the linewidth. On the basis of their calculations they predicted that the widths of the excitation lines at 0 K are about 3.6 meV for shallow impurities in Si. Using the simple Lorentz broadening approach Sampson and Margenau (1956) calculated a low-temperature width of ~ 1.6 meV. These values are larger by about two orders of magnitude than the observed linewidths of the donor lines in Si, which are about 0.02 meV! The full width at half-maximum, $W_{1/2}$, of the $2p_0$ and $3p_{\pm}$ lines of the excitation spectrum of phosphorus donors introduced in silicon by neutron transmutation shown in figure 6 was measured to be 0.021 and 0.030 meV, respectively, taking into account instrumental function (Jagannath *et al* 1981). The $W_{1/2}$ of the $2p_{\pm}$ line was measured to be ~ 0.027 meV. The $W_{1/2}$ for the $2p_0$ and $3p_{\pm}$ lines for arsenic donors were obtained from the spectrum shown in figure 7; these values, 0.024 and 0.028 meV, respectively, are in excellent agreement with the linewidths of the phosphorus donor spectrum. The corresponding values of the linewidths for the lithium and lithium-oxygen donor complex (series A) in figure 18 are also in close agreement with the above values. The $W_{1/2}$ for the $2p_0$ and $3p_{\pm}$ lines in a sample in which the phosphorus dopant is introduced during crystal growth was measured to be 0.026 and 0.033 meV, respectively, by Jagannath *et al* (1981).

It was pointed out by Kane (1960) that the linewidths reported in earlier studies in

Si may be entirely instrumental. He suggested that, due to the weakness of the electron-phonon interaction in silicon, the broadening, free from instrumental effects, arises from a 'lifetime effect' due to a transition to a lower state with the emission of a phonon. At $T=0$ K he estimated such linewidths to be ~ 0.05 meV. Later, Barrie and Nishikawa (1963) confirmed that for a weak electron-phonon interaction, the observed linewidths do arise from a 'lifetime effect' and that the process discussed by Lax and Burstein (1955), where the emission or absorption of phonons gives rise to line broadening, only contributes a broad, weak background on which the peak is superimposed. Numerical estimates of the zero-phonon—'lifetime broadening'—and the one-phonon process indicate that for the $1s \rightarrow 2p_0$ transition at 0 K the height of the peak for the zero-phonon process is about 10^3 times larger than that for the one-phonon process while the full width at half-maximum ($W_{1/2}$) for the one-phonon process is $\sim 10^2$ times larger than that for the zero-phonon process (Barrie and Nishikawa 1963). In the light of these considerations the measured $W_{1/2}$ of Si donor lines at 0 K arises from the broadening caused by the 'lifetime effect'.

6.2. Resonant electron-phonon interaction

Resonant interaction between phonons and electronic excitations of donors and acceptors in Si was observed by Onton *et al* (1967b). They reported an anomalous broadening of the $1s(A_1) \rightarrow 2p_0$ line in the spectrum of Si(Bi). The chemical shift of the ground state of this donor places the excitation spectrum in the energy range of the optical phonons of the host. The coincidence of the excitation energy of this transition with that of the optical phonons with wavevectors approximately along $\langle 110 \rangle$ suggested that a resonance interaction between the two excitations together with appropriate selection rules was the underlying cause of this dramatic broadening (Onton *et al* 1967b, Rodriguez and Schultz 1969). On applying uniaxial stress, the stress-induced components can be tuned out of resonance, with a resultant decrease in the resonant interaction and the consequent

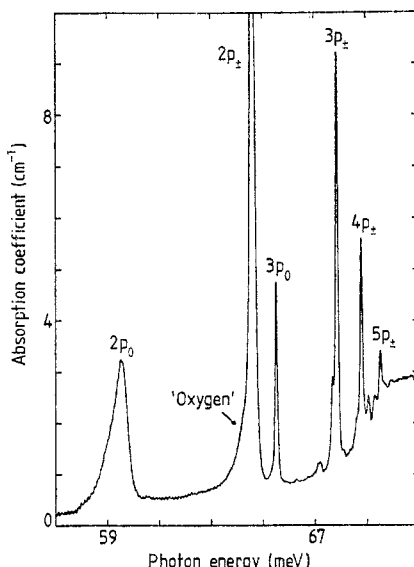


Figure 55. The $1s(A_1) \rightarrow np$ transitions in Si(Bi). Liquid helium used as coolant. Room-temperature resistivity $\sim 2.5 \Omega \text{ cm}$ (after Butler *et al* 1975).

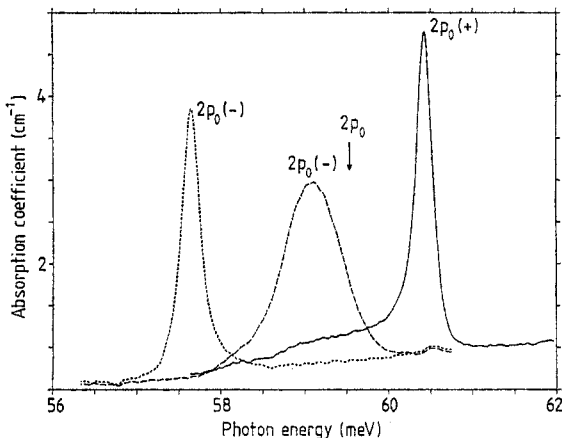


Figure 56. The sharpening of the $1s(A_1) \rightarrow 2p_0(+)$, $2p_0(-)$ transitions in Si(Bi) under increasing stress (after Butler *et al* 1975). Si(Bi) no 16.3, $F \parallel \langle 100 \rangle$. ---, $E \parallel F$, 2.96×10^8 dyn cm $^{-2}$; ——, $E \parallel F$, 4.7×10^7 dyn cm $^{-2}$; —, $E \perp F$, 2.96×10^8 dyn cm $^{-2}$.

sharpening of the excitation lines. The $2p_0$ line of bismuth donors in silicon was observed to have a width eight times larger than that of the other prominent lines. When uniaxial stress was used to 'switch off' the interaction, sharp lines corresponding to $1s(A_1) \rightarrow 2p_0(-)$ and $1s(A_1) \rightarrow 2p_0(+)$ were observed; $2p_0(-)$ and $2p_0(+)$ originate due to the regrouping of the conduction band minima along $\langle 100 \rangle$. We reproduce in figures 55 and 56 the results of Butler *et al* (1975) which illustrate the large half-width at zero stress and the sharpening of the stress-induced components as they move off from resonance. Another striking example of such a resonant interaction is the near-absence of line 2 in the excitation spectrum of Si(Ga) as can be seen in figure 26; the spectrum of Si(Ga) under a high resolution is given in figure 57 (Chandrasekhar *et al* 1976). The transition labelled 2 occurs very close to the zone centre optical phonon ($\hbar\omega_0 = 64.8$ meV). Notice

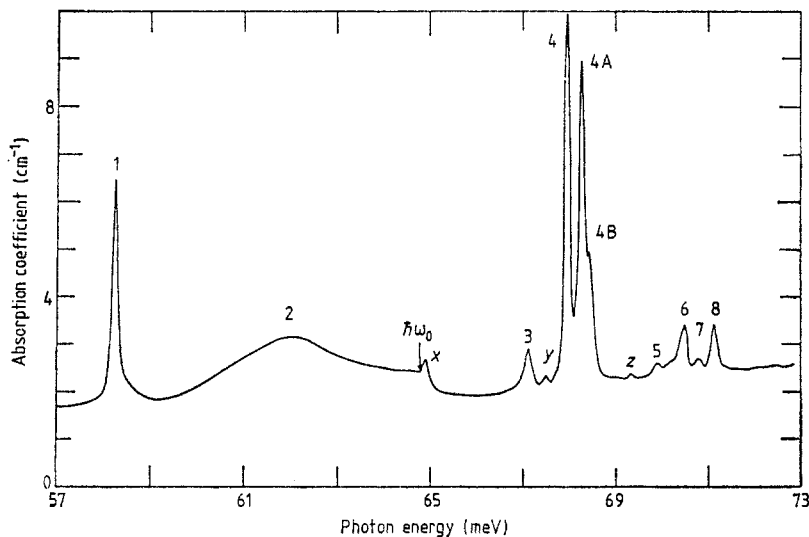


Figure 57. Excitation spectrum of Si(Ga). Liquid helium used as coolant. $p(300\text{ K}) = 2.6 \times 10^{15}$ cm $^{-3}$; $\hbar\omega_0$ = energy of zone-centre optical phonon (after Chandrasekhar *et al* 1976).

the sharp feature labelled X just above $\hbar\omega_0$. We give below the essentials of the theory for the resonant interaction (Rodriguez and Schultz 1969).

We consider an optical transition from the ground state to an excited level lying at an energy ϵ above it. In the absence of interactions with other excitations of the crystal, the linewidth associated with the transition is the natural linewidth determined by the interaction with the electromagnetic field. If, however, the electronic excitation can decay by emission of, say, phonons there will be an additional line broadening. We study a simple model of this effect when the phonon spectrum has a branch with energy in the vicinity of the energy ϵ of the electronic excitation. We calculate the transition rate from the initial state to each of the 'exact' eigenstates in the space spanned by the unperturbed states of an excited impurity and a de-excited impurity plus a phonon. We denote the states by

$$\begin{aligned} |u\rangle &= \text{impurity excited, no phonons and no photons} \\ |q\mu\rangle &\equiv \text{impurity in the ground state, one phonon in state } q\mu \text{ and no photons.} \end{aligned}$$

(6.1)

We enumerate all lattice modes by the labels q and μ , where q is the wavevector of the phonon and μ is the particular branch to which it belongs. If the crystal contains N_c primitive cells and z_0 atoms per primitive cell there are $3z_0N_c$ phonon modes. Thus the label μ indicates whether the phonons are longitudinal or transverse, optical or acoustical. We assume that the Hamiltonian can be decomposed into a diagonal and non-diagonal part

$$H = H_0 + H_1 \quad (6.2)$$

in the representation given by equation (6.1). We have

$$\begin{aligned} H_0|u\rangle &= \epsilon|u\rangle & H_0|q\mu\rangle &= \hbar\omega_{q\mu}|q\mu\rangle \\ H_1|u\rangle &= \sum_{q\mu} \beta_{q\mu}|q\mu\rangle & H_1|q\mu\rangle &= \beta_{q\mu}^*|u\rangle. \end{aligned} \quad (6.3)$$

H_1 is the electron-phonon interaction. Thus H is represented by a $(3z_0N_c+1) \times (3z_0N_c+1)$ matrix whose diagonal components are ϵ and $\hbar\omega_{q\mu}$ for all $q\mu$. The non-diagonal matrix elements are $\langle q\mu | H_1 | u \rangle = \beta_{q\mu}$, $\langle u | H_1 | q\mu \rangle = \beta_{q\mu}^*$ while all other matrix elements vanish.

The rate at which photons of energy E are absorbed is proportional to

$$P(E) = 2\pi \sum_{\lambda} |\langle u | \lambda \rangle|^2 \delta(E - E_{\lambda}) \quad (6.4)$$

where the $|\lambda\rangle$ are the exact eigenstates of H with eigenvalues E_{λ} . Using the well-known relation

$$\delta(E - E_{\lambda}) = -(1/\pi) \operatorname{Im}(E - E_{\lambda} + i\eta)^{-1} \quad (6.5)$$

where η is a positive infinitesimal, we have

$$P(E) = -2 \operatorname{Im} \sum_{\lambda} \langle u | \lambda \rangle (E - E_{\lambda} + i\eta)^{-1} \langle \lambda | u \rangle = -2 \operatorname{Im} \langle u | (E - H + i\eta)^{-1} | u \rangle. \quad (6.6)$$

If we define

$$|\chi_E\rangle = (E - H + i\eta)^{-1} |u\rangle \quad (6.7)$$

and expand in our subspace

$$|\chi_E\rangle = B(E)|u\rangle + \sum_{q\mu} D_{q\mu}(E)|q\mu\rangle \quad (6.8)$$

then

$$P(E) = -2 \operatorname{Im} B(E). \quad (6.9)$$

To obtain $B(E)$ we combine equations (6.7) and (6.8), obtaining the set of linear equations

$$(E - \varepsilon + i\eta) B(E) - \sum_{q\mu} \beta_{q\mu} * D_{q\mu}(E) = 1 \quad (6.10)$$

$$-\beta_{q\mu} B(E) + (E - \hbar\omega_{q\mu} + i\eta) D_{q\mu}(E) = 0. \quad (6.11)$$

These equations are solved simply:

$$D_{q\mu}(E) = [\beta_{q\mu} (E - \hbar\omega_{q\mu} + i\eta)^{-1}] B(E) \quad (6.12)$$

and

$$B(E) = \left(E - \varepsilon + i\eta - \sum_{q\mu} \frac{|\beta_{q\mu}|^2}{E - \hbar\omega_{q\mu} + i\eta} \right)^{-1}. \quad (6.13)$$

In the limit in which N_c approaches infinity, the summation over q can be replaced by an integral. We define

$$\rho(\omega) |\beta(\omega)|^2 = \sum_{q\mu} \frac{N_c v_0}{(2\pi)^3} \int \frac{dS_\mu |\beta_{q\mu}|^2}{|\nabla_q \omega_{q\mu}|} \quad (6.14)$$

where the integral over dS_μ is to be taken over the surface in q space for which $\omega_{q\mu} = \omega$. It might appear at first sight that $\rho(\omega) |\beta(\omega)|^2$ is proportional to the volume of the crystal. However, in general, $\beta_{q\mu}$ is proportional to $N_c^{-1/2}$ so that $|\beta(\omega)|^2 \rho(\omega)$ is independent of N_c ; $\rho(\omega)$ is the density of phonon states of energy ω . The quantity $|\beta(\omega)|^2$ is thus the average of $|\beta_{q\mu}|^2$ over all phonon modes having energy ω . We can now rewrite equation (6.13) as follows:

$$B(E) = \left[E - \varepsilon - \mathcal{P} \int \frac{|\beta(\omega)|^2 \rho(\omega) d\omega}{E - \hbar\omega} + i \left(\eta + \frac{\pi}{\hbar} |\beta(E/\hbar)|^2 \rho(E/\hbar) \right) \right]^{-1}. \quad (6.15)$$

Thus, for E such that $\beta(E/\hbar) \neq 0$,

$$P(E) = \frac{2\pi}{\hbar} |\beta(E/\hbar)|^2 \rho(E/\hbar) \left[\left(E - \varepsilon - \mathcal{P} \int \frac{|\beta(\omega)|^2 \rho(\omega) d\omega}{E - \hbar\omega} \right)^2 + \left(\frac{\pi}{\hbar} |\beta(E/\hbar)|^2 \rho(E/\hbar) \right)^2 \right]^{-1}. \quad (6.16)$$

Here \mathcal{P} before an integral signifies that the principal value of the integral is to be taken. The energy eigenvalues are obtained also in a simple fashion. They are the poles of $B(E)$ after setting $\eta = 0$. Thus we find them by solving for E the equation

$$E - \varepsilon = \sum_{q\mu} \frac{|\beta_{q\mu}|^2}{E - \hbar\omega_{q\mu}}. \quad (6.17)$$

The solution of this equation is exhibited schematically in figure 58 in which we plot the left- and right-hand members of equation (6.17). The eigenvalues of $H = H_0 + H_1$ are the abscissae of the intersections of the two graphs. The solution of highest energy is identified as line X of Si(Ga) in figure 57. The sharpness of this feature can be understood if we remark that the strongest interaction between the hole and the phonons

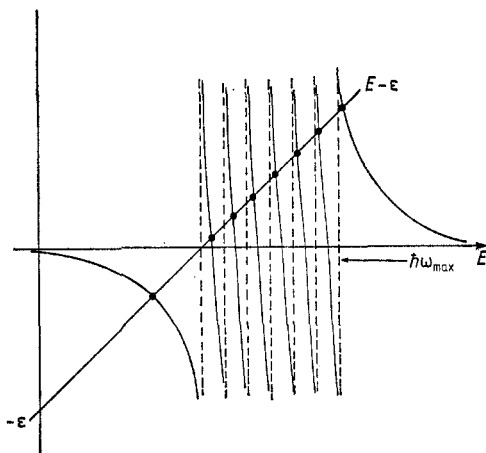


Figure 58. Schematic graphical solution of equation (6.17). The ordinates represent either $\Sigma_{q\mu} |\beta_{q\mu}|^2$ ($E - \hbar\omega_{q\mu}$) $^{-1}$ or $E - \epsilon$. The vertical broken lines are at the positions of the optical phonon energies. The intersections of the graph yield the energy eigenvalues of the mixed electronic-phonon states.

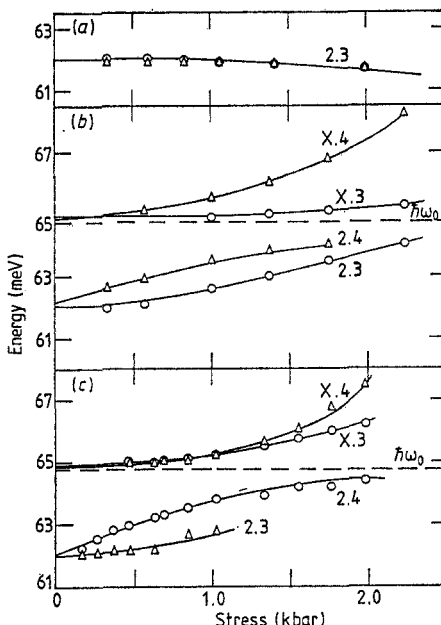


Figure 59. Stress dependence of the components of lines 2 and X of Si(Ga). For $F \parallel [110]$, the direction of propagation k was parallel to $[1\bar{1}0]$. The triangles and circles represent data points for $E \perp F$ and $E \parallel F$, respectively (after Chandrasekhar *et al* 1976). (a) Si(Ga) no 12.3, $F \parallel \langle 100 \rangle$. (b) Si(Ga) no 12.4, $F \parallel [110]$, $q \parallel [1\bar{1}0]$. (c) Si(Ga) no 12.1 and 12.8, $F \parallel \langle 111 \rangle$.

occurs in the vicinity of the highest phonon energy. In contrast for Si(Bi), the strongest electron-phonon coupling occurs for a $\langle 110 \rangle$ phonon near the BZ boundary and is thus within the limits of the phonon spectrum. In the piezospectroscopic investigation of line 2 of Si(Ga), Chandrasekhar *et al* (1976) reported non-linear stress dependence of the positions of the stress-induced components, the ‘pinning’ of some components to $\hbar\omega_0$

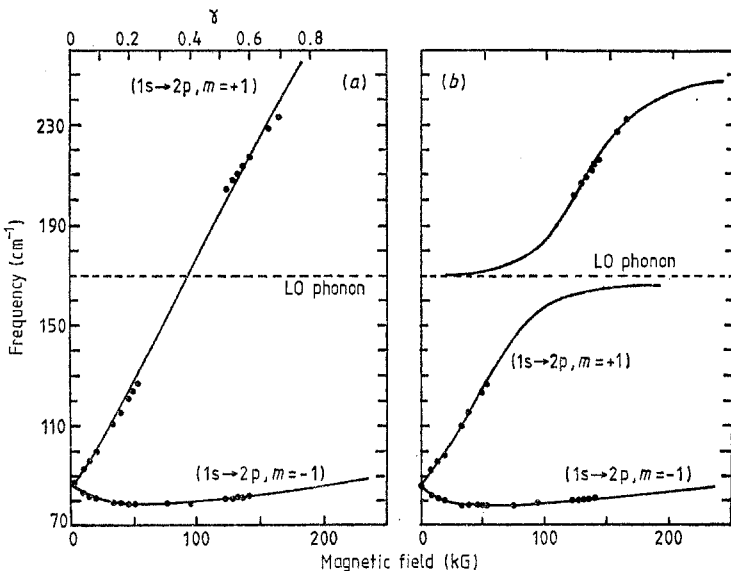


Figure 60. Experimental and theoretical magnetic-field dependence of the position of the $1s \rightarrow 2p_+$ transition. The full curve represents the no-electron-LO phonon interaction ($\alpha=0$) (a) and for an electron-LO phonon interaction characterised by a coupling constant $\alpha=0.4$ (b). The experimental results are for shallow donors in n-CdTe (after Cohn *et al* 1970). Note $r=\hbar\omega_c/2R$ where $\hbar\omega_c$ is the cyclotron resonance energy and R is the Rydberg constant.

and hence the observation of an otherwise infrared-inactive zone-centre optical phonon (figure 59). An interesting example of a ‘pinning’ effect has been observed by Cohn *et al* (1970, 1972) in the Zeeman splitting of the $1s \rightarrow 2p$ transition of a shallow donor in CdTe; the $1s \rightarrow 2p$, $m=+1$ component interacts strongly with the zone-centre longitudinal optical phonon as their energies are brought into coincidence by the applied magnetic field (figure 60).

6.3. Electric-field broadening

The potential energy due to the interaction of the charge carrier with all ionised impurities in the crystal, $V(r)$, evaluated at a point r near the neutral donor can be written as (Jackson 1975)

$$\begin{aligned} V(r) &= \sum_i \frac{e_i}{\kappa |R_i - r|} \\ &= 4\pi \sum_i \frac{e_i}{R_i \kappa} \sum_{l=0}^{\infty} \sum_{m=-l}^l \frac{1}{2l+1} \left(\frac{r}{R_i}\right)^l Y_{lm}^*(\theta_i, \varphi_i) Y_{lm}(\theta, \varphi) \end{aligned} \quad (6.18)$$

where e_i denotes the charge on the i th impurity ion, R_i , θ_i , φ_i its position in spherical coordinates, and r , θ , φ are the spherical coordinates of r . For $l=0$ equation (6.18) reduces to $\sum_i e_i / \kappa R_i$ which is the potential evaluated at the donor centre $r=0$. This term shifts all the levels of the neutral donor up or down by the same amount and therefore leaves the transition energies unchanged.

The $l=1$ terms reduce to $-E(0) \cdot r$ where $E(0)$ is the electric field associated with the potential $V(r)$ also evaluated at the donor centre, $r=0$. Physically this term produces

the Stark effect. For weak electric fields the general formula for bound-state energy levels with quantum numbers n , m , n_1 and n_2 is (Landau and Lifshitz 1977)

$$\mathcal{E} = -\frac{e^2}{2a_0n^2} + \frac{3}{2} n(n_1 - n_2) e E a_0 - \frac{E^2 n^4}{16} a_0^3 [17n^2 - 3(n_1 - n_2)^2 - 9m^2 + 19] + \dots \quad (6.19)$$

where n is the principal quantum number and m is the magnetic quantum number for the component of the orbital angular momentum along the electric-field direction, a_0 is the effective Bohr radius, and n_1 and n_2 are integers greater than or equal to zero which obey

$$n = n_1 + n_2 + |m| + 1. \quad (6.20)$$

In equation (6.19) the second term, proportional to the electric field, is the linear Stark term; the term proportional to E^2 leads to the quadratic Stark shift. These perturbations introduce shifts in infinitely sharp transitions. In the case of donors and acceptors we are always sampling large numbers of them and, in general, the electric fields vary from donor to donor according to a more or less random spatial distribution of charged impurities producing these fields. The shift in the energy levels due to the Stark effect will vary from one donor to another. Thus the net absorption spectrum, observed in the infrared, is a superposition of a large number of sharp absorption lines centred at different frequencies. This leads to a broadening of the transition and the peak position and shape of the absorption line will then reflect the statistical distribution of the electric fields. To estimate the magnitude of the broadening resulting from the Stark effect we can define an average electric field $\langle E \rangle$ created by an ion at the donor site to be

$$\langle E \rangle \approx \frac{e}{\kappa \langle r \rangle^2} \approx \frac{e}{\kappa} (N_i)^{2/3} \quad (6.21)$$

where $\langle r \rangle$ is the mean distance between the ions and N_i is their concentration. Thus for a simple hydrogenic system the ratio of the linear to the quadratic Stark effect is $\approx 10^{-2} (N_i a_0^3)^{-2/3}$ for the 3p orbit; even for $N_i \approx 10^{16} \text{ cm}^{-3}$ this ratio is greater than one. However, donors in silicon are not simple hydrogenic systems in that the levels with the same n quantum number and different angular momentum, l , are not degenerate. Hence we do not expect significant linear Stark broadening of the 2p, 3p, ..., levels. As can be seen from equation (6.19) the quadratic Stark effect, for a given electric field, shifts the line to the lower energy side; with a random spatial distribution of charges the lineshape would be asymmetric producing a tail towards the lower energy side.

The third term in the multipole expansion (6.18), the quadrupole term, can be shown to contain terms that are linear in the electric-field gradients (Larsen 1973, 1976). The broadening due to this effect has been estimated to be of the order of $(e^2 a_0^2 / \kappa) N_i$; this becomes comparable to the broadening expected due to quadratic Stark broadening (Kogan and Lifshitz 1977), which is $\sim (e^2 a_0^3 / \kappa) N_i^{4/3}$, when the concentration of charged defects is about 10^{15} cm^{-3} .

Korn and Larsen (1973) have presented a quantitative study of the quadratic Stark broadening of $1s \rightarrow np$ transitions of donors in GaAs and its decrease at high magnetic field. The effect of charged defects on the linewidths and lineshapes of the excitation spectrum of donors in silicon can be conveniently studied using neutron-transmutation-doped silicon. Prior to any annealing there is considerable radiation damage produced by the fast neutron component of the neutron flux and the displacement of the phosphorus produced by the neutron transmutation process. It is well known (Lark-Horovitz 1951, Billington and Crawford 1961) that neutron irradiation of silicon produces defects

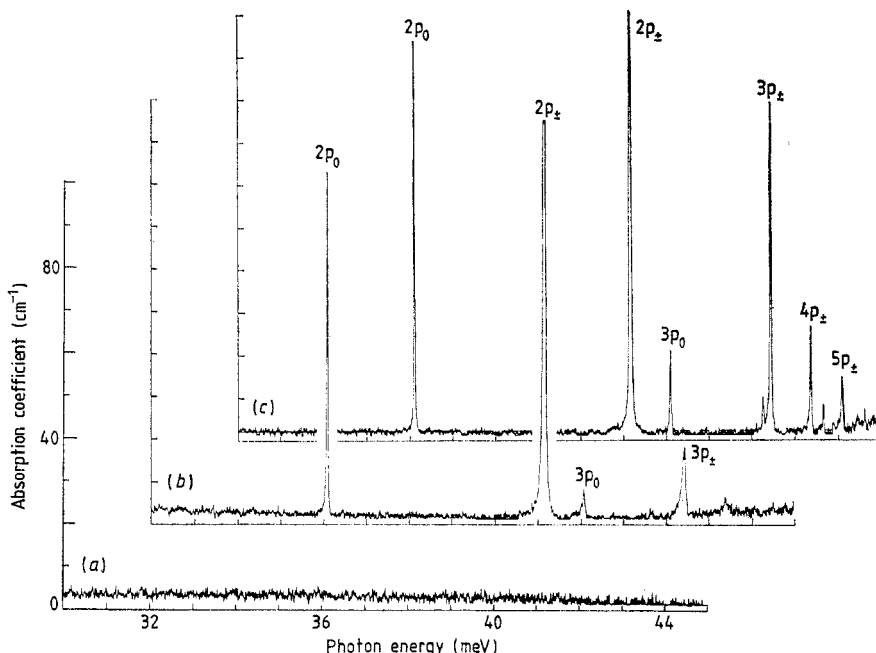


Figure 61. Lineshapes and intensities of $1s(A_1) \rightarrow np$ transitions in Si(P), the phosphorus donors being generated by the transmutation of ^{30}Si by slow neutron capture. The concentration of phosphorus $\sim 2 \times 10^{15} \text{ cm}^{-3}$. (a) Before annealing; (b) after annealing for 2 h at 650°C ; (c) after further annealing for 1 h at 800°C . The spectra were recorded with liquid helium as coolant. The instrumental resolution is 0.06 cm^{-1} without apodisation (after Jagannath *et al* 1981).

which are effective in trapping carriers and that such defects exhibit a characteristic annealing behaviour. Figure 61(a) shows the spectrum of a sample irradiated with a neutron flux of $1.1 \times 10^{14} \text{ neutrons cm}^{-2} \text{ s}^{-1}$ for 30.6 h. The phosphorus added to the sample is estimated to be $2 \times 10^{15} \text{ cm}^{-3}$. The ratio of fast to slow neutrons being 1:10, we expect $\sim 10^{20} \text{ cm}^{-3}$ defects to be produced by the fast neutrons. It is clear that the presence of these defects has compensated all the phosphorus donors and consequently the excitation spectrum is not seen. The sample was then annealed in an atmosphere of flowing helium for 2 h at 650°C . Figure 61(b) shows the spectrum after this annealing. The $2p_0$, $2p_{\pm}$, $3p_0$ and $3p_{\pm}$ lines are clearly observed in the spectrum whereas the $4p_{\pm}$ and $5p_{\pm}$ lines cannot be separated from the background. The $2p_0$ line has a $W_{1/2}$ of $\sim 0.025 \text{ meV}$ whereas the $3p_0$ and $3p_{\pm}$ lines are broad and asymmetric. Figure 61(c) shows the spectrum after the sample was further annealed for 1 h at 800°C . The $3p_0$ and $3p_{\pm}$ lines became narrower and the $4p_{\pm}$ and $5p_{\pm}$ lines could now be clearly distinguished from the background. Within experimental errors, the intensity and $W_{1/2}$ of the $2p_0$ line remained the same after the first anneal, indicating that the same number of donors are responsible for the transitions in figure 61(b) and 61(c). Figure 62 compares the $3p_{\pm}$ line on an expanded energy scale after the two anneals. The quadratic Stark broadening can account for the absence of the $4p_{\pm}$ and the higher transitions in figure 61(b) as well as the asymmetric lineshape and the lower peak heights of the $3p_0$ and the $3p_{\pm}$ lines; with the expanded energy scale in figure 62 one can easily appreciate this asymmetry in the lineshape and the lower peak height of the $3p_{\pm}$ line after the first anneal. Electrically charged radiation damage centres are evidently present even after the first

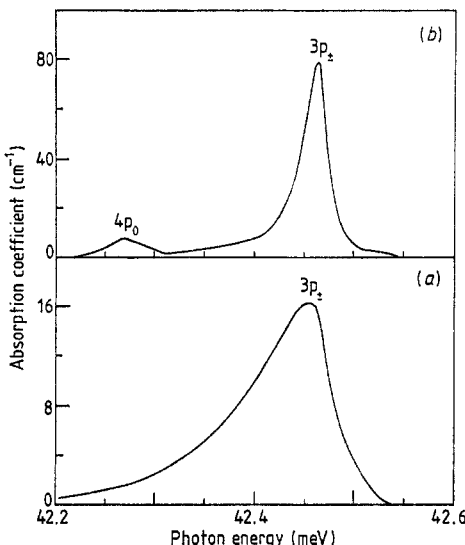


Figure 62. Comparison of the $1s(A_1) \rightarrow 3p_{\pm}$ line during successive annealings for the sample used for figure 61. (a) First annealing: 650°C for 2 h; (b) second annealing: 800°C for 1 h. The spectra were recorded using liquid helium as coolant (after Jagannath *et al* 1981).

anneal. Jagannath *et al* (1981) have also observed pronounced quadratic Stark broadening of the $2p_0$, $2p_{\pm}$ lines of phosphorus donors introduced by neutron transmutation doping in a boron-doped Si; after annealing at a sufficiently high temperature, the observed asymmetry can be ascribed to P^+ and B^- produced by compensation.

6.4. Concentration broadening

On increasing the concentration of impurities the resulting overlap of the wavefunctions gives rise to a broadening of the various energy levels. Baltensperger's (1953) calculations of the $1s$, $2s$, $2p$ bands for a lattice of hydrogen-like impurities show that the broadening of the 'hydrogenic' lines becomes important when

$$r_s \approx 6 n a_0 \quad (6.22)$$

where n is the principal quantum number of the level, a_0 is the effective Bohr radius of the bound carrier in a crystal with dielectric constant κ and r_s is defined by

$$\frac{4\pi r_s^3}{3} = \frac{1}{N_i} \quad (6.23)$$

N_i being the impurity concentration. The half-width of the $2p_0$ line does not change when the donor concentration is increased from $1.2 \times 10^{14} \text{ cm}^{-3}$ (figure 6) to $2 \times 10^{15} \text{ cm}^{-3}$ (figure 61), indicating that the broadening due to the overlap of the wavefunction does not contribute to the observed linewidth up to at least $2 \times 10^{15} \text{ cm}^{-3}$ donor atoms. Experimental data of Newman (1956) on the line spectra of acceptors in silicon demonstrated that the lines begin to broaden when the acceptor concentration is $\sim 10^{16} \text{ cm}^{-3}$. This is in close agreement with the theoretical value obtained from equation (6.22). However, this does not agree with the data obtained by Colbow (1963), which showed that con-

centration broadening starts below $1.2 \times 10^{15} \text{ cm}^{-3}$ for boron acceptors in silicon; this disagreement with Baltensperger's theory was explained by considering a random distribution of impurities as opposed to a regular spacing of impurities assumed in the calculations.

7. Concluding remarks

In this review it has not been possible to discuss many additional topics of importance. A few are mentioned below.

Electron paramagnetic resonance (EPR) especially when coupled with nuclear magnetic resonance (electron-nuclear-double-resonance or ENDOR) has provided unusually detailed information on the nature of the ground-state wavefunctions of donors (Feher 1959a, b, Feher and Gere 1959, Feher *et al* 1959, Hale and Mieher 1969a, b, 1971, Ivey and Mieher 1972, 1975a, b). Wilson and Feher (1961), Wilson (1964), Watkins and Ham (1970) and Hale and Castner (1970) studied EPR and ENDOR in donors in Si and Ge under uniaxial stress. We also cite the EPR of acceptors in Si studied by Feher *et al* (1960). Baxter and Ascarelli (1973) have reported the EPR of Si(Mg⁺). There has always been a strong interest in the effects arising from the overlap of wavefunctions as the donor concentration is increased; starting with the formation of molecular species which are analogues of the H₂ molecule, band formation is a phenomenon of basic interest. The investigations of Newman (1956) on the excitation spectra of acceptors in Si, of Imatake (1973) on donors in Ge, and of Carter *et al* (1977a) on donors in Si and CdTe are of particular interest in this context. The electronic Raman spectra of donor impurities involving the ground-state multiplet in the range where the metal-insulator transition occurs have been reported for Si by Jain *et al* (1976) and for Ge by Doepler *et al* (1974). Capizzi *et al* (1980) have recently reported the spectra of Si(P) in the concentration range of 2×10^{16} to $2 \times 10^{17} \text{ cm}^{-3}$ where they found evidence for the formation of donor-pair bonds. The formation of such pairs was previously inferred in the study of the magnetic susceptibility of n-type Si (Sonder and Stevens 1958) and n-type Ge (Damon and Gerritsen 1962).

For a recent account of deep impurities, a field closely allied to the subject of the present article, we refer the reader to Jaros (1980).

In analogy with the negative hydrogen ion (H⁻) (Bethe and Salpeter 1957), there has been interest in the study of the binding of an electron to a neutral donor (D⁻) and of a hole to a neutral acceptor (A⁺). It is expected that as in H⁻ there will occur only one bound state of very small binding energy. Scaling the known value of the binding energy of H⁻ (0.747 eV) one expects the corresponding value for Si to be 1.7 meV. Experimental evidence for D⁻ was found by Dean *et al* (1976b) in their study of radiative recombination processes in doped Si and Ge. The far-infrared photoconductivity of D⁻ and A⁺ in Si and Ge was observed by Gershenson *et al* (1973), Norton (1976) and Narita (1980). A theoretical fit of the binding energy of D⁻ in Si under uniaxial stress has been given by Larsen (1981).

Photoluminescence line spectra of multi-exciton complexes bound to donors and acceptors in Si are particularly relevant to the theme of this review. First predicted by Lampert (1958) and observed by Haynes (1960), the subject has received a new impetus in recent years in the context of the discovery of the electron-hole droplets (see, for example, Kaminskii *et al* 1971, Kosai and Gershenson 1974, Thewalt 1979). We have already referred to the 'two-electron' spectra reported by Dean *et al* (1967a) in §4.6.

Mayer and Lightowers (1980) have observed similar spectra in Ge(Bi), Ge(As) and Ge(P) and deduced the energies of the even parity states.

Donors and acceptors in uniaxial semiconductors is a subject which is a natural extension of the subject matter of this review. In this context we cite the comprehensive studies on (*a*) the electronic Raman scattering of nitrogen donors in the polytypes of SiC (Colwell and Klein 1972) and (*b*) the far-infrared photoconductivity measurements on Bi, Sb and As acceptors in Te (von Klitzing 1980).

Acknowledgments

Our thanks are due to R L Aggarwal and L Browning for a careful reading of the manuscript. Support from the National Science Foundation during the preparation of this review is gratefully acknowledged (Grant No DMR 77-27248 and NSF-MRL Program No DMR 77-23798).

References

- Aggarwal RL 1964 *Solid St. Commun.* **2** 163-6
- 1965 *PhD Thesis* Purdue University, unpublished
- Aggarwal RL, Fisher P, Mourzine V and Ramdas AK 1965 *Phys. Rev.* **138** A882-93
- Aggarwal RL, People R, Wolff PA and Larsen DM 1980 *Proc. 15th Int. Conf. on Physics of Semiconductors, Kyoto. J. Phys. Soc. Japan. Suppl. A* pp197-300
- Aggarwal RL and Ramdas AK 1965a *Phys. Rev.* **137** A602-12
- 1965b *Phys. Rev.* **140** A1246-53
- 1965c unpublished
- Ahlburn BT and Ramdas AK 1968 *Phys. Rev.* **167** 717-29
- 1969 *Phys. Rev.* **187** 932-42
- Altarelli M and Bassani F 1980 *Handbook of Semiconductors* vol 1, ed W Paul (Amsterdam: North-Holland)
- Anastassakis E 1969 *Phys. Rev.* **186** 760-7
- Arai T, Asanuma N, Kudo K and Umemoto S 1972 *Japan. J. Appl. Phys.* **11** 206-12
- Austin IG and Wolfe R 1956 *Proc. Phys. Soc. B* **69** 329-38
- Baldereschi A and Bassani F 1968 *Proc. 9th Int. Conf. on Physics of Semiconductors, Moscow* vol 1, ed S M Ryvkin (Leningrad: Nauka) pp280-6
- 1970 *Proc. 10th Int. Conf. on Physics of Semiconductors, Cambridge, Mass.* ed S P Keller, J C Hensel and F Stern (Washington, DC: USAEC Division of Technical Information) pp191-6
- Baldereschi A and Lipari NO 1973 *Phys. Rev. B* **8** 2697-709
- 1974 *Phys. Rev. B* **9** 1525-39
- 1976 *Physics of Semiconductors* ed F G Fumi (Rome: Tipografia Marves) pp595-8
- Balslev I 1966 *J. Phys. Soc. Japan* **21 Suppl.** 101-6
- Baltensperger W 1953 *Phil. Mag.* **44** 1355-63
- Bardeen J and Shockley W 1950 *Phys. Rev.* **80** 72-80
- Barra F, Fisher P and Rodriguez S 1973 *Phys. Rev. B* **7** 5285-98
- Barrie R and Nishikawa K 1963 *Can. J. Phys.* **41** 1823-35
- Bassani F, Iadonisi G and Preziosi B 1974 *Rep. Prog. Phys.* **37** 1099-210
- Bassani F and Pastori Parravicini G 1975 *Electronic States and Optical Transitions in Solids* (Oxford: Pergamon)
- Baxter JE and Ascarelli G 1973 *Phys. Rev. B* **7** 2630-9
- Becker WM, Ramdas AK and Fan HY 1961 *J. Appl. Phys.* **32** 2094-102
- Bell RJ 1972 *Introductory Fourier Transform Spectroscopy* (New York: Academic)
- Berlincourt D, Jaffe H and Shiozawa LR 1963 *Phys. Rev.* **129** 1009-17
- Bethe HA 1942 *Theory of the Boundary Layer of Crystal Rectifiers. MIT Radiation Lab. Rep. No 43-12*
- Bethe HA and Salpeter EE 1957 *Quantum Mechanics of One- and Two-electron Atoms* (Berlin: Springer-Verlag) pp154-7

- Bhagavantam S 1966 *Crystal Symmetries and Physical Properties* (New York: Academic)
- Bhatia KL 1971 *Can. J. Phys.* **49** 374–80
- Bhattacharjee AK and Rodriguez S 1972 *Phys. Rev. B* **6** 3836–56
- Billington DS and Crawford JH 1961 *Radiation Damage in Solids* (Princeton: Princeton University)
- Bir GL, Butikov EJ and Pikus GE 1963 *J. Phys. Chem. Solids* **24** 1467–74
- Bir GL and Pikus GE 1974 *Symmetry and Strain-induced effects in Semiconductors* (New York: Wiley) pp226–38
- Bosomworth AR, Crandall RS and Enstrom RE 1968 *Phys. Lett.* **28A** 320–1
- Bouckaert LP, Smoluchowski R and Wigner EP 1936 *Phys. Rev.* **50** 58–67
- Boyle WS 1959 *J. Phys. Chem. Solids* **8** 321–3
- Boyle WS and Howard RE 1961 *J. Phys. Chem. Solids* **19** 181–8
- Bratt PR 1977 *Semiconductors and Semimetals* vol 12, ed RK Willardson and AC Beer (New York: Academic) pp39–142
- Breit G and Wigner EP 1936 *Phys. Rev.* **49** 519–31
- Broeckx J and Clauws P 1978 *Solid St. Commun.* **28** 355–8
- Broeckx J, Clauws P, Van Den Steen K and Vennick J 1979 *J. Phys. C: Solid St. Phys.* **12** 4061–79
- Brophy JJ 1956 *Physica* **22** 156–8
- Burstein E, Bell EE, Davison JW and Lax M 1953 *J. Phys. Chem.* **57** 849–52
- Burstein E, Picus G, Henvis B and Wallis R 1956 *J. Phys. Chem. Solids* **1** 65–74
- Butler NR and Fisher P 1974 *Phys. Lett.* **47A** 391–2
- 1976 *Phys. Rev. B* **13** 5465–75
- Butler NR, Fisher P and Ramdas AK 1975 *Phys. Rev. B* **12** 3200–9
- Buzdin VV, Demeshina AI and Kurskii Yu A 1973 *Sov. Phys.–Semicond.* **6** 1792–6
- Bykova EM, Goncharov LA, Lifshitz TM, Sidorov VI and Hall RN 1976 *Sov. Phys.–Semicond.* **9** 1228–31
- Callaway J 1958 *Solid State Physics* vol 7, ed F Seitz and D Turnbull (New York: Academic) pp99–212
- Capizzi M, Thomas GA, DeRosa F, Bhatt RN and Rice TM 1980 *Phys. Rev. Lett.* **44** 1019–22
- Carlson RO 1957 *Phys. Rev.* **108** 1390–3
- Carter AC, Skolnick MS, Stradling RA, Leotin JP and Askenazy S 1976 *Proc. 13th Int. Conf. on Physics of Semiconductors* ed FG Fumi (Rome: Tipografia Marves) pp619–22
- Carter AC, Carver GP, Nicholas RJ, Portal JC and Stradling RA 1977a *Solid St. Commun.* **24** 55–60
- Carter AC, Dean PJ, Skolnick MS and Stradling RA 1977b *J. Phys. C: Solid St. Phys.* **10** 5111–29
- Chamberlain JM, Ergun HB, Gehring KA and Stradling RA 1971a *Solid St. Commun.* **9** 1563–6
- Chamberlain JM, Simmonds PE, Stradling RA and Bradley CC 1971b *J. Phys. C: Solid St. Phys.* **4** L38–42
- Chandrasekhar HR, Fisher P, Ramdas AK and Rodriguez S 1973 *Phys. Rev. B* **8** 3836–51
- Chandrasekhar HR and Ramdas AK 1980 *Phys. Rev. B* **21** 1511–5
- Chandrasekhar HR, Ramdas AK and Rodriguez S 1975 *Phys. Rev. B* **12** 5780–9
- 1976 *Phys. Rev. B* **14** 2417–21
- Chapman RA and Hutchinson WG 1965 *Solid St. Commun.* **3** 293–6
- 1967a *Phys. Rev.* **157** 615–22
- 1967b *Phys. Rev. Lett.* **18** 443–5
- Chelikowsky JR and Cohen ML 1976 *Phys. Rev. B* **14** 556–82
- Chen CS, Corelli JC and Watkins GD 1972 *Phys. Rev. B* **5** 510–26
- Cherlow JM, Aggarwal RL and Lax B 1973 *Phys. Rev. B* **7** 4547–60
- Cohn DR, Larsen DM and Lax B 1970 *Solid St. Commun.* **8** 1707–9
- 1972 *Phys. Rev. B* **6** 1367–75
- Colbow K 1963 *Can. J. Phys.* **41** 1801–22
- Collins AT, Dean PJ, Lightowers EC and Sherman WF 1965 *Phys. Rev.* **140** A1272–4
- Collins AT and Lightowers EC 1968 *Phys. Rev.* **171** 843–55
- Collins CB and Carlson RO 1957 *Phys. Rev.* **108** 1409–14
- Collins CB, Carlson RO and Gallagher CJ 1957 *Phys. Rev.* **105** 1168–73
- Colwell PJ and Klein MV 1972 *Phys. Rev. B* **6** 498–515
- Crouch RK, Robertson JB and Gilmer TE 1972 *Phys. Rev. B* **5** 3111–9
- Crowther PA, Dean PJ and Sherman WF 1967 *Phys. Rev.* **154** 772–85
- Custers JFH 1952 *Physica* **18** 489–96
- Damon DH and Gerritsen AN 1962 *Phys. Rev.* **127** 405–13
- Darken LS 1977 *Bull. Am. Phys. Soc.* **22** 42
- Dean PJ, Bimberg D and Mansfield F 1977 *Phys. Rev. B* **15** 3906–16
- Dean PJ, Cuthbert JD, Thomas DG and Lynch RT 1967a *Phys. Rev. Lett.* **18** 122–4

- Dean PJ, Haynes JR and Flood WF 1967b *Phys. Rev.* **161** 711–29
Dean PJ and Herbert DC 1976 *J. Lumin.* **14** 55–79
Dean PJ, Lightowlers EC and Wight DR 1965 *Phys. Rev.* **140** A352–68
de Kock AJR 1980 *Handbook on Semiconductors* vol 3, ed S P Keller (Amsterdam North-Holland)
Dexter RN, Zeiger HJ and Lax B 1956 *Phys. Rev.* **104** 637–44
Dickey DH and Dimmock JO 1967 *J. Phys. Chem. Solids* **28** 529–42
Doehler J, Colwell PJ and Solin SA 1974 *Phys. Rev. B* **9** 636–9
— 1975 *Phys. Rev. Lett.* **34** 584–7
Dresselhaus G, Kip AF and Kittel C 1955 *Phys. Rev.* **98** 368–84
Duff KJ, Fisher P and Butler NR 1980 *Aust. J. Phys.* **33** 73–90
Elliot JP and Dawber PG 1979 *Symmetry in Physics* vols 1 and 2 (Oxford: Oxford University Press)
Elliot RJ and Loudon R 1960 *J. Phys. Chem. Solids* **15** 196–207
Fan HY and Fisher P 1959 *J. Phys. Chem. Solids* **8** 270–2
Fano U 1961 *Phys. Rev.* **124** 1866–78
Faulkner RA 1969 *Phys. Rev.* **184** 713–21
Feher G 1959a *Phys. Rev.* **114** 1219–44
— 1959b *J. Phys. Chem. Solids* **8** 486–9
Feher G and Gere EA 1959 *Phys. Rev.* **114** 1245–56
Feher G, Hensel JC and Gere EA 1960 *Phys. Rev. Lett.* **5** 309–11
Feher G, Wilson DK and Gere EA 1959 *Phys. Rev. Lett.* **3** 25–8
Fetterman HR, Larsen DM, Stillman GE, Tannenwald PE and Waldman J 1971 *Phys. Rev. Lett.* **26** 975–8
Fisher P 1962 *J. Phys. Chem. Solids* **23** 1346–8
Fisher P and Fan HY 1959 *Phys. Rev. Lett.* **2** 456–8
— 1960 *Phys. Rev. Lett.* **5** 195–7
Fisher P, Haak WH, Johnson EJ and Ramdas AK 1963 *Proc. 8th Symp. on the Art of Glass Blowing* (Wilmington, Delaware: The Scientific Glassblowers Society) pp136–47
Fisher P, Jones RL, Onton A and Ramdas AK 1966 *J. Phys. Soc. Japan* **21 Suppl.** 224–9
Fisher P and Ramdas AK 1969 *Physics of the Solid State* ed S Balakrishna, M Krishnamurthi and B Ramachandra Rao (New York: Academic) pp149–82
Fletcher RC, Yager WA, Pearson GL, Holden AN, Read WT and Merritt FR 1954a *Phys. Rev.* **94** 1392–3
Fletcher RC, Yager WA, Pearson GL and Merritt FR 1954b *Phys. Rev.* **95** 844–5
Flynn CP 1972 *Point Defects and Diffusion* (Oxford: Clarendon)
Franks RK and Robertson JB 1967 *Solid St. Commun.* **5** 479–81
Fuller CS 1960 *Semiconductors* ed N B Hannay (New York: Reinhold) pp192–221
Gershenson EM 1977 *Sov. Phys.–Usp.* **20** 456–62
Gershenson EM, Gol'tsman GN and Ptitsina NG 1973 *Sov. Phys.–JETP* **37** 299–304
— 1977 *JETP Lett.* **25** 539–43
Ghanekhar KM and Sladek RJ 1966 *Phys. Rev.* **146** 505–12
Gilman JJ 1963 *The Art and Science of Growing Crystals* (New York: Wiley)
Gilmer TE, Franks RK and Bell RJ 1965 *J. Phys. Chem. Solids* **26** 1195–204
Golka J, Trylski J, Skolnick MS, Stradling RA and Couder Y 1977 *Solid St. Commun.* **22** 623–6
Gorman M and Solin SA 1977 *Phys. Rev. B* **16** 1631–47
Hadni A 1967 *Essentials of Modern Physics Applied to the Study of the Infrared* (Oxford: Pergamon)
Haering RR 1958 *Can. J. Phys.* **36** 1161–7
Hale EB and Castner TG Jr 1970 *Phys. Rev. B* **1** 4763–83
Hale EB and Mieher RL 1969a *Phys. Rev.* **184** 739–50
— 1969b *Phys. Rev.* **184** 751–9
— 1971 *Phys. Rev. B* **3** 1955–65
Haller EE and Falicov LM 1978 *Phys. Rev. Lett.* **41** 1192–4
Haller EE and Hansen WL 1974 *Solid St. Commun.* **15** 687–92
Hannay NB 1960 *Semiconductors* (New York: Reinhold)
Hardy JR, Smith SD and Taylor W 1962 *Proc. Int. Conf. on Semiconductor Physics, Exeter* (London: The Institute of Physics and The Physical Society) pp521–8
Hasegawa H and Howard RE 1961 *J. Phys. Chem. Solids* **21** 179–98
Hass M 1967 *Semiconductors and Semimetals* vol 3, ed R K Willardson and A C Beer (New York: Academic) pp3–16

- Hass M and Henvis BW 1962 *J. Phys. Chem. Solids* **23** 1099–104
 Haynes JR 1960 *Phys. Rev. Lett.* **4** 361–3
 Henry CH, Hopfield JJ and Luther LC 1966 *Phys. Rev. Lett.* **17** 1178–80
 Hilsom C, Fray S and Smith C 1969 *Solid St. Commun.* **7** 1057–9
 Hinkeley ED, Nill KW and Blum FA 1976 *Laser Spectroscopy of Atoms and Molecules* ed H Walther (Berlin: Springer-Verlag) pp125–96
 Ho LT and Ramdas AK 1970 *Phys. Lett.* **32A** 23–4
 —— 1972 *Phys. Rev. B* **5** 462–74
 Hopfield JJ, Thomas DG and Gershenzon M 1963 *Phys. Rev. Lett.* **10** 162–4
 Horii K and Nisida Y 1971 *J. Phys. Soc. Japan* **31** 783–91
 Hrostowski HJ and Kaiser RH 1958 *Phys. Rev. Lett.* **1** 199–200
 Huggins CM and Cannon P 1962 *Nature* **194** 829–30
 Humphreys RG, Rössler U and Cardona M 1978 *Phys. Rev. B* **18** 5590–605
 Imatake A 1973 *J. Phys. Soc. Japan* **35** 164–71
 Ivey JL and Mieher RL 1972 *Phys. Rev. Lett.* **29** 176–8
 —— 1975a *Phys. Rev. B* **11** 822–48
 —— 1975b *Phys. Rev. B* **11** 849–57
 Jackson JD 1975 *Classical Electrodynamics* (New York: Wiley) 2nd edn, p102
 Jagannath C 1980 *PhD Thesis* Purdue University, unpublished
 Jagannath C, Grabowski ZW and Ramdas AK 1979 *Solid St. Commun.* **29** 355–9
 —— 1981 *Phys. Rev. B* **23** 2082–98
 Jagannath C and Ramdas AK 1980 *J. Phys. Soc. Japan* **49 Suppl. A** 201–4
 —— 1981 *Phys. Rev. B* **23** 4426–40
 Jain K, Lai S and Klein MV 1976 *Phys. Rev. B* **13** 5448–64
 Jaros M 1980 *Adv. Phys.* **29** 409–525
 Jones RL 1968 *PhD Thesis* Purdue University, unpublished
 Jones RL and Fisher P 1964 *Solid St. Commun.* **2** 369–71
 —— 1965 *J. Phys. Chem. Solids* **26** 1125–31
 —— 1970 *Phys. Rev. B* **2** 2016–29
 Kaiser W 1962 *J. Phys. Chem. Solids* **23** 255–60
 Kaiser W, Frisch HL and Reiss H 1958 *Phys. Rev.* **112** 1546–54
 Kaminskii AS, Pokrovskii YaE and Alkeev NV 1971 *Sov. Phys.–JETP* **32** 1048–53
 Kanazawa KK and Brown FC 1964 *Phys. Rev.* **135** A1757–60
 Kane EO 1960 *Phys. Rev.* **119** 40–2
 —— 1966 *Semiconductors and Semimetals* vol 1, ed R K Willardson and A C Beer (New York: Academic) pp75–100
 Kaplan R 1969 *Phys. Rev.* **181** 1154–62
 —— 1973 *Solid St. Commun.* **12** 191–4
 Kaplyanskii AA 1964a *Sov. Phys.–Opt. Spectrosc.* **16** 557–65
 —— 1964b *Sov. Phys.–Opt. Spectrosc.* **16** 329–37
 Kartheuser EP, Rodriguez S and Fisher P 1974 *Phys. Stat. Solidi b* **64** 11–28
 Keyes RW and Sladek RJ 1956 *J. Phys. Chem. Solids* **1** 143–5
 Kirkman RF, Stradling RA and Lin-Chung PJ 1978 *J. Phys. C: Solid St. Phys.* **11** 419–33
 Kittel C and Mitchell AH 1954 *Phys. Rev.* **96** 1488–93
 Kleiner WH and Krag WE 1970 *Phys. Rev. Lett.* **25** 1490–2
 Kleiner WH and Roth LM 1959 *Phys. Rev. Lett.* **2** 334–6
 Kogan ShM and Lifshits TM 1977 *Phys. Stat. Solidi a* **39** 11–39
 Kohn W 1957 *Solid State Physics* vol 5, ed F Seitz and D Turnbull (New York: Academic) pp257–320
 Kohn W and Luttinger JM 1955 *Phys. Rev.* **98** 915–22
 Kopylov AA and Pikhtin AN 1977 *Sov. Phys.–Semicond.* **11** 510–6
 Korn DM and Larsen DM 1973 *Solid St. Commun.* **13** 807–10
 Kosai K and Gershenzon M 1974 *Phys. Rev. B* **9** 723–36
 Koster GF 1957 *Solid State Physics* vol 5, ed F Seitz and D Turnbull (New York: Academic) pp173–256
 Koster GF, Dimmock JO, Wheeler RG and Statz H 1963 *Properties of the Thirty-two Point Groups* (Cambridge, Mass.: MIT Press)
 Krag WE, Kleiner WH and Zeiger HJ 1970 *Proc. 10th Int. Conf. on Physics of Semiconductors, Cambridge, Mass.* ed S P Keller, J C Hensel and F Stern (Washington, DC: USAEC Division of Technical Information) pp271–7

- Krag WE, Kleiner WH, Zeiger HJ and Fischler S 1966 *J. Phys. Soc. Japan* **21 Suppl.** 230–3
- Krag WE and Zeiger HJ 1962 *Phys. Rev. Lett.* **8** 485–7
- Kuchar F, Fantner E and Bauer G 1977 *J. Phys. C: Solid St. Phys.* **10** 3577–87
- Lampert MA 1958 *Phys. Rev. Lett.* **1** 450–3
- Landau LD and Lifshitz EM 1977 *Quantum Mechanics (Non-relativistic Theory)* (Oxford: Pergamon) 3rd edn
- Lark-Horovitz K 1951 *Semi-Conducting Materials* ed H K Henisch (London: Butterworths) pp47–69
- 1954 *The Present State of Physics* (New York: AAAS) pp57–127
- Larsen DM 1973 *Phys. Rev. B* **8** 535–52
- 1976 *Phys. Rev. B* **13** 1681–91
- 1981 *Phys. Rev.* to be published
- Laude LD, Cardona M and Pollak FH 1970 *Phys. Rev. B* **1** 1436–42
- Laudise RA 1970 *The Growth of Single Crystals* (Englewood Cliffs, NJ: Prentice-Hall)
- Lawaetz P 1971 *Phys. Rev. B* **4** 3460–7
- 1975 *Solid St. Commun.* **16** 65–7
- Lax M and Burstein E 1955 *Phys. Rev.* **100** 592–602
- Lax B, Roth LM and Zwerdling S 1959 *J. Phys. Chem. Solids* **8** 311–8
- Lee N, Larsen DM and Lax B 1973 *J. Phys. Chem. Solids* **34** 1817–25
- Leotin J, Ousset JC, Barbaste R, Askenazy S, Skolnick MS, Stradling RA and Poiblaud G 1975 *Solid St. Commun.* **16** 363–6
- Lifshits TM and Nad' FYa 1965 *Sov. Phys.-Dokl.* **10** 532–3
- Lightowlers EC 1962 *Anal. Chem.* **34** 1398–402
- Lin-Chung PJ and Henvis BW 1975 *Phys. Rev. B* **12** 630–40
- 1976 *Proc. 13th Int. Conf. on Physics of Semiconductors* ed F G Fumi (Rome: Tipografia Marves) pp587–90
- Lin-Chung PJ and Wallis RF 1969 *J. Phys. Chem. Solids* **30** 1453–64
- Lipari NO and Baldereschi A 1970 *Phys. Rev. Lett.* **25** 1660–4
- 1972 *Proc. Int. Conf. on Physics of Semiconductors* ed M Miasek (Warsaw: Polish Scientific Publications) pp1009–15
- 1978 *Solid St. Commun.* **25** 665–8
- Litton CW, Dennis RB and Smith SD 1969 *J. Phys. Chem.* **2** 2146–55
- Long D 1968 *Energy Bands in Semiconductors* (New York: Interscience)
- Lorimor OG and Spitzer WG 1965 *J. Appl. Phys.* **36** 1841–4
- Luttinger JM 1956 *Phys. Rev.* **102** 1030–41
- Luttinger JM and Kohn W 1955 *Phys. Rev.* **97** 869–83
- Manchon DD Jr and Dean PJ 1970 *Proc. 10th Int. Conf. on Physics of Semiconductors, Cambridge, Mass.* ed S P Keller, J C Hensel and F Stern (Washington, DC: USAEC Division of Technical Information) pp760–6
- Martin AD, Fisher P and Simmonds PE 1979 *Phys. Lett.* **73A** 331–2
- 1981 to be published
- Mayer AE and Lightowlers EC 1980 *J. Phys. Soc. Japan* **49 Suppl. A** 441–4
- Mehran F, Morgan TN, Title RS and Blum SE 1972 *Phys. Rev. B* **6** 3917–26
- Mendelson KS and James HM 1964 *J. Phys. Chem. Solids* **25** 729–39
- Mendelson KS and Schultz DR 1969 *Phys. Stat. Solidi* **31** 59–69
- Merlet F, Pajot B, Arcas Ph and Jean-Louis AM 1975 *Phys. Rev. B* **12** 3297–317
- Messiah A 1966 *Quantum Mechanics* (Engl. transl. G M Temmer (vol 1) and J Potter (vol 2) (New York: Wiley))
- Möller KD and Rothschild WG 1971 *Far-Infrared Spectroscopy* (New York: Wiley-Interscience)
- Mooradian A 1972 *Laser Handbook* vol 2, ed F T Arecchi and E O Schulz-DuBois (Amsterdam: North-Holland) pp1409–56
- Mooradian A and McWhorter AL 1967 *Phys. Rev. Lett.* **19** 849–52
- Mooradian A and Wright GB 1966a *Phys. Rev. Lett.* **16** 999–1001
- 1966b *Solid St. Commun.* **4** 431–4
- Moore WJ 1965 *Solid St. Commun.* **3** 385–8
- 1971 *J. Phys. Chem. Solids* **32** 93–102
- Morgan TN 1968 *Phys. Rev. Lett.* **21** 819–23
- Morin FJ, Maita JP, Schulman RG and Hannay NB 1954 *Phys. Rev.* **96** 833
- Mott NF and Gurney RW 1940 *Electronic Processes in Ionic Crystals* (Oxford: Clarendon)
- Murzin VN, Demeshina AI and Umarov LM 1969 *Sov. Phys.-Semicond.* **3** 367–9

- 1972 *Sov. Phys.-Semicond.* **6** 419–25
 Nara H and Morita A 1967 *J. Phys. Soc. Japan* **23** 831–5
 Narita S 1980 *J. Phys. Soc. Japan* **49 Suppl. A** 173–80
 Nelson DF, Johnson LF and Gershenzon M 1964 *Phys. Rev.* **135** A1399–406
 Newman R 1956 *Phys. Rev.* **103** 103–6
 Newman RC 1973 *Infra-red Studies of Crystal Defects* (London: Taylor and Francis)
 Nisida Y and Horii K 1971 *J. Phys. Soc. Japan* **31** 776–82
 Nisida Y and Muro K 1975 *Prog. Theor. Phys. Suppl.* **57** 77–86
 Norton P 1976 *Phys. Rev. Lett.* **37** 164–8
 Onton A 1969 *Phys. Rev.* **186** 786–90
 — 1971 *Phys. Rev. B* **4** 4449–52
 Onton A, Fisher P and Ramdas AK 1967a *Phys. Rev.* **163** 686–703
 — 1967b *Phys. Rev. Lett.* **19** 781–3
 Onton A and Taylor RC 1970 *Phys. Rev. B* **1** 2587–91
 Onton A, Yacoby Y and Chicotka RJ 1972 *Phys. Rev. Lett.* **28** 966–9
 Pajot B and Darviot Y 1966 *Phys. Lett.* **21** 512–4
 Pajot B, Kauppinen J and Anttila R 1979 *Solid St. Commun.* **31** 759–63
 Pajot B, Merlet F and Taravella G 1972a *Can. J. Phys.* **50** 2186–93
 Pajot B, Merlet F, Taravella G and Arcas Ph 1972b *Can. J. Phys.* **50** 1106–13
 Pantelides ST 1978 *Rev. Mod. Phys.* **50** 797–858
 Patel CKN and Shaw ED 1970 *Phys. Rev. Lett.* **24** 451–5
 Patrick L and Dean PJ 1969 *Phys. Rev.* **188** 1254–6
 Pearson GL and Bardeen J 1949 *Phys. Rev.* **75** 865–83
 Pell EM 1960 *Solid State Physics in Electronics and Telecommunications* vol 1, ed M Désirant and JL Michiels (New York: Academic) pp261–76
 Picus G, Burstein E and Henvis B 1956 *J. Phys. Chem. Solids* **1** 75–81
 Pikus GE and Bir GL 1960 *Sov. Phys.-Solid St.* **1** 1502–17
 Pine AS 1974 *J. Opt. Soc. Am.* **64** 1683–90
 Price PJ 1956 *Phys. Rev.* **104** 1223–39
 Putley EH 1964 *Phys. Stat. Solidi* **6** 571–614
 Ramdas AK, Lee PM and Fisher P 1963 *Phys. Lett.* **7** 99–101
 Rauch CJ, Stickler JJ, Zeiger HJ and Heller GS 1960 *Phys. Rev. Lett.* **4** 64–6
 Reiss H and Fuller CS 1960 *Semiconductors* ed NB Hannay (New York: Reinhold) pp222–68
 Reuszer JH and Fisher P 1964 *Phys. Rev.* **135** A1125–32
 — 1965 *Phys. Rev.* **140** A245–51
 — 1968 *Phys. Rev.* **165** 909–16
 Rodriguez S, Fisher P and Barra F 1972 *Phys. Rev. B* **5** 2219–33
 Rodriguez S and Schultz TD 1969 *Phys. Rev.* **178** 1252–63
 Rose-Innes AC 1973 *Low-temperature Laboratory Techniques* (London: English Universities Press) 2nd edn
 Sampson D and Margenau H 1956 *Phys. Rev.* **103** 879–85
 Schechter D 1962 *J. Phys. Chem. Solids* **23** 237–47
 Sclar N 1976 *Infrared Phys.* **16** 435–48
 — 1977 *Infrared Phys.* **17** 71–82
 Scott W and Onffroy JR 1976 *Phys. Rev. B* **13** 1664–74
 Seccombe SD and Korn DM 1972 *Solid St. Commun.* **11** 1539–45
 Shenker H, Swiggard EM and Moore WJ 1967 *Trans. Metall. Soc. AIME* **239** 347–9
 Simmonds PE, Stradling RA, Birch JR and Bradley CC 1974 *Phys. Stat. Solidi b* **64** 195–203
 Sladek RJ 1958 *J. Phys. Chem. Solids* **5** 157–70
 Soepangkat HP and Fisher P 1973 *Phys. Rev. B* **8** 870–93
 Sonder E and Stevens DK 1958 *Phys. Rev.* **110** 1027–34
 Stillman GE, Wolfe CM and Dimmock JO 1969 *Solid St. Commun.* **7** 921–5
 Stillman GE, Larsen DM, Wolfe CM and Brandt RC 1971 *Solid St. Commun.* **9** 2245–9
 Stirn RJ and Becker WM 1966 *Phys. Rev.* **141** 621–8
 Stoelinga JHM, Larsen DM, Walukiewicz W, Aggarwal RL and Bozler CO 1978 *J. Phys. Chem. Solids* **39** 873–7
 Street RA and Senske W 1976 *Phys. Rev. Lett.* **37** 1292–5
 Summers CJ, Dingle R and Hill DE 1970 *Phys. Rev. B* **1** 1603–6
 Suzuki K, Okazaki M and Hasegawa H 1964 *J. Phys. Soc. Japan* **19** 930–44

- Swartz JC, Lemmon DH and Thomas RN 1980 *Solid St. Commun.* **36** 331–4
Tannenbaum M and Mills AD 1961 *J. Electrochem. Soc.* **108** 173–8
Tekippe VJ, Chandrasekhar HR, Fisher P and Ramdas AK 1972 *Phys. Rev. B* **6** 2348–56
Thewalt MLW 1979 *Physics of Semiconductors 1978. Inst. Phys. Conf. Ser. No 43* ed B L H Wilson (Bristol: The Institute of Physics) pp605–14
Thomas DG, Gershenson M and Hopfield JJ 1964 *Phys. Rev.* **133** A269–79
Tokumoto H and Ishiguro T 1977 *Phys. Rev. B* **15** 2099–117
Torrey HC and Whitmer CA 1948 *Crystal Rectifiers* (New York: McGraw-Hill)
Vink AT and Van Doorn CZ 1962 *Phys. Lett.* **1** 332–3
von Klitzing K 1980 *Phys. Rev. B* **21** 3349–57
Wagner RJ and McCombe BD 1974 *Phys. Stat. Solidi b* **64** 205–12
Wannier GH 1962 *Rev. Mod. Phys.* **34** 645–55
Watkins GD 1965 *Radiation Damage in Semiconductors* ed P Baruch (Paris: Dunod) pp97–113
Watkins GD and Fowler WB 1977 *Phys. Rev. B* **16** 4524–9
Watkins GD and Ham FS 1970 *Phys. Rev. B* **1** 4071–98
Wedepohl PT 1957 *Proc. Phys. Soc. B* **70** 177–85
——— 1968 *J. Phys. C: Solid St. Phys.* **1** 1773–4
Wentorf RH and Bovenkerk HP 1962 *J. Chem. Phys.* **36** 1987–90
Whelan JM 1960 *Properties of Some Covalent Semiconductors in Semiconductors* ed N B Hannay (New York: Reinhold) pp389–436
Wilson DK 1964 *Phys. Rev.* **134** A265–86
Wilson DK and Feher G 1961 *Phys. Rev.* **124** 1068–83
Wilson EB, Decius JC and Cross PC 1955 *Molecular Vibrations* (New York: McGraw-Hill)
Wolf HF 1969 *Silicon Semiconductor Data* (Oxford: Pergamon)
Wood RA, Khan MA, Wolff PA and Aggarwal RL 1977 *Opt. Commun.* **21** 154–7
Wright GB and Mooradian A 1967 *Phys. Rev. Lett.* **18** 608–10
Zwerdling S, Button KJ and Lax B 1960a *Phys. Rev.* **118** 975–86
Zwerdling S, Button KJ, Lax B and Roth LM 1960b *Phys. Rev. Lett.* **4** 173–6